# Ablation laser femtoseconde pour le contrôle de la micro et nano structuration

David Bruneel

## To cite this version:

David Bruneel. Ablation laser femtoseconde pour le contrôle de la micro et nano structuration. Autre [cond-mat.other]. Université Jean Monnet - Saint-Etienne; Universität des Saarlandes, 2010. Français. NNT : 2010STET4007 . tel-00675144

HAL Id: tel-00675144
https://theses.hal.science/tel-00675144

Submitted on 29 Feb 2012

# Femtosecond laser ablation for controlling micro and nano structuration

Dissertation

zur Erlangung des Grades des Doktors der Ingenieurwissenschaften

der Naturwissenschaftlich-Technischen Fakultät II

- Physik und Mechatronik -

der Universität des Saarlandes

Cotutelle-Promotion mit der Universität St. Etienne (Frankreich)

von

David Bruneel

Saarbrücken

(2010)

*“When a […] scientist states that something is possible,*
*He is almost certainly right*
*When he states that something is impossible,*
*He is very probably wrong.”*

*Arthur C. Clarke*

# Abstract

The current development of technology makes constant the necessity of getting smaller and smaller features sizes down to micrometer and sub micrometer scales. Laser ablation, which has the great advantage of precise material removal, is a promising candidate. In this dissertation we have demonstrated the feasibility to take advantage of the interaction of femtosecond laser pulses with matter for micro- and nano-structuration and this by having developed a compact and high accurate and flexible apparatus. An analyse of the specific physical mechanisms of laser-matter interaction in the femtosecond regime is presented. Investigations on processing time efficiency as well as the effect of the repetition rate during ablation of metals have been performed. The potential of the multifunctional tool coupled with a compact high repetition rate femtosecond oscillator is shown for different applications in biotechnology. Results on large area mapping as well as accurate nanoprocessing of biological tissue and various materials are presented. This versatile tool covers wide research fields from the nanoprocessing of biological samples as well as the nanostructuring of different type of materials. It is of great interest for many applications in material science, nanobiotechnology and nanomedicine.

# Kurzdarstellung

Die augenblickliche Technologieentwicklung macht ein Design immer kleinerer Bauteile, bis hin zu mikrometer- und sub-mikrometer Bereichen notwendig. Materialabtragung durch einen Laser wird durch die erreichbare hohe Präzision zu einer vielversprechenden Methode, diese gewünschten Bereiche zu erreichen. In dieser Dissertation wird die Möglichkeit, den Vorteil der Interaktion von femtosekunden Laserpulsen mit für eine Mikro- und Nanostrukturierung geeignetem Material durch ein eigens entwickeltes, kompaktes, hochpräzises und flexibles System demonstriert. Eine Analyse der spezifischen physikalischen Mechanismen der Laser – Materie Interaktion im femtosekunden Bereich wird präsentiert. Untersucht wurden sowohl die Effizienz unterschiedlicher Bearbeitungsdauern als auch der Einfluss der Repetitionsrate während des Materialabtrags. Das Potential des erstellten multifunktionellen Gerätes in Kopplung mit einem kompakten femtosekunden Oszillator hoher Repetitionsrate wird für verschiedene Applikationen in der Biotechnologie aufgezeigt. Ergebnisse einer Abbildung von Bereichen, die mehr als den eigentlichen

Scanbereich umfassen, und präziser Nanoabtrag biologischen Gewebes und verschiedener Materialien werden präsentiert. Das entwickelte vielfältige System deckt wichtige Bereiche der aktuellen Forschung von der Nanobearbeitung biologischer Proben bis hin zur Nanostrukturierung verschiedener Materialien ab. Dies ist von großem Interesse für viele Anwendungen in Materialwissenschaften, Nanobiotechnologie und Nanomedizin.

## Résumé succinct

Le développement actuel de la technologie induit une constante nécessité d'obtenir des tailles de plus en plus petites pouvant descendre jusqu'à des dimensions micrométriques et sub micrométriques. L'ablation laser, qui a le grand avantage d'un enlèvement de matière très précis, et un candidat prometteur. Dans cette thèse on démontre la faisabilité de tirer avantage des impulsions laser femtosecondes avec la matière pour la micro et nano structuration, et ceci en ayant développé une machine compacte de grande précision et flexibilité. Une approche théorique comparant les régimes d'interaction à haute et basse cadence est présentée. Des investigations de l'efficacité du temps de procédé aussi bien que l'effet de la cadence pendant l'ablation de métaux ont été effectuées. Le potentiel de l'outil multifonctionnel couplé avec un oscillateur laser femtoseconde à haute cadence est montré pour différentes applications en biotechnologie. Les résultats sur la cartographie d'une large zone aussi bien que la nano découpe de précision de tissus biologiques et de matériaux variés sont présentés. Cet outil polyvalent couvre de larges domaines de recherche de la nano découpe d'échantillons biologiques aussi bien que la nanostructuration de différents types de matériaux. C'est d'un grand intérêt pour de nombreuses applications en science des matériaux, nanobiotechnologie et nanomédecine.

# Summary

The current development of technology makes constant the necessity of getting smaller and smaller features sizes down to micrometer and sub micrometer scales. Such small sizes strongly restrict the use of conventional tools. However several concurrent technologies attempt to push limits of small feature sizes. In this race, the laser is a promising candidate.

In this dissertation, the feasibility to take advantage of the interaction of femtosecond laser pulses with matter for micro- and nano-structuration is demonstrated and this by having developed a compact and high accurate and flexible apparatus.

An overview of actual nanostructuring technologies, especially focusing on benefits of femtosecond lasers are discussed in this work. An analyse of the specific physical mechanisms of laser-matter interaction in the femtosecond regime is presented. In the case of high repetition rate laser matter interaction, physical mechanisms seem to be governed by heat accumulation effect phenomenon. A theoretical approach comparing high and low repetition rate interaction regime is given.

A detailed description of the consequent work performed in engineering for the development of the multifunctional tool for nanostructuring and imaging is given in this dissertation. This development implies the implementation and control of a multitude of parameters and devices such as translation stages, piezo driven, shutter, camera,... as well as a good knowledge in optics engineering. Hardware and software have been intensively developed under LabVIEW in an easy to manage and user-friendly environment. The flexibility of the device allows to perform complex 2D as well as 3D patterns.

A new method for processing time calculation on metals in the case of laser machining at kilohertz repetition rate is presented in this work. primary results are demonstrated on the possibility to get an estimation of processing time for femtosecond machining. This method put in evidence the physical time, the time during which ablation processes are active in the machining. The comparison of calculated processing time and measured total process time can give concrete information on process characteristics, which have to be optimized to improve the manufacturing efficiency. Furthermore, results on the influence of laser repetition rate show the way to another field of improvements. Indeed, in our experiments, the ablation rate is not affected by the increase of laser repetition rate up to some tens of KHz. Hence, it means that it is possible to decrease the processing time by increasing the repetition rate. On the other hand, experimental results on the effects of the repetition rate at megahertz repetition rate show different characteristics and put in evidence a controllable phenomenon of "growing" matter. It seems to grow up depending on the strength of the heat accumulation effect. This phenomenon is discussed.

This dissertation focuses finally on the potential of the multifunctional tool for different applications in biotechnology. Results on large area mapping with a very high resolution, in transmission, in reflexion, or using two photons imaging are presented. This allows targeting a precise location on a large area of a sample and makes possible the nanodissection of biological samples, cells, chromosomes… Nanodissection with ultra short laser pulses opens new horizons for scientists, who are primarily interested in investigation of cells, and tissues processes. This versatile tool allows to covers wide research fields from the nanoprocessing of biological samples as well as the nanostructuring of different type of materials as polymers, dielectrics or metals. It is of great interest for many applications in material science, nanobiotechnology and nanomedicine.

# Zusammenfasung

Die gegenwärtige Technologieentwicklung verlangt immer kleinere Bauteile mit Größen im Mikrometer- und Submikrometerbereich. Diese winzigen Abmessungen schränken den Gebrauch konventioneller Werkzeuge stark ein. Gegenwärtig versuchen verschiedene Technologien die machbaren Grenzen für immer kleinere Bauteile nach unten zu verschieben. Hier kommt die Lasertechnologie als aussichtsreiche Technik ins Spiel.

In dieser Dissertation wird Machbarkeit und Vorteil der Interaktion von femtosekunden Laserpulsen mit Materie bei Mikro- und Nanostrukturierungen mit einem eigens entwickelten kompakten, flexiblen und hochpräzisen Gerät untersucht.

Ein Überblick über aktuelle Technologien zur Nanostrukturierung mit besonderem Schwerpunkt auf den Vorteilen von femtosekunden Lasern wird in dieser Arbeit gegeben und diskutiert. Eine Analyse der spezifischen physikalischen Mechanismen der Laser / Materie Interaktion im Femtosekundenbereich wird präsentiert. Interagiert ein Laser mit hoher Repetitionsrate mit Materie, scheinen diese physikalischen Vorgänge durch das Phänomen der Hitze-Akkumulation beeinflusst zu werden. Ein theoretischer Ansatz hierzu wird durch einen Vergleich von hohen und niedrigen Repetitionsraten während der Interaktion, gegeben.

Anschließend wird in dieser Dissertation eine detaillierte Beschreibung der Entwicklungsarbeit für ein Multifunktionsgerät für Nanostrukturierung und Abbildung gegeben. Diese Entwicklung beinhaltete die Implementierung und Kontrolle von sehr verschiedenen Parametern und Bauteilen, wie Verschiebetisch, Piezo-Antrieb, Shutter, Kamera,....in Verbindung mit einer guten Kenntnis in optischer Konstruktion und Entwicklung. Hard- und Software wurden unter LabVIEW so konstruiert, dass eine einfach zu handhabende und benutzerfreundliche Oberfläche entstand. Die Flexibilität des Gerätes erlaubt Entwicklung und Ausführung komplexer 2D und 3D Strukturen.

In dieser Arbeit wird eine neue Methode für die Kalkulation der Bearbeitungszeit von Metallen mit einem Laser mit Kilohertz- Repetitionsrate vorgestellt. Erste Ergebnisse für eine mögliche Bestimmung der Bearbeitungszeitdauer mit einem Femtosekunden-System werden dargestellt. Diese Methode berücksichtigt die physikalische Zeitdauer, die Zeit während der Abtragprozesse tatsächlich aktiv in der Bearbeitung stattfinden. Der Vergleich der kalkulierten Bearbeitungszeitdauer und der gemessenen gesamten Prozessdauer kann konkrete Informationen über Prozesscharakteristika geben, die optimiert die Effizienz der Bearbeitung steigern können. Außerdem zeigen die Resultate aus den Versuchen zum Einfluss der Laser-Repetitionsrate, dass sich hier ein anderes Feld für Verbesserungen ergibt. Tatsächlich ergaben unsere Experimente, dass die Abtragsrate nicht durch einen Anstieg der Laser-Repetitionsrate bis hin zu einigen KHz beeinflusst wird. Dies bedeutet, dass es möglich ist, die eigentliche Bearbeitungszeit zu reduzieren, wenn die Repetitionsrate erhöht wird. Andererseits zeigen die Ergebnisse aus den Untersuchungen zu Effekten der Repetitionsrate, dass im MHz Bereich andere Charakteristika zu Berücksichtigen sind und Anzeichen für ein kontrollierbares Phänomen von "wachsendem" Material zum Tragen kommen. Dieses Phänomen scheint abhängig von der Stärke der akkumulierten Hitze zu sein und wird diskutiert.

Abschließend liegt der Fokus dieser Dissertation auf dem Potential des multifunktionellen Systems für verschiedene Anwendungen in der Biotechnologie. Die Resultate der Implementierung der Darstellung großer Areale mit sehr hoher Auflösung in Transmission, Reflexion oder durch Zwei-Photonen angeregte Fluoreszenz werden präsentiert. Dies erlaubt eine präzise Lokalisation und Ansteuerung interessierender Punkte innerhalb eines größeren Areals und macht eine gezielte Nanodissektion von biologischen Proben, Zellen, Chromosomen, ...usw. möglich. Nanodissektion mit ultrakurzen Laserpulsen eröffnet neue Horizonte für Wissenschaftler, die primär in Untersuchungen von Prozessen in

Zellen und Geweben eingebunden sind. Dieses innovative System deckt eine Reihe von wissenschaftlichen Gebieten von Nanoprozessierung von biologischen Proben bis hin zu Nanostrukturierung verschiedener Materialien wie Polymere, Nicht-Leiter und Metalle, ab. Dies ist für viele Anwendungen in Materialwissenschaften, Nanobiotechnologie und Nanomedizin von großem Interesse.

# Résumé

Le développement actuel de la technologie induit une constante nécessité d'obtenir des tailles de plus en plus petites pouvant descendre jusqu'à des dimensions micrométriques, et sub micrométriques. De telles tailles d'objet restreint énormément l'utilisation des outils conventionnels. Cependant plusieurs technologies concurrentes tentent de repousser les limites des petites dimensions. Dans cette course, le laser se présente comme un candidat prometteur.

Dans cette thèse est démontré la faisabilité de tirer avantage de l'interaction des impulsions laser femtosecondes avec la matière pour la micro et nano structuration, et ceci en ayant développé une machine compacte de grande précision et haute flexibilite.

Une vue d'ensemble des technologies actuelles de nanostructuration, mettant l'accent sur les avantages des lasers femtosecondes est discutée dans ce travail. Une analyse des mécanismes physiques particuliers de l'interaction laser-matière en régime femtoseconde est présentée. Dans le cas de l'interaction laser-matière à haute cadence, les mécanismes physiques semblent être gouvernés par le phénomène d'accumulation de chaleur. Une approche théorique comparant les régimes d'interaction à haute et basse cadence est présentée.

Une description détaillée du travail conséquent effectué en ingénierie pour le développement de l'outil multifonctionnel pour la structuration et l'imagerie est donnée dans cette thèse. Ce développement implique l'implémentation et le control d'une multitude de paramètres et d'appareils tels que des platines de déplacement, des drivers piezoélectriques, un shutter, une caméra, … mais aussi une bonne connaissance en ingénierie optique. Les parties matérielle et logicielle ont été développées sous LabVIEW dans un environnement

convivial et simple d’utilisation. La flexibilité de la machine permet d’effectuer des motifs complexes 2D et 3D.

Dans ce travail une nouvelle méthode est présentée pour le calcul du temps de procédé sur les métaux dans le cas d’usinages laser à des taux de repetition dans la gamme du kilohertz. Les résultats préliminaires démontrent la possibilité d’avoir une estimation du temps de procédé pour l’usinage femtoseconde. Cette méthode met en évidence le temps physique, le temps pendant lequel les processus d’ablation sont actifs. La comparaison du temps de procédé calculé avec le temps de procédé total mesuré peut donner une information concrète sur les caractéristiques du processus à optimiser pour améliorer l’efficacité de la fabrication. De plus, les résultats de l’influence de la cadence laser montre le chemin d’un autre domaine d’améliorations. En effet, dans nos expériences, le taux d’ablation n’est pas affecté par l’augmentation de la cadence jusqu’à plusieurs dizaines de kilohertz. Par conséquent, ceci signifie qu’il est possible de diminuer le temps de procédé en augmentant le taux de répétition. D’un autre côté, les résultats expérimentaux sur les effets de la cadence à une cadence de l’ordre du mégahertz montre différentes caractéristiques et mettent en évidence un phénomène de « croissance » de la matière. Il semble croître de façon dépendante de la force de l’effet cumulatif. Ce phénomène est discuté.

Pour finir, cette these se concentre finalement sur le potentiel de l’outil multifonctionnel pour différentes applications en biotechnologie. Les résultats de cartographie de grande surface avec une très haute résolution, en transmission, en réflexion, ou en utilisant l’imagerie à deux photons sont présentés. Ceci permet le ciblage précis sur une grande zone de l’échantillon et rend possible la nanodissection d’échantillons biologiques, cellules, chromosomes … La nanodissection avec des impulsions laser ultracourtes ouvre de nouveaux horizons aux scientifiques, qui sont premièrement intéressés dans l’investigation des processus de cellules et tissus organiques. Cet outil polyvalent permet de couvrir de larges domaines de recherche du traitement d’échantillons biologiques aussi bien que de nanostructuration de différents types de matériaux comme les polymères, les diélectriques ou les métaux. C’est d’un grand intérêt pour de nombreuses applications en science des matériaux, nanobiologie et nanomédecine.

# Contents

# Introduction

The current development of technology leads to more and more important necessity of miniaturization. Scientists and industrial try hard to develop these micro and nano technologies, in different fields such as physics, chemistry and biology. The market of these technologies is estimated at several billion in 2020. Many industries are concerned by these future advances that have applications in many fields such as medical, military, cosmetics, marketing, traceability, etc. Applications in nanomanufacturing fields such as material nanostructuring, nanoelectronics, nanobiotechnology are widely recognized to be critical. The integration of nanoscale elements into nano/micro scale products needs to achieve a great development in the various branches of science and engineering such as surface chemistry, electrostatics, fluid flow, adhesion, etc.

The production of these nano-technologies requires the development of 2D and 3D dedicated tools. Ultrafast lasers thanks to its intrinsic properties enable to reach a very high precision and a very good quality. Femtosecond lasers meet the quality requirements necessary to reach features sizes down to nanometre scale. Indeed, the interaction of pulses of the order of femtosecond with the matter has got properties making a femtosecond laser a very precise tool for mechanics. For constant energy inside a pulse, the decrease to such pulse duration results in a high increasing of the peak power of the pulse. The focal volume is high confined and the matter is ablated with a very high precision. This property enables many developments in surface micro- nano-structuration.

These arguments are the reason of the work done during this thesis. This work is organised into several chapters:

- The chapter I presents an overview of nanostructuring technologies, especially focused on benefits of femtosecond lasers and their place in the market. A discussion of physical mechanisms of the interaction of such short laser pulses with the matter is done.
- The chapter II gives a detailed description of the multifunctional tool developed in order to use multiple promising possibilities given by the femtosecond pulses. This implies the control of many parameters for 2D and 3D micro and nano processing, as well as high resolution imaging.
- In the chapter III, the effects of the repetition rate on the ablation of materials and in particularly on metals is studied. Phenomenon known as heat accumulation at repetition rates in the MHz range are expected. Results of the litterarure have been discussed...Experimental results on the effects of the repetition rate on copper are presented. Results put in evidence a controllable phenomenon of “growing” matter. A short discussion is done about this phenomenon.
- In the chapter IV the potential of the multifunctional tool for different applications in biotechnology is shown. Results on large area multiphoton imaging as well as nanoprocessing of biological tissue and various materials are presented.

# Chapter I

# Overview of nanostructuring techniques

# 1. Introduction

In the following we will shortly present several types of current nanostructuring technologies. At first, we will present different types of lithography and their principles, which are the most widely used technology both in industry and in research. Moreover, nanostructuring can be performed also with lasers which are another growing technology with a huge potential. In this work we are mainly interested in femtosecond lasers, their benefits and their place in the market. A brief discussion of specific physical mechanisms of laser-matter interaction in the femtosecond regime is presented which explains why it is specific and huge of interest, and then we will focus on different techniques for nanostructuring achievable with femtosecond laser. Finally self-nanostructuring of the matter under single laser irradiation is also presented, even if this is not the topic of the present work. The mechanisms of such structures formation are not yet well understood and many fundamental studies are still under progress.

## 2. Nanostructuring with lithography

For several years, the semiconductor industry has been able to maintain a continuous integration and miniaturization of transistors. The most widely used processes for semiconductor fabrication in industry is lithography with electron beam for the formation of designed patterns on a set of masks, then an optical projection lithography for the reproduction of the mask patterns at a high throughput level. It is possible to design micro and nanostructures as we want for specific applications. The next step after lithography is the pattern transfer from the resist to the substrate.

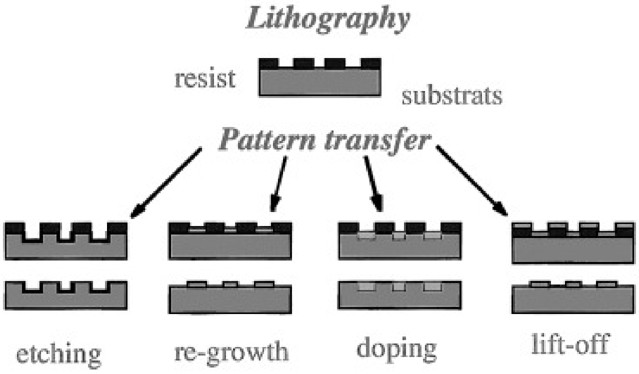

**Figure 1** ***Schematic representation of pattern transfer techniques [1].***

A typical lithography consists on three steps:

- Coating a substrate with a layer of a resist (irradiation sensitive polymer)
- Exposition of the resist under light, electron or ion beams
- Developing the resist image with a suitable chemical

Patterns are imparted by steering an energetic beam of electrons over a material which undergoes a physical or chemical change under the influence of the energy deposited from the electron beam. The energy deposition creates a latent image in the material, also called a resist. A chemical development washes away the exposed (positive resist) or unexposed (negative resist) leaving the pattern wanted. Other energetic beams such as ions or photons can be used in this way. The principle is the same but each type of beam has its own particular set of advantages and disadvantages. For example, energetic ions deposit energy much more locally than electrons but the shorter range of ions requires thin resists. A further disadvantage is that the most mature ion source is gallium, a liquid metal ion, which is left behind, i.e., implanted, in the sample. But, and perhaps most telling, the available tooling for electron beam lithography is much more sophisticated, which is perhaps the single-most reason it is much more widely used.

In order to produce a tightly focused spot of electrons on the sample, highly energetic (>25 keV) beams are needed in conventional electron optical columns. However it is possible to use very low energy beams (<100 eV) where the energy deposition can be constrained much more locally.

## 2.1. Energetic beams

In the case of energetic beams, electron passes through the resist material, it undergoes a series of elastic and inelastic scattering events which determine the volume over which the energy is deposited and the resist exposed. As a narrow beam of energetic electrons passes through a thin suspended layer of resist, secondary electrons are generated which deposit their energy radially. The equi-energy contours in resist tend to have a higher radial gradient as the incident beam energy increases. Since the energy contour is strongly correlated with the developed width, finer features are possible. As a result, the trend in today's state-of-the-art e-beam nanolithography systems typically is toward high beam energy and bright, i.e., field emission, electron sources to give a few nanometer focused beam diameter. With such equipment, feature sizes in relatively complex structures approaching 10 nm are relatively routine. Advances in resist materials and better understanding of their processing are gradually pushing the resolution limit down. For example, Ochiai *et al.* described sub-10 nm e-beam nanolithography in a modified calixarene [2].

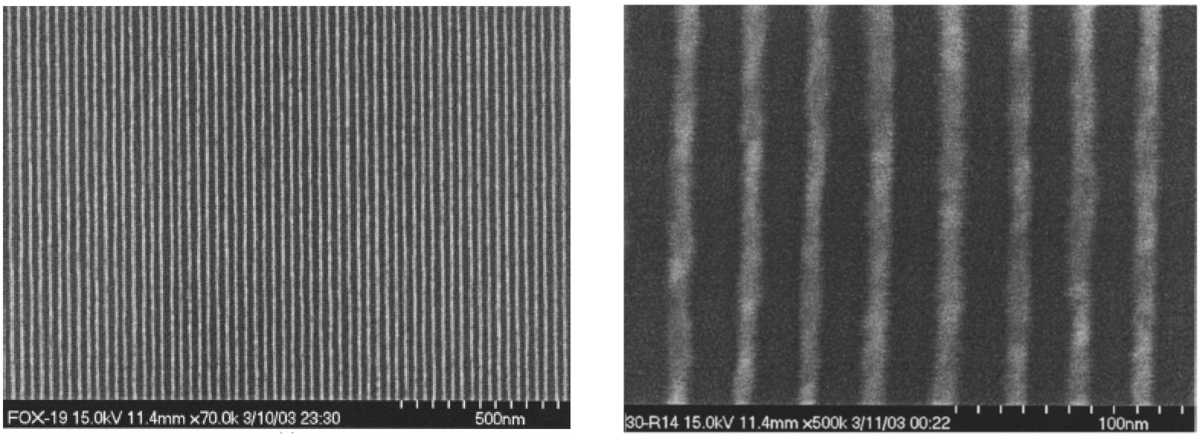

(a) (b)

**Figure 2** ***Overview of 30 nm grating exposed in HSQ resist on silicon (a) and zoom on lines of 10 nm width (b) [3].***

## 2.2. Low energetic beams

The detrimental effect of electron scattering has led many researchers to consider using very low energy primary electrons as a way of mitigating the resolution degradation caused by inelastic electron scattering. Various techniques have been and, no doubt, will continue to be explored in this context. Most of the early work on the advantages of the low energy e-beam approach used the scanning tunnelling microscope (STM) and/or atomic force microscope (AFM) as electron sources to perform resist exposure [4]. These experiments demonstrated the advantages of such an approach. In addition, a number of other nanofabrication techniques based on proximal probes have been identified. These include selective oxidation [6], [7], field ionization [8], field induced evaporation [9], indentation [10], and chemical etching [11].

Industrial applications need fast, reliable and cost-effective techniques. Optical projection lithography with deep UV light is now used. As next generation lithography, several non-optical techniques have been developed including extreme UV, X-ray lithography and projection lithography with either ions or electrons.

## 2.3. Extreme UV lithography

Extreme UV lithography refers to the exposure technique developed with 13,4 nm radiation and a reflective reduction system [12]. For this selective wavelength, the radiation is obtained from laser-induced plasmas or synchrotron radiation. The radiation is first projected on the reflective mask with a couple of mirrors acting as the condenser. Then, it is focused with another mirror system onto the wafer. The advantage of extreme UV lithography relies on its projection configuration and its high potentiality for several generation manufacturing. Fabrication of 100 nm line-and-space and 70 nm isolated lines have already been demonstrated [13].

## 2.4. X-ray lithography

For smaller wavelengths ranging from 0.5 to 4 nm (soft X-rays), no materials can be used for the construction of a projection system but a shadow technique is relevant. A typical X-ray mask consists of 2 μm thick membrane of silicon carbide and absorber features of heavy metals such as Au, W, or Ta. The resolution of X-ray lithography is defined by the Fresnel diffraction and the diffusion of photoelectrons in the resist. From 50 nm to 30 nm lines were reproduced. The X-ray lithography is nearly ready for industrial use [14][15][16] but some technical issues remain open such as the mechanical and radiation stability of the masks, the avaibility of high throughput e-beam systems for mask making, and the reliability of high accuracy alignment.

## 2.5. Imprint lithography

The need for a simple parallel ‘‘printing’’ method capable of filling the 10–100 nm gap has caused a rapid proliferation in the variety of imprint lithographic techniques. These methods hold great promise as flexible, high resolution, replication methods. Most prominent among these methods are stamping methods or ‘‘soft lithography’’ such as microcontact printing [17] and nanotransfer printing (µCP) [18] which use elastomer molds to ‘‘ink’’ or directly transfer a pattern, nanoimprint lithography34 which uses compression molding of thermoplastic polymers, and step and flash lithography (SFIL) [19], [20] which uses photopolymerization molding.

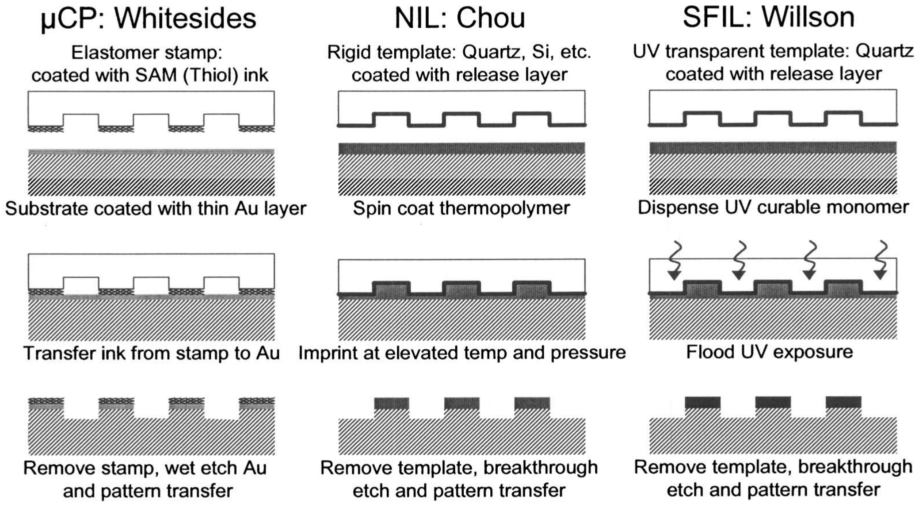

**Figure 3** ***Simplified comparison of imprint lithography techniques [21].***

Nanoimprint lithography (NIL) is a nonconventional and low-cost technique for high resolution pattern replication [22] [23]. Nanoimprint is an update of the hot embossing process used to make copies of relief structures such as compact disks. Rather than forcing an impression in a bulk plastic substrate, the imprint is made in a thin film of thermoplastic polymer using a combination of heat and pressure. The process is often described as “copy exact”.

Nanoimprint consists in a rigid mold used to physically deform a heated polymer layer coated on a substrate. The mold can be made of metal or thermal silicon dioxide produced on a silicon substrate. The imprint can be done by applying a typical pressure of 50 bars in the temperature range of 100°C-200°C depending on the polymer in use. After imprinting, the resist pattern is followed by reactive ion etching in order to produce a useful profile for the subsequent hard material pattern transfer. The mold can be re-used many times without damage. Structures as small as 6 nm can be produced[23].

## 2.6. Laser stereolithography

Laser stereolithography allows real three-dimensional microfabrication [25][26]. An object designed in 3D with CAD software is sliced into a series of 2D layers. The distance between each layer stay constant and each layer has the same thickness. A code is created for each slide and saved into a file which is then sent and executed by a motorized x-y-z platform immersed in a photopolymer liquid. This liquid is then exposed to a laser beam which is focused inside the liquid. The polymer forms a solid where the intensity of the light is high enough, that is to say in the focal point region. Once the first layer has solidified, the sample moves downward and a new layer is exposed. This process is repeated layer by layer (Fig. 4.a).

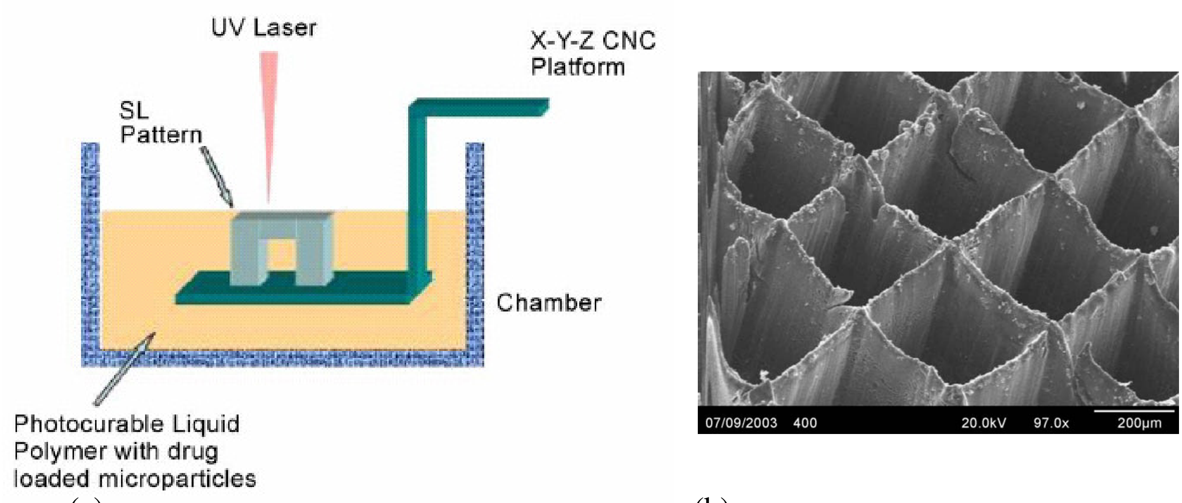

(a) (b)

**Figure 4** ***Scheme of a laser stereolithography setup (a). Cellular-type structure made with stereolithography (b) [25][26].***

This process enables complex internal structures such as curved surfaces, or passageways with high accuracy. This tool is very useful for fabrication of cellular structure (Fig. 4.b) composed of vertical walls with a 400 µm interline spacing and a thichness < 800 nm. It is also possible to control the spatial distribution of fluorescein and rhodamine microparticles inside a polymer layer. This kind of structures is very used in biological researches on cell adhesion or cell growth in specific conditions.

Lithography enables to reach up to sizes of fabrication down to tens of nanometers. This technology of micro/nano fabrication can be applied on big surfaces and consequently allows a high throughput level of production. However, this technology is not very flexible. In another hand, we can see that in the case of stereolithography, such small sizes are reached thanks to laser. Indeed, in this example size of the feature depends on optical parameters such as wavelength, focusing strength and on the interaction of the laser beam with the polymer. This put the laser to the front of the nanofabrication stage. Laser process is not known to fabricate nanostructures with a high throughput level but brings more flexibility. Pulsed lasers are used for machining. High repetition rate lasers enable to increase machining speed while preserving same sizes of machining.

# 3. Laser approach

Advantages of laser processing is to be a noncontact and flexible setup that can operate in air, vacuum or liquid environment, making it very attractive as manufacturing tool in many applications. Lasers can be easily focused down to the micrometer scale. These advantages are exploited extensively in modern microelectronics industries applications such as marking, drilling, annealing and surface modification. As a concrete example, wafer singulation is one of the key processes in microelectronics production lines using laser microfabrication to separate thousands of integrated circuits on wafers. The dicing technique using a fast diamond saw rotating over the wafer surface usually causes chipping and cracking of the thin wafers. There are also technical difficulties in separating different and multilayered substrates such as glass, sapphire, diamond, and glass/Si/glass multilayered device structures [26].

Pulsed lasers are a good solution to these problems. Short laser pulses ablation is a fast and explosive process useful for removal of substrate materials thanks to the possibility to focus a laser beam down to few micrometers. The heat-affected zone (HAZ), which depends on the pulse duration and the light absorption depth, can be limited to a small volume. Currently, the shortest pulse duration available are produced by femtosecond laser. These lasers can delivers laser pulses with duration down to few tens of femtoseconds. This kind of laser is a good solution for micro and nanomachining because of the specificity of the interaction. Indeed, such short pulses interacting with a material induce a very small heat-affected zone which allows to machine down to sub-micrometer sizes. The whole femtosecond technology is based on this originality of the interaction.

## 3.1. Physical aspect of interaction for ultrafast pulses

This section discusses about femtosecond pulse accuracy and of the phenomena of the interaction of femtosecond laser pulses with a metal. A presentation of the phenomena is described as a function of the time, for each instant from the absorption of the pulse until the removal of material. A solid can be described as a network of ions surrounded by an electron cloud in which each electron is more or less connected, depending more or less on the conductive nature of the material. We focus primarily on the case of metals which have a high conductivity due to their quasi-free electrons. These quasi-free electrons absorb linearly energy of the incident photons in a quasi-instantaneous time (<1 fs). This radiation is absorbed on a thin surface layer whose thickness is of the order of the inverse of the linear absorption coefficient. The electrons acquire energy and their temperature rises very quickly. The interest of pulses in the order of hundred femtoseconds is that their duration is shorter than the energy transfer duration from electronic network to the network of ions, typically from 1 to 10 ps, which means that the evolution of ionic and electronic dynamics are decoupled. It has to be noticed that for pulses of duration in the order of picosecond or nanosecond, this decoupling is neglected because the energy transfer occurs in a few picoseconds. The solid is formed of a gas of hot electrons surrounding an ion in which the temperature is still at its initial value. This fast increase in temperature is equivalent to a thermal shock.

## 3.2. Thermalization

The solid returns in a steady state after the transfer of energy between electrons network to ion network. This energy transfer is via the electron-phonon coupling, phonons point out own vibration modes of the ionic network. The electron-phonon coupling is a characteristic of the material. During this phase of energy transfer, the system is out of balance, electron temperature is higher than the temperature of the ion, that’s why thermalization is most often described by a two temperatures model:

$$\begin{aligned} C_e \frac{\partial T_e}{\partial t} &= \frac{\partial}{\partial z}\left( K_e \frac{\partial T_e}{\partial z} \right) - g \times (T_e - T_i) + S(z,t) \\ C_i \frac{\partial T_i}{\partial t} &= g \times (T_e - T_i) \end{aligned} \tag{1.1}$$

$C_e$ and $C_i$ are the volumetric heat capacity electronic and ionic. The constant g is the coefficient of electron-phonon coupling which describes the energy transfer to the ion network. $K_e$ is the thermal conductivity of the material and S (z, t) is the source term, it represents the energy deposited by the laser for a period of time $\Delta t$ in the hot electrons gas. This system of coupled differential equations describes the evolution of electronic and ionic temperatures as a function of time. This energy transfer has a relatively long period compared to the process of optical absorption of photons by electrons. This is largely due to the large difference in mass between electrons and ions. These are the electron-phonon interactions which are responsible for this transfer of heat. These phonons created during the transfer are such as sound and play an important role in laser-matter interactions.

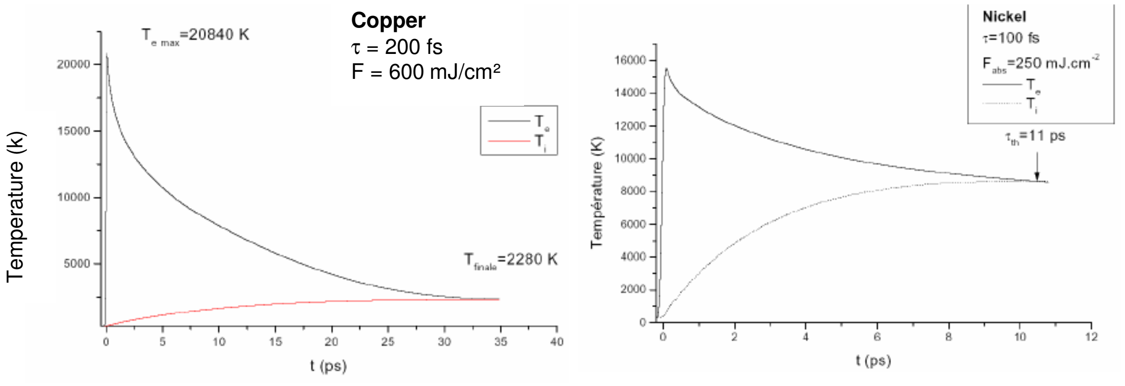

a.

b.

**Figure 5** ***Results obtained with the two temperature model for a fluence of 600 mJ/cm² and a pulse duration of 200 fs on copper (a), and for a fluence of 250 mJ/cm² for a pulse duration of 100fs on Nickel [28].***

Fig. 5 [28] illustrates two examples of the two temperatures model applied on two different materials. The first (a) on copper, the absorbed fluence is 600 mJ/cm ² for a pulse of 200 fs, and the second (b) on Nickel, the absorbed fluence is 250 mJ/cm ² for a pulse duration of 100 fs. These graphs show the evolution of the temperature of electrons and ions as a function of time. At time $t = 0 + \varepsilon$ it can be clearly seen that the electron temperature rises sharply and in a very short time while the temperature of ions increases much more slowly After a period of a few picoseconds, the energy is transferred from electrons to the ionic network via the electron-phonon coupling. This transfer has the effect of lowering the electron temperature and increase the temperature of ions. These two temperatures tend to a point of thermodynamic equilibrium, which is about 35 ps in the case of copper and 11 ps in the case of Nickel.

## 3.3. Femtosecond pulses and longer pulses (ps or ns)

In the case of a longer pulse, we are talking here of a pulse whose duration is higher than the thermalization time of the solid, there is also a change in the material. But this change is governed by a classical heat deposition to electrons, the impulse is longer so the energy deposition is accompanied at the same time by a heat transfer between electrons and ions. Throughout the duration of the pulse, the electrons and the crystal remain in thermodynamical equilibrium. This type of long interaction is purely thermal. This process explains the difference in quality machining achieved with femtosecond pulses and nanosecond pulses. The following figure illustrates the difference between two impacts made on a sheet of copper 100 µm thick at a fluence of 8 J/cm ², with a pulse of 180 fs (a) and a pulse of 8 ns (b) [105] and the evolution of the influence of pulse duration on the threshold of damage (c). According to this curve, for pulses longer than ~10 ps, we see clearly the increase of the influence of pulse duration that would follow a law in $\tau^{1/2}$ as verified by many experiments [29] , where $\tau$ is the pulse duration.

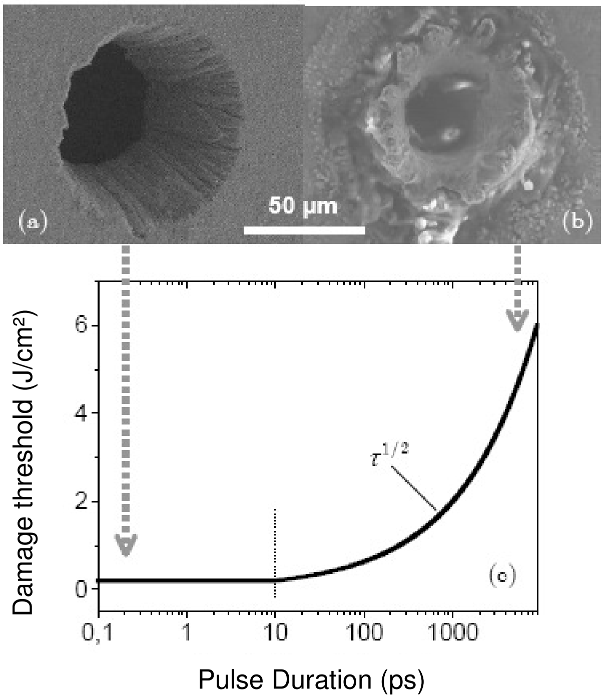

**Figure 6** ***Comparison of impacts on 100µm thick copper samples between ultrafast pulses (a) of 180 fs, and longer pulses (b) of 8ns. Both have been done with a fluence of 8J/cm$^2$. The influence of pulse duration seems to follow a law in $\tau^{1/2}$ after ~10 ps (c) [32][33][34].***

On Fig. 6, the influence of pulse duration is of importance only above10 ps. As already explained, this time corresponds to the duration of thermalization of the material, that is to say the ability of the material to distribute the heat gained by the laser pulse. Obviously this time is variable depending on the materials. Focused pulses from a high-power laser can damage virtually any material if the electric field is high enough to produce optical breakdown, which is typical of femtosecond lasers.

This deterministic behaviour of femtosecond pulses in interaction with the matter enables very clean micro machining. Such characteristics give to femtosecond micro machining a very good repeatability as well as for the control of the size than for the quantity of removed matter for one pulse. This makes possible the calculation of the processing time which can be of huge interest for industrial and economical reasons. An efficient ablation rate can be determined for each material, in a corresponding fluence range [97][98][99][100][97]. This deterministic behaviour offers the possibility to decrease machining sizes down to sub micrometric scales. Such small sizes are reachable by pulses with very small energy in order to be close to the threshold of the matter. This range of energy is very easy to reach with high repetition rate lasers with a good control of the amount of the energy per pulse down to nano joule.

## 3.4. UV laser micromachining

Most of materials absorb light more strongly as the optical wavelength decreases. Many polymers, crystals and metals that either highly transmit or reflect light for wavelengths in infrared and visible range, absorb strongly in the UV range. This means that the penetration depth is small. This allows a very fine control of the drilling depth. Another benefit of ultraviolet lasers is that they can be focused into a spot of the order of its wavelength. Indeed, this is due to the linear dependence of the minimum feature size and the wavelength [35].

UV wavelengths correspond to high energy photons (3-7 eV) [36] can be used to break the chemical bonds especially for plastics. Indeed polymers absorb ultraviolet light of sufficiently short wavelength. The material escapes as small particles and gaz. This is considered as “cold cutting”, and so very few damage are observed to surrounding material. However, for metals even more energy is required. Moreover, electrons absorb first the laser pulse energy and transform it into heat which leads to the melting and the evaporation of the metal.

That’s why femtosecond lasers are another good option. Pulse durations are so short that many photons are delivered on a time that electrons are hit by several photons simultaneously. This kind of absorption has the same effect than absorption of one photon of higher energy. This brings the benefit to lower the importance of the wavelength, because the energy is transferred by several photons simultaneously. This gives an advantage for ultrafast lasers. Indeed, these lasers do not need specific optics to operate with.

## 3.5. Principle of nanomachining

The deterministic character of damages induced by ultrafast laser pulses makes numerous applications possible for nanomachining. One of the goals of nanotechnology is to produce well-defined features much smaller than the wavelength of visible light. As already said above, the pulse duration decreases from picosecond regime to femtosecond regime, the damage threshold moves from stochastic to deterministic. This implies a strongly nonlinear dependence of the optical breakdown on intensity. This feature allows decreasing limits of the size to regions smaller than the spot size of the focused laser.

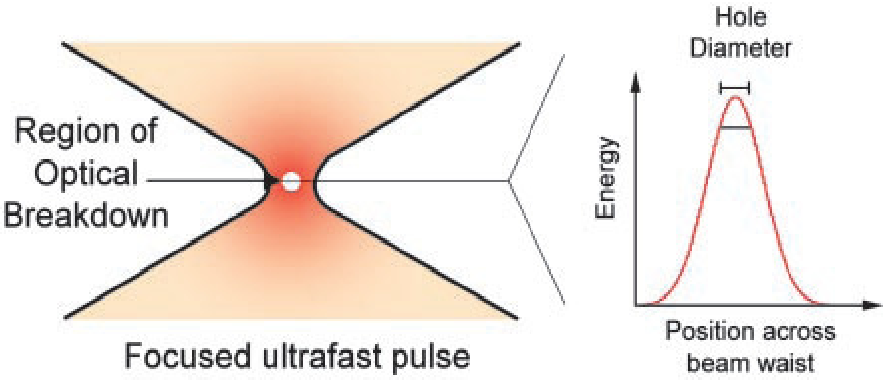

**Figure 7** ***Schematic representation of how an ultrashort laser pulse can damage a material on an area smaller than the diffraction limit. The size of the modified area decreases with energy per pulse [38][39].***

As illustrated on Fig. 7, only a small section of the Gaussian focused spot can be selected by controlling the power of the laser beam. This “thresholding” effect has been applied to fabricate micrometer and sub-micrometer patterns as small as 300nm [40][41][42][43] and single holes as small as 40 nm (Fig. 8) [38][39]. Thanks to this deterministic feature, femtosecond pulses find many applications. In the following some techniques which take advantage of ultrafast pulses for nanomachining are presented.

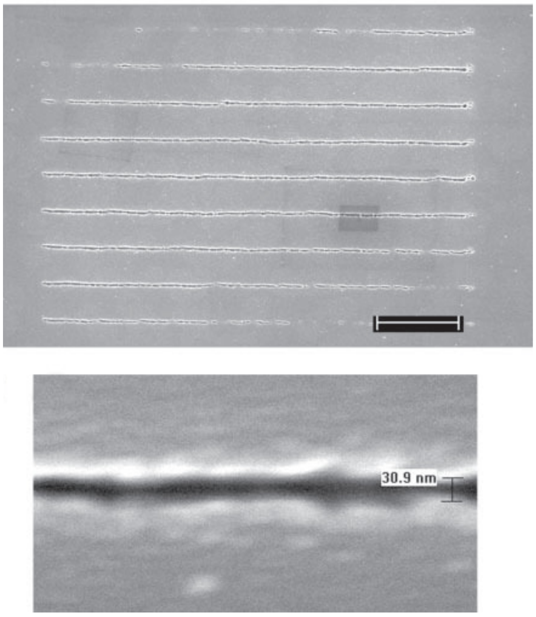

**Figure 8** ***SEM images of 30-nm-wide channels machined in glass[38].***

## 3.6. Ultrafast nanomachining techniques

### 3.6.1. Direct grating writing

This technique is based on direct ablation with a special optical setup (Fig.9) in which the principle of interfering femtosecond pulses is used. This technique enables to adjust the line-width of gratings in a simple way. This method offers a new approach for the fabrication of gratings on a surface.

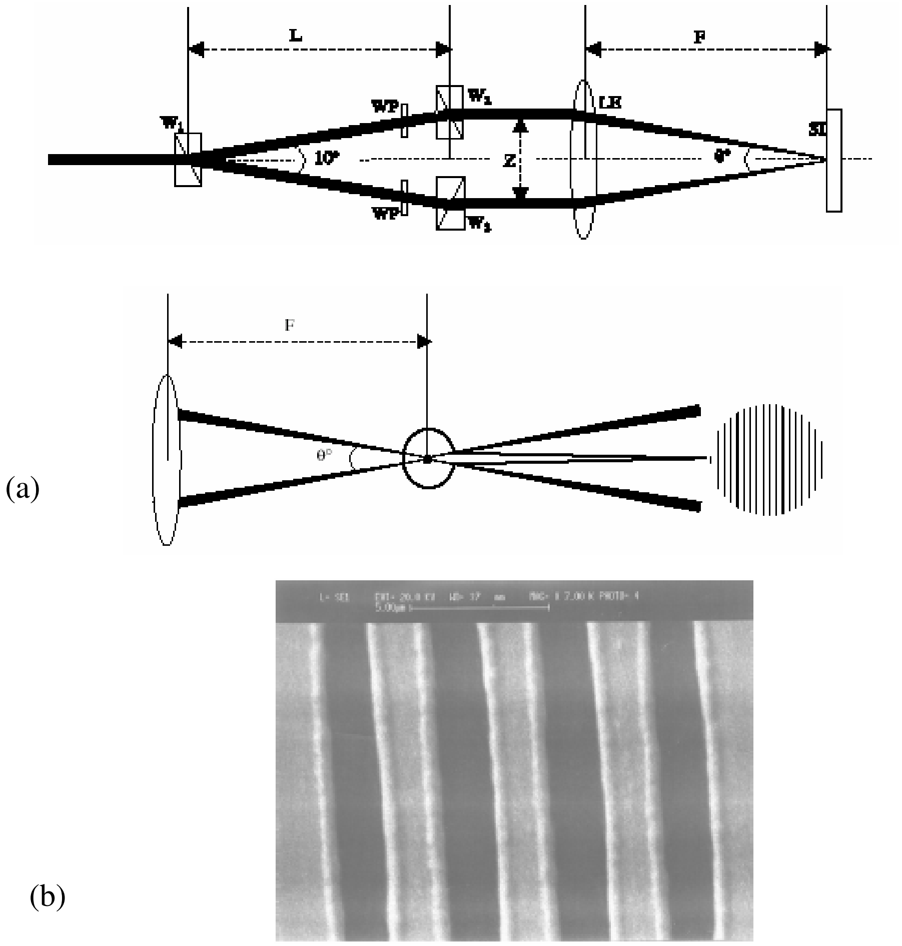

**Figure 9** ***(a) Scheme of the setup for grating fabrication. One beam is split in two beams and focused thanks to a big lense. (b) Grating formed with a line-width of 4μm [44].***

Interfering two femtosecond laser beams have been reported [45][46]. The angle between two beams can vary. The synchronization between the two lines can be adjusted by using an optical delay line. To overcome important drawbacks, like the need of a very precise adjustment of two focusing lenses or the realignment of the whole system for each change of the distance between the two incoming beam, an alternative is to use a common lens. The main advantage of this setup is to directly focus the two beams exactly to the same point on the sample.

## 3.6.2. Illumination of an atomic microscope tip

This method consists on illuminate an atomic force microscope tip by a femtosecond laser beam [47][48]. Two different mechanisms are advanced to explain this phenomenon: one is an enhancement of the laser electric field in the neighbourhood of the tip. This effect combined with characteristics of femtosecond laser on the matter led to the removal of the material [49][50]. The other mechanism advanced is the warming of the tip due to absorption of laser radiation and creates a mechanical stress which led to a thermal elongation [51][52].

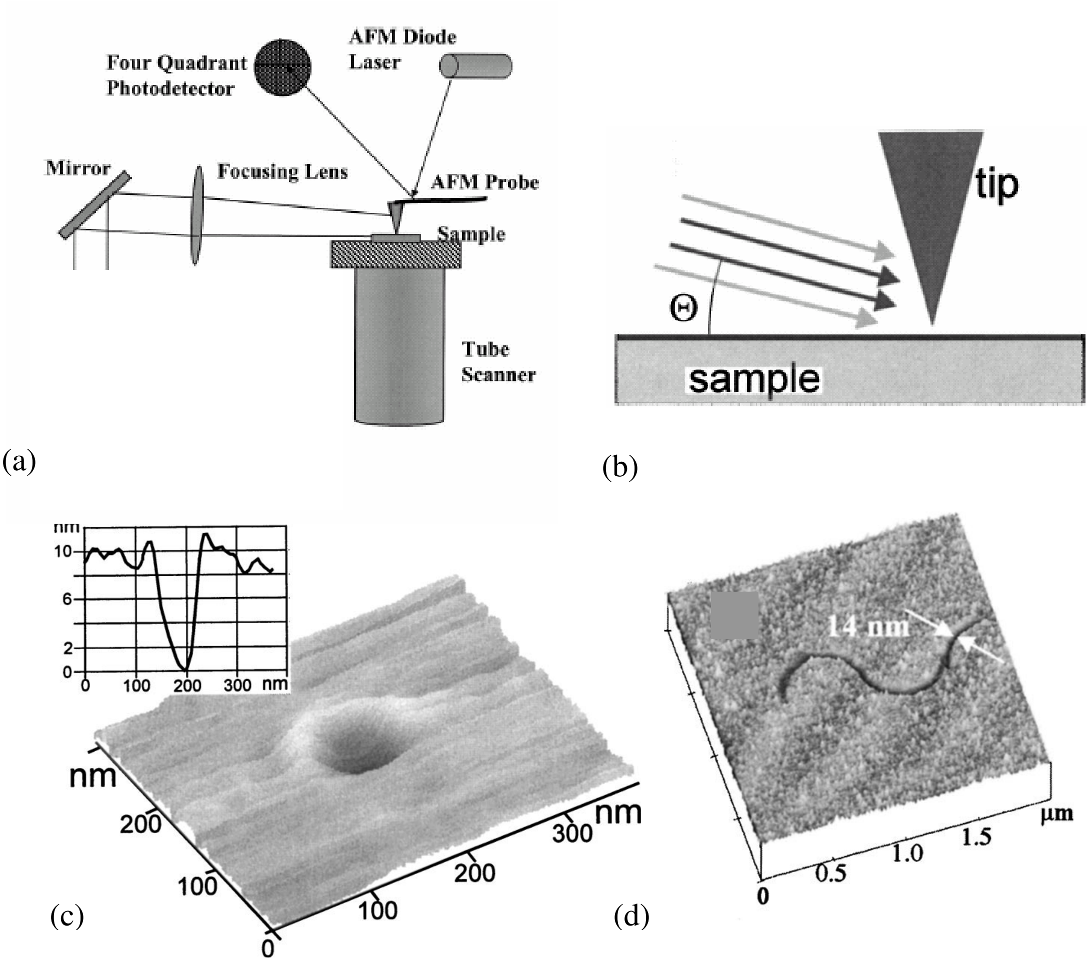

(a) (b)

(c) (d)

**Figure 10** ***Scheme of the experimental setup with a very low aperture lens (a) or without aperture (b). AFM image of crater made on FeCr film (c). Curve obtained on gold film surface (d)[47][48].***

This technique enables to produce complex shapes like curves (Fig. 10.d), grid patterns, with a constant width less than 20 nm. This process combines advantages of femtosecond laser pulses with accuracy of atomic force microscope. Spacing can be done with a very high accuracy. This technique can be improved to multi-array structure with several tips. Thanks to the very high confinement of the tip on the surface, scattering should not be significant. A spatial resolution less than 10 nm has been demonstrated on a thin gold film.

### 3.6.3. Interference of ultrafast laser pulses

As already seen above, the ultrafast laser has a Gaussian beam profile and by controlling the intensity it is possible to decrease the size of machining. However it is possible to go further in decreasing of machining size methods. Another technique taking advantage of femtosecond laser pulses consists on interfering the laser light circularly and then using the central bright fringe to machine [53].

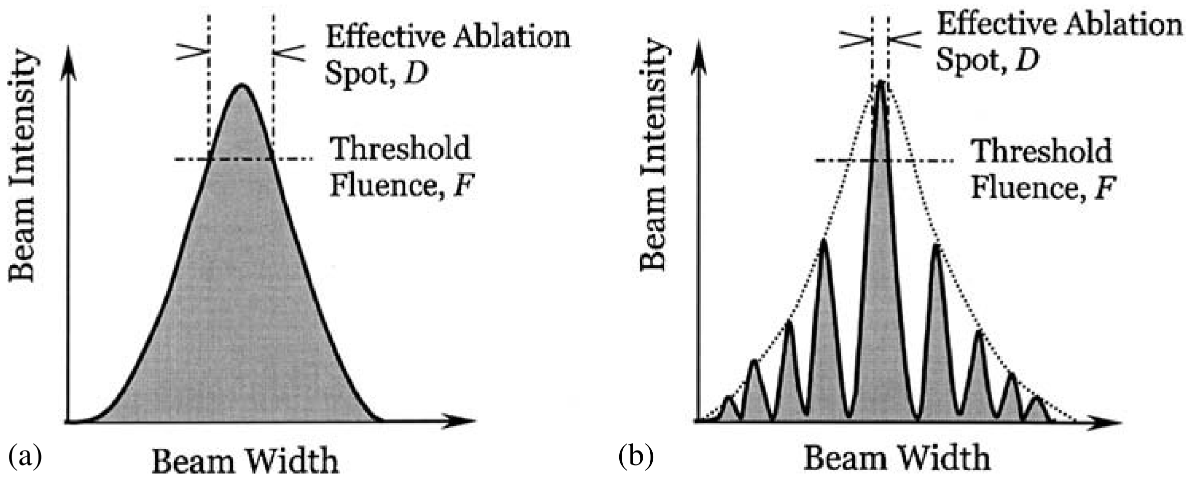

**Figure 11** ***Profiles of a normal gaussian beam (a) and profile of a Gaussian-like interfered laser beam (b)[53].***

The effective ablation spot can be significantly reduced in comparison with a classical Gaussian profile. This kind of profile is obtained by using a Newton's ring interferometer setup.

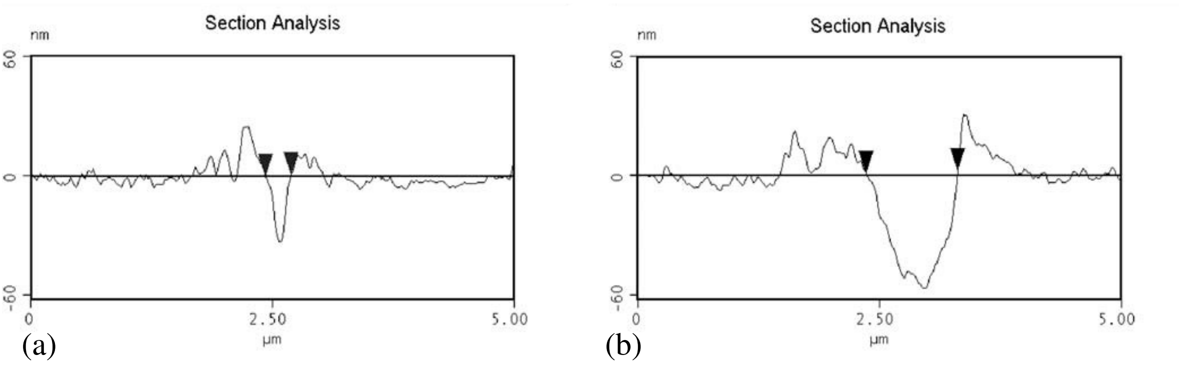

**Figure 12** ***Profile comparison of sub-micrometer holes obtained using a Gaussian-like interfered beam (a) and a classical Gaussian beam (b)[53].***

Samples have been machined with and without interferometer at the same energy per pulse. Profiles of each structure drilled show clearly a much smaller hole for the structure done with the interferometer setup (Fig. 12). With the interferometer setup, the diameter of the hole drilled is around 270 nm while it is around 930 nm without the interferometer setup.

### 3.6.4. Self-organized structures (LIPSS)

Periodic nanostructuring of materials is a much studied topic due to their increasing applications in many sciences fields [54][55][56][57]. Indeed, well defined surface structures may have new properties. Understanding and controlling the fabrication of such structures may be of great interest for industrial applications. It has been proved that microstructures and nanostructures influence biological processes at implant interfaces [58][59]. A lot of attention is focused also on semiconductor nanostructures because of the interests in fundamental physics as well as the great potential for industrial applications. For example, nanostructuring of ZnO which is a promising material for a broad range of high technology applications such as field emission, UV light-emitting diodes, piezo-electric devices, nanoresonators and biosensors[60][61][62]. The development of simple and reliable methods to control the morphology of self assembled nanostructures is a huge challenge. As we saw in a previous paragraph, methods to form nanostructures mainly use electron beam lithography, nanoimprint lithography, or chemical methods [63][64] but the possibility to do nanostructures with lasers is now well known. In the past, surface structures were produced using long-pulse lasers, including nanosecond Nd:YAG laser, copper vapour laser, nanosecond excimer lasers.

The formation of ripples has been observed long time ago by many researchers who study the interaction between intense lasers and material with a power laser beam near or equal to the threshold of damage. The formation of a pattern of damage similar to a grating, resulting from the illumination of a single laser beam of high intensity, has often been observed on the surfaces of metals, dielectrics and semiconductors. These observations were made with both continuous lasers and with pulsed lasers. We saw that most patterns are similar and independent of material properties. When the beam arrives at a normal incidence to the surface of the material, the damage appears as parallel and periodical lines. The period is in the range of the wavelength of the beam.

Several explanations for such periodic damage have been advanced based on the properties of the laser beam [65][66], or surface acoustic waves [67], or condensation of plasmon [68][69][70][71]. We also noticed that the orientation of the ripples depends strongly on the polarization of the incident laser beam. These observations have made a model evolved explaining the formation of ripples as a result of inhomogeneity in the energy arriving, which could be due to interference between the incident laser beam and a surface wave scattered maybe from a scratch on the surface of the material [72][73]. Indeed fringes created nearly a scratch have been observed, suggesting that roughness plays a role in the creation of periodic structures. Interference creates the energy arriving directly translated into a variation of ablation depth and the structure of ripples is an image of the interference pattern. The frequency modulation pattern of ripples is controlled by the wavelength of the incident beam, the angle of incidence and taking into account the refractive index of the material, it is given by the formula:

$$\Lambda = \frac{\lambda}{n(1 \pm \sin\theta)} \qquad ((1.2)$$

This model was applied for years to explain the observations of different kinds of periodic structures. However this model does not take into account certain structures generated more or less in contradiction with this model, such as bifurcations in the lines of ripples, sinuous structures or the formation of cones.

Recently much attention is paid to formation of LIPSS with ultrafast lasers. In general, the pulse lengths are shorter than the assumed time of ablation. However structures are always observed [74][75] As in previous observations, two different systems of ripples appear perpendicular to each other which one of them has a characteristic size smaller than the wavelength.

As already demonstrated, ripples with large ridges and grooves very narrow were obtained and the structures of cones auto-arranged in two dimensions [77][78][79]. Most experiments were made with linear polarization. The orientation of structures is strongly dependent on polarization, fine ripples are always formed perpendicular to the electric field of the beam [76] (Fig.13)

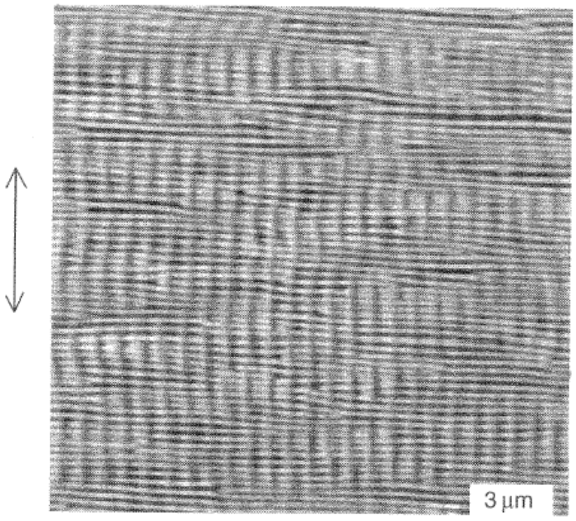

**Figure 13** ***Two systems of ripples perpendicular to each other. The laser polarization is given by the double arrow. This result has been obtained with a Ti:Sapphire laser with a wavelength of 800 nm on BaF2 [76].***

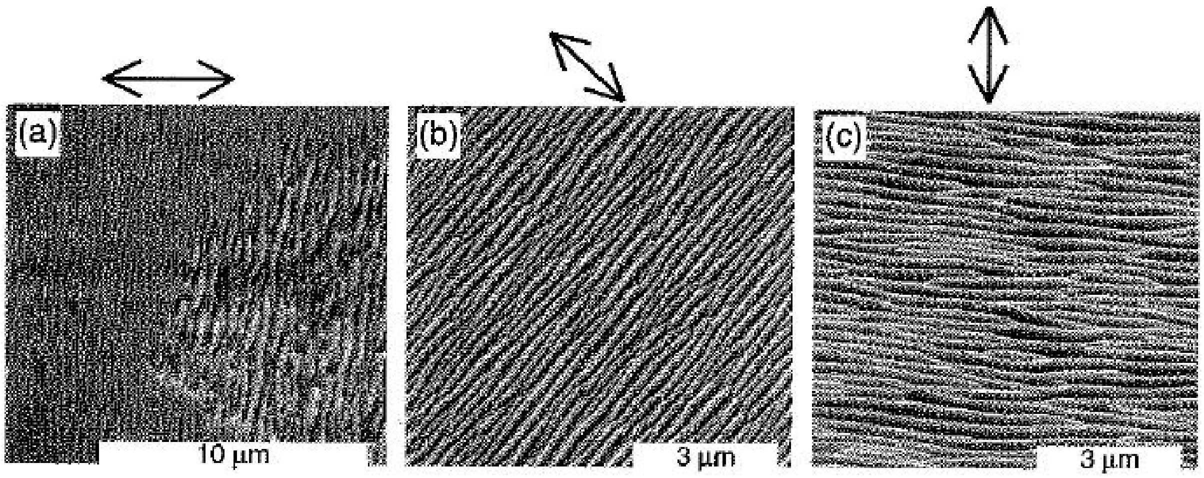

.

**Figure 14** ***Arrows indicate the polarization's orientation of the beam respectively of 0° (a), 40° (b) and 90° (c). The dependence of the orientation of ripples on the polarization is obvious. Notice that in the picture (a) there are both coarse and fine ripples oriented in the same direction. Fine ripples are on the edge of the crater, coarse ripples are in the center [76].***

Fig. 14 shows fine ripples on the crater edge, and coarse ripples in the center of the crater where the beam intensity is the highest. The period of ripples depends on the intensity, but in a non-continuous way. In the centre of the crater, period of ripples is approximately 10 times higher than the ripples from the edge. In many experiments no influence of the wavelength or angle of incidence was observed over the period of ripples. However periodic structures have also been obtained under the effect of ion bombardment [80]. These structures have approximately the same size as the ripples obtained under laser irradiation [81][82][83]. This result brought the idea of self-organization of matter from instabilities [75].

To summarize, in the current state of our knowledge, several physical phenomena are responsible for the formation of ripples. Firstly, when a laser pulse hit the surface of a material, the electric field E interacts with the surface electrons vibrate at the same frequency than the laser wave. Then the energy is absorbed by the ionic network which is accompanied by a sudden increase in temperature, pressure waves are formed, the material arrives in unstable states which gives way to a phenomenon of nucleation, with formation of cavities or bubbles that may appear in the material. Then a self-organization is set up comparable with the ripples observed on the sand dunes. This effect of self-organization currently remains to be explained and is the subject of extensive research in order to approach a global understanding of the phenomenon.

# 4. Effect of heat accumulation: theoretical approach

The use of high repetition rate lasers asks the question to know if the interaction with the matter is the same than with low repetition rate lasers, around kilohertz, such as amplified laser systems. The next paragraph gives a theoretical approach of the interaction and tries to answer this question.

In order to have a better understanding of the interaction at high repetition rates, it is possible to use results obtained from a simulation program. For instance a code is developed in our laboratory by Jean-Philippe Colombier [84][85][86].

## 4.1. Description of the simulation code

This code has been developed in collaboration with the CEA Saclay (Commissariat à l'Energie Atomique). Its applications are oriented to study materials behaviour when they are excited by an ultra fast laser pulse. The approach of fluids' dynamics is based on multi-phase states equations of the material. The absorption of the electromagnetic energy is taken into account by this code named "ESTHER" by the heating of the material through several steps. In a first step, the resolve of the Helmholtz equation enables to determine the electromagnetic field in the illuminated area by the laser. This resolve takes into account the amplitude of the electric field, the frequency of the laser and the complex conductivity of the material.

As previously said in paragraph (3.1), the electromagnetic energy is absorbed by electrons of conduction. This energy is stacked in the electronic system and redistributed in electron-electron collisions. Three types of collisions occur: electron-electron, electron-ion, and electron-phonon. All of them describe the thermalization process, particularly the collisions electron-phonon which contributes to the heating of the crystalline network. The effect of the energy absorption on optical properties is taken into account step by step in order to reproduce in the most realistic way the laser-matter coupling. The two temperatures model describes the thermal forwarding of the energy from electrons to the ionic network.

Ultrafast irradiation is associated with the decoupling between electronic and ionic temperatures. It makes necessary to introduce specific electronic parameters. It so supposed that free electrons follows a thermal distribution law during the interaction. The Fermi-dirac distribution is used to determine electronic properties (energy, pressure and calorific capacity) depending on the density and the temperature. These parameters make possible to write hydrodynamics equations in there Lagrangian form not only for the ionic system but also by taking into account the contribution of the electronic system. These equations are coupled with multi-phase state equations which represents the studied material in order to reproduce the changing process of this material after a laser irradiation. In particular, simulations give thermodynamic paths of the matter through the pressure, the density and the temperature also by taking into account possible effects in relation with the non-equilibrium regime of first times of the irradiation. So a wide spectrum of states is available thanks to this code.

## 4.2. Results for heat accumulation

This algorithm deals with mono-atomic metal but not with alloys like stainless steel. Fig. 15 presents results of simulations of the evolution of the temperature at the surface of the material 12.5 ns after one shot for different fluences for aluminium.

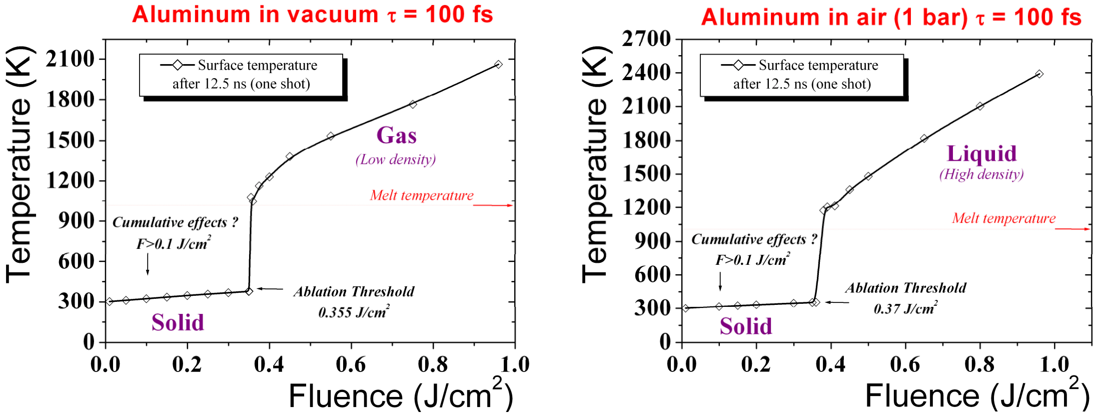

**Figure 15** ***Comparison of the evolution of the temperature at the surface of the material 12.5 ns after one shot for different fluences.***

Simulations have been done with an initial temperature of 300 K, into the air and into vacuum for pulse duration of 100 fs. These simulations show the evolution of the temperature after a time delay of 12,5 ns after one pulse. This delay corresponds to the time when the second pulse arrives on the material. The evolution of the temperature has been done in terms of fluence of one pulse. The ablation threshold of the aluminium is around 0,36 J/cm², as well as for air than for vacuum environment. However, in the case of air environment, after ablation the material is in a liquid state whereas it is in a gas state in the case of vacuum environment.

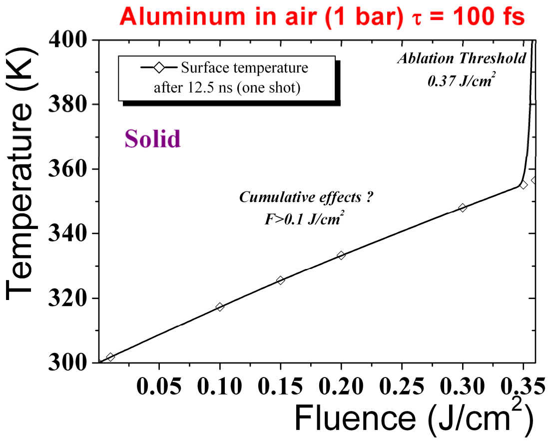

**Figure 16** ***Evolution of the temperature 12,5 ns after one pulse for several fluences.***

We can see on fig. 16 the detail of the fluence range lower than the threshold ablation, the temperature after 12,5 ns evolves linearly. Before the ablation, we notice that it is not possible to reach all temperatures at the surface of the sample. The maximum temperature reachable before ablation is around 370 K.

Up to now, we have spoken of temperature after one pulse. The algorithm has been used with several pulses to see the evolution of the temperature in terms of time. The time of calculation of the algorithm is very long, so simulations have been limited to a small number of pulses. Fig. 17 illustrates the evolution of temperature during a shooting of 4 pulses and for fluences of 0,25 J/cm² and 0,29 J/cm² per pulse. These two fluences have been chosen. The ablation threshold is not reached after four pulses of 0,25 J/cm², whereas for the second fluence of 0,29 J/cm², the ablation threshold is reached after the fourth pulse. The ablation is reached after the fourth pulse at 0,3 J/cm². After ablation, the material is in liquid state.

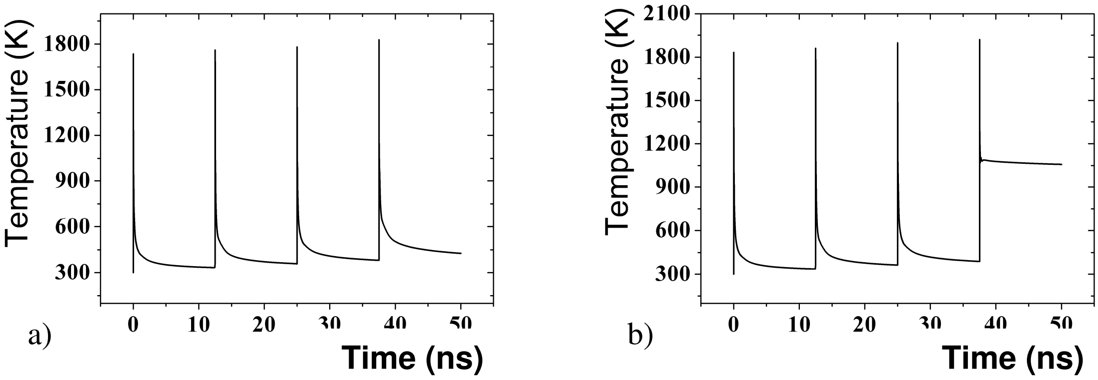

**Figure 17** ***Comparison of the evolution of the temperature at the surface of the material after irradiation of 4 pulses: (a) at 0.25 J/cm² and (b) at 0.29 J/cm².***

In parallel to the temperature approach, it is possible to present simulation results regarding the density. Fig. 18 illustrates a simulation which gives the evolution of the density of the material for four pulses. Each pulse is delayed by 12.5 ns from the previous pulse and has a fluence of 0.3 J/cm².

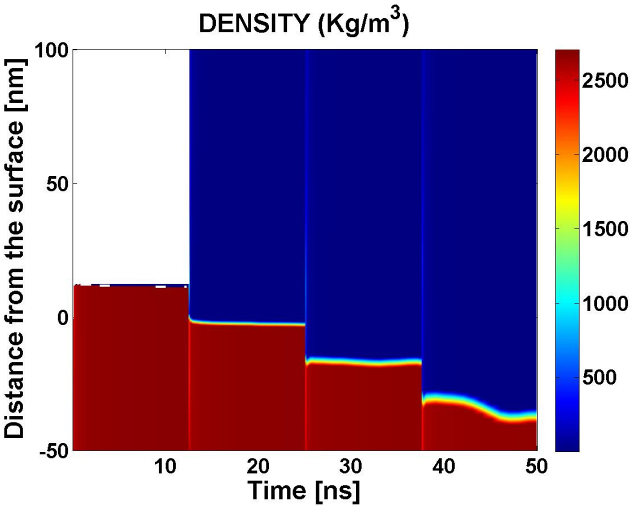

**Figure 18** ***Simulation of the density and of the surface evolving after each pulse.***

According to the simulation, for the first pulse, there is no change of the density, no ablation occurs. The red part illustrates high density which corresponds to the solid state of the material. But from the second and next pulses, the density of the material changes very strongly. Indeed, after one pulse, the density of a small thickness of the material, becomes very low, this corresponds to a density of a non-solid state. The material starts being ablated from the second pulse. In agreement with the strong decrease of the density, after each pulse the level surface goes few nanometers lower.

The calculations allow investigating the evolution of the temperature after ablation at the surface and under the surface of the sample (fig. 19). With a fluence fixed to 0,3 J/cm², the ablation at the surface is reached after two pulses. The material is transformed into a gas state with low density. The electronic density is lower than the critical plasma density, so the material is transparent for following pulses. However, at 100 nm depth inside the material, the electronic density is very high so the material absorbs pulses. This results in the increase of temperature due to cumulative effect occurring under the surface.

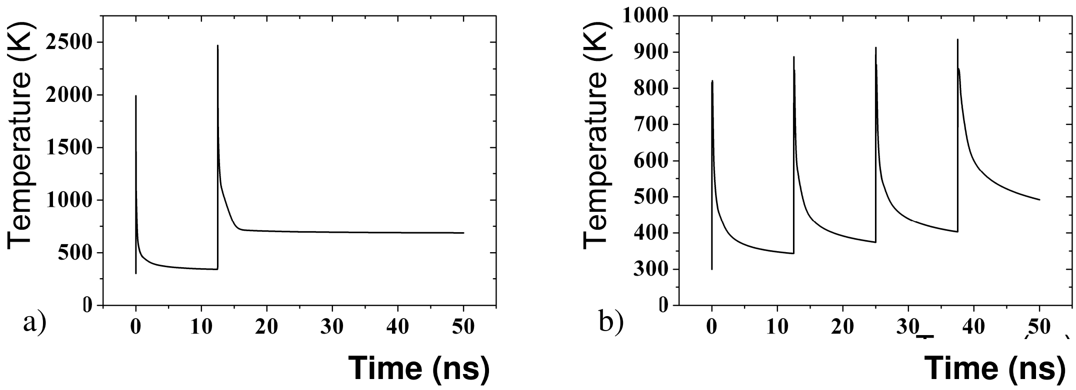

**Figure 19** ***Comparison of the evolution of the temperature after 4 pulses of 0.3 J/cm² (a) at the surface, and (b) at 100 nm depth.***

An investigation of the evolution of the temperature inside the material has been done in two different cases (fig. 20). The first case corresponds to one pulse of 1,2 J/cm² and the second case corresponds to four pulses of 0,3 J/cm².

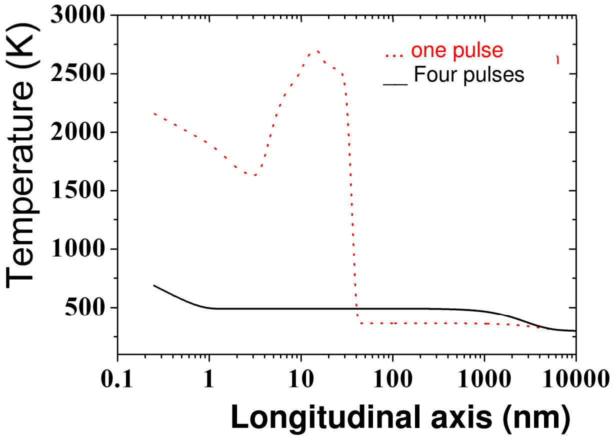

**Figure 20** ***Comparison of the evolution depending on the depth from the surface of the material. Two cases are presented with the same total energy: irradiation by one pulse of 1.2 J/cm², and irradiation by four pulses of 0.3 J/cm².***

We investigate the temperature after 50 ns, which corresponds to the time after four pulses spaced by 12,5 ns. We can see that the temperature is very high, around 2000 K and evolves in a chaotic way until 30 nm depth. After that, the temperature decreases to the initial temperature and stays constant. In the second case, the temperature is relatively high, around 700 K at the surface then decreases to a constant value from 1 nm to 1 µm depth.

# 5. Conclusion

Ultrafast lasers have long been confined to a sleepy corner of the laser market, reserved for the most exotic R&D applications. Now, not only does it seem that every laser supplier is offering an ultrafast laser, but a great many of them are offering ultrafast fiber lasers, and some of suppliers even offer ultrafast thin-disk lasers. What has happened to this sleepy corner? Ultrafast lasers have been confined to the R&D corner of the market for a simple reason. If lasers are often the tool of last resort, then ultrafast lasers are the last resort among lasers. In other words, the end-user will use a drill, a surgical knife, or a lamp if it can do the job more easily and cheaply. And when a laser is used as a tool, a CW or Q-switched laser will usually do the job more easily and cheaply than an ultrafast laser.

However, these other lasers are like jagged saws compared to the fine scalpel of the ultrafast laser. The ultrafast laser is perfect for making very clean cuts in materials, with little or no thermal damage. These materials could be microfluidic devices, patterned semiconductors, human tissue, explosives, and so on. The reason is that the ultrafast pulse imparts energy very quickly. It can boil away material or initiate multiphoton processes in a controlled fashion, before the heat that is created diffuses away. This allows for an athermal process, or at least a process with minimal heat damage. But this fine-toothed saw is simply too fine for most laser-processing applications. The ultrafast pulses are also very efficient for producing nonlinear effects, like wavelength conversion and multiphoton absorption, for use in wafer inspection and biomedical imaging, and can provide a very stable, high-frequency pulse train for metrology.

We have attempted to do a comparison between several techniques for nanofabrication. In material processing, patterns are generated either via lithography that implies the use of masks, or via direct writing that implies to use a multi axis translation stages. The specific area of direct writing, where the sample or the laser beam moves, has the capability to increase the resolution to sub micron to nanometer dimensions. We see that these two technologies are competing. Indeed, they reach equivalent size of patterns but with different advantages. Indeed the specificity of the interaction of femtosecond pulses with a material allows doing micro/nano machining, micro/nano surgery, multiphotonic imaging, and also 3D machining thanks to multiphoton photopolymerization.

The work presented here concerns the development of a tool allowing multiple applications. This tool has been developed in order to simplify and to make easily available benefits of femtosecond laser pulses.

# Chapter II

# Development of a tool for nanostructuring and multiphoton imaging

# 1. Introduction

This chapter describes the development of the multifunctional tool for nanostructuring and imaging. This development implies the implementation and control of a multitude of devices such as translation stages, piezo driven, shutter, camera,... as well as a good knowledge in optics engineering. Hardware and software have been intensively developed under LabVIEW in an easy to manage and user-friendly environment. Such a flexible apparatus can be used for a wide range of materials from metals to biological samples.

## 2. Short description of the laser source

The femtosecond laser source used in all the work of this thesis is an ultrashort pulses tuneable oscillator (Mai Tai, Spectra-Physics, USA) as shown in fig. 21 (a). The Mai Tai comprises two lasers, a CW diode-pumped laser and a mode-locked Ti:sapphire pulsed laser. The CW diode pump laser is an intracavity frequency-doubled, solid-state Millenia type 532 nm laser. Because of Ti:sapphire broad absorption band in the blue and green, the 532 nm output of the CW laser is an ideal pump source for the Ti:sapphire laser.

The tuneable Ti-sapphire laser provides an average power of 1.5W at 800nm (fig.21 (b)) and has a repetition rate of 80MHz and pulse duration of 100fs. Tuning the wavelength is accomplished by changing the position of a slit between a sequence of prisms inside the cavity that disperse the beam spatially. Varying the position of the slit would select a different wavelength within the range from 710nm to 990nm.

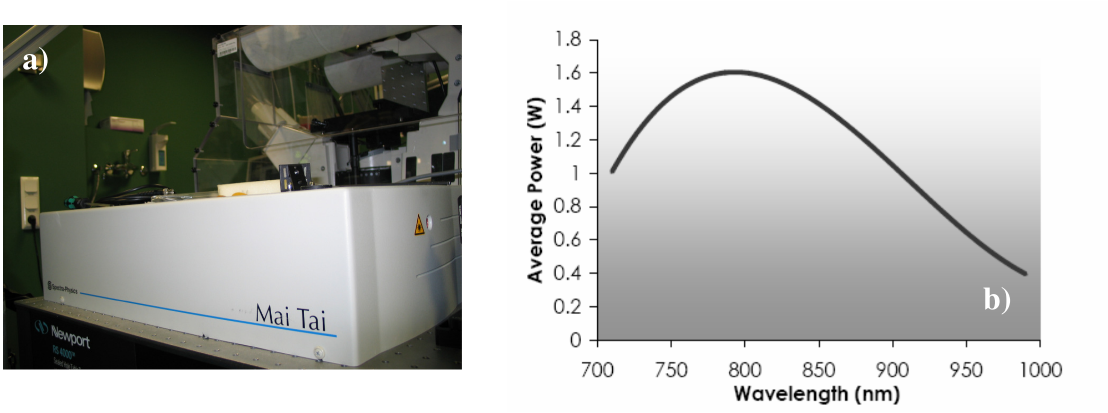

**Figure 21** ***(a) photograph of the Ti-sapphire Mai Tai laser, (b) Variation of the power depending on the wavelength.***

# 3. Device development

The nanostructuring tool is based on the bulk of an inverted microscope (fig. 22 (a)) (ZEISS axiovert 200, Germany) which has been modified. Two open flat plates have been designed with three screws allowing adjusting the planarity of the sample. On these plates, a compact open x,y translation stage based on piezo linear motorization (fig. 22 (b)) (KDT180-LM, Feinmess Dresden GmbH) is fixed. The piezo technology allow high resolution and repeatability which is fundamental for accurate nanoprocessing. These stages have a travel range of 100 mm, with a resolution of 5 nm. The repeatability is +/- 40 nm. The relative deviation is given to be 1µm on the 100 mm travel range. The maximal speed is 5 mm/s.

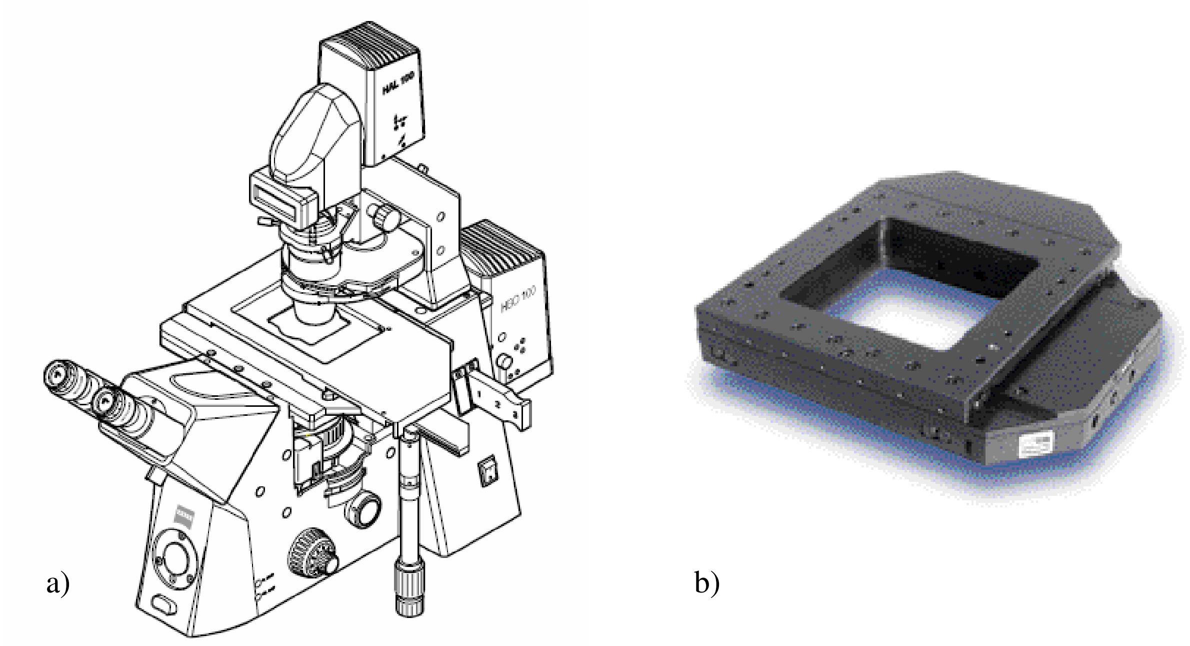

**Figure 22** ***Scheme of the inverted microscope ZEISS axiovert 200 (a). Translation stages KDT180-LM Feinmess Dresden GmbH (b.)***

These stages are provided with a 19 ˝ motion controller hardware rack connected to the serial port RS 232 of a computer, which allow the control of the two axes (Galil Motion Control, USA). The programming of the stage is performed by the use of a dedicated software based on C language with specific drivers for programming under LabVIEW environment (National Instrument, USA). LabVIEW (short for Laboratory Virtual Instrumentation Engineering Workbench), a platform and development environment for a visual programming language is a powerful tool for the control and connection of several instruments.

Sample holders have been designed and adjusted on the top of the stages as shown in fig.23.

**Figure 23** ***Picture of the sample holder fixed on translation stages.***

A piece has been specially designed for reflecting the beam to the top of the microscope. This piece can supports a dichroïc plate with an angle of 45°, three small screws allow to adjust the orientation of the plate, which transmits wavelength from 400 to 675 nm and reflects 100% of the light at 800 nm. A cube of the microscope's revolver has been modified and contains a beam splitter which transmits 90% of the light and reflects 10%. The reflected light coming from the sample goes back through the objective. A small amount of light is reflected on the beam splitter and focused, via a lens, on a programmable CCD camera (Imaging Source, USA) for imaging the surface of the sample. It is possible to use lenses with different focal in order to change the magnification of the visualization system.

The magnification is calibrated thanks to a micrometer scale or grid which we know the size as illustrated on fig. 24. The corresponding size of the area observed with the camera (µm) can hence be deduced.

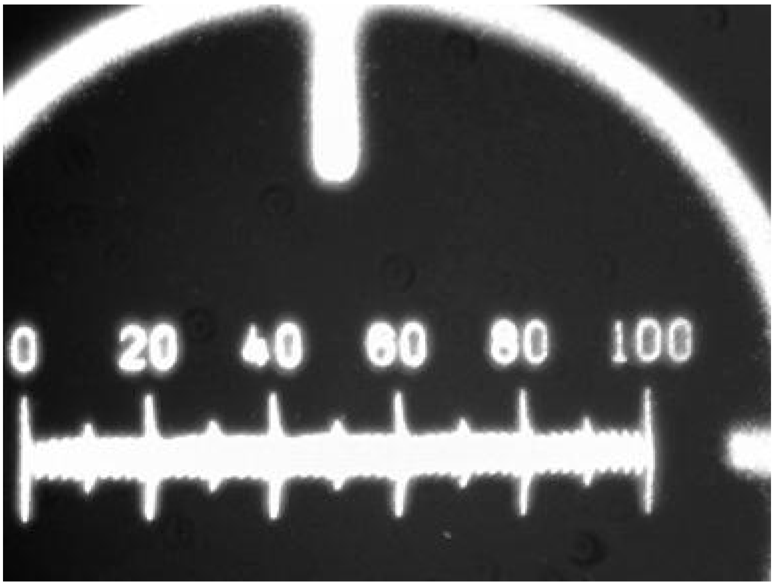

**Figure 24** ***100 micrometer scale seen by the CCD camera in the objective focal plan.***

The white light source setup is composed of a 90 W halogen lamp, several lenses, and a diaphragm. It provides a parallel white light beam. The intensity can be modulated. This white light source is located in the place of the binocular of the microscope which has been removed. The white light beam goes through the aperture on the binocular side, is reflected on a mirror in the bottom of the bulk of the microscope, then cross the dichroïc plate until the high numerical aperture objective. The focal plane of the objective is conjugate with the plane of the CCD camera which provides a picture of the sample surface and of the laser beam reflection. A polarizer was inserted on the optical path up to the camera to reduce the intensity of the laser beam reflected to ensure no saturation. The polarizer is oriented so as to minimize reflection. The fraction of the light detected by the camera is enough to show the spot as shown in fig. 25. The whole setup is depicted in the fig. 26 below.

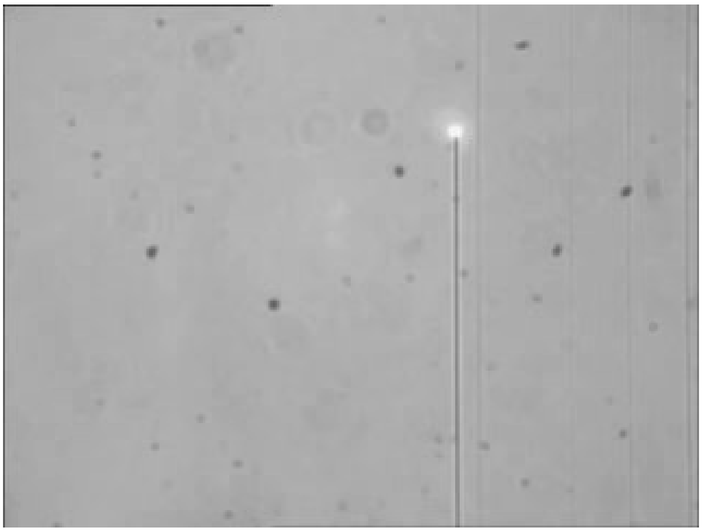

**Figure 25** ***Example of spot visualisation of the laser spot on the material surface during laser nanostructuring.***

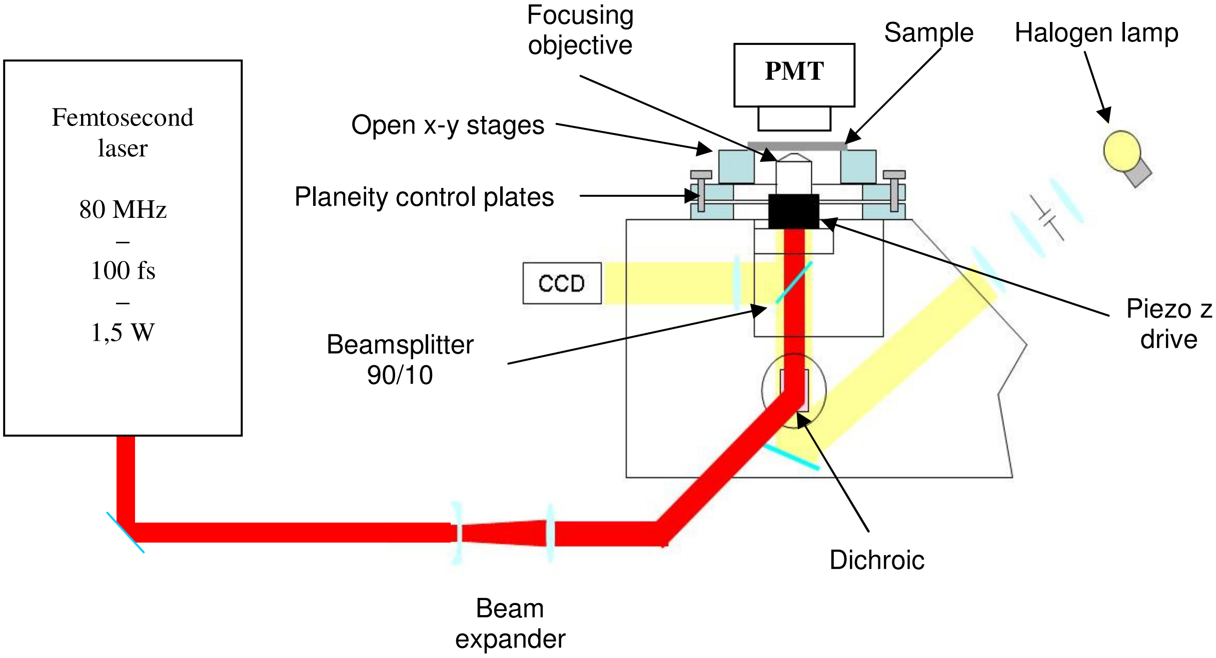

**Figure 26** ***Global scheme of the nanostructuring device.***

To perform sub-µm structuring, optics with tightly focusing are necessary. Using high NA objectives, a smaller region above the ablation threshold is produced, thus enabling the creation of structures below the diffraction limit. The objective used (ZEISS, Germany) is an oil immersion high numerical aperture of 1.3 with a magnification of 40 times. The objective's diameter input is 11 mm. The diameter at 1/e² of the laser beam has been measured with a beam analyser (Ophir-Spiricon, LLC, USA). The software gives linear profiles of the beam that we can see on edges of the picture on fig. 27. The software can give diameters of the beam for different value according to the point of maximum of power. In our case we are interested in the diameter at 1/e² which corresponds approximately to 13.5 % of the maximum of the Gaussian. In this case we have a mean diameter of 5.2 mm.

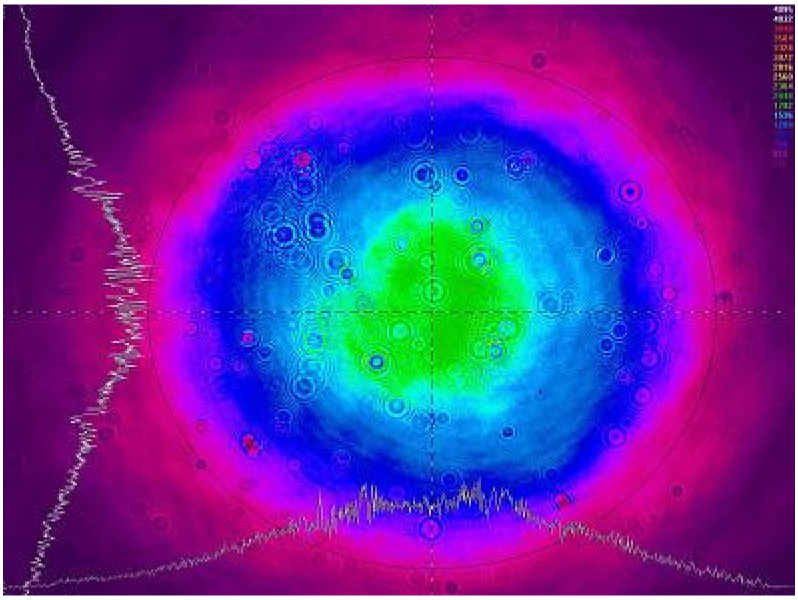

**Figure 27** ***Spatial laser beam profile before the setup***

In order to obtain the higher power of focalization with a minimal spot size, one has to illuminate the whole diameter of the input of the objective. The beam has then been expanded twice and the diameter before objective at 1/e² is 10.4 mm now. This objective is mounted on a piezoelectric stage (P-722 PIFOC, Physics Instrusments, Germany) as shown in fig.28.

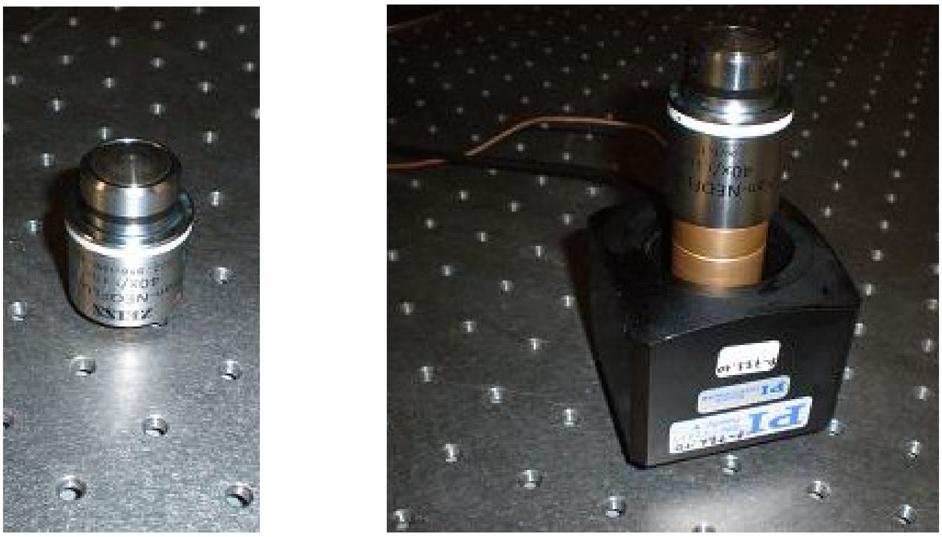

**Figure 28** ***1.3 NA oil objective (ZEISS) mounted on an extension screwed on piezoelectric stage.***

Small developments have been done to hollow the control of the piezoelectric stage under LabVIEW. A 0-10V signal is send from the acquisition card, this signal is then amplified 10 times before being applied to the piezoelectric stage as shown in the fig. 29.

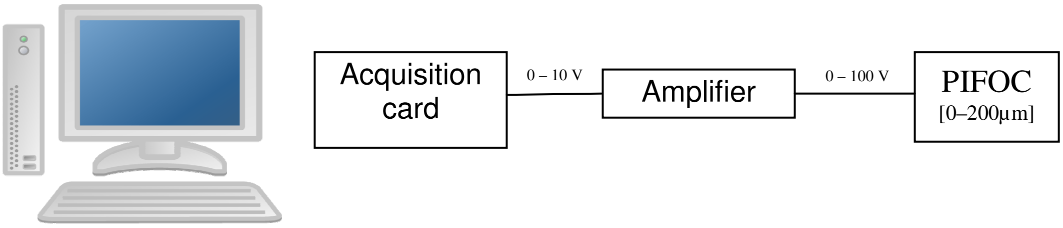

**Figure 29** ***Scheme of the computer controlled Z-axis.***

This microscope objective piezo stage nanopositioning system is fast and compact and can be mounted on most microscopes. It provides a positioning and scanning range from up to 200 µm with nanometer resolution while extending the optical path by only 13 mm. In this instance, for mechanical reasons, an extension has been added before the objective. An infinity corrected objective is required. The variation of the z position of the spot is given in fig. 30.

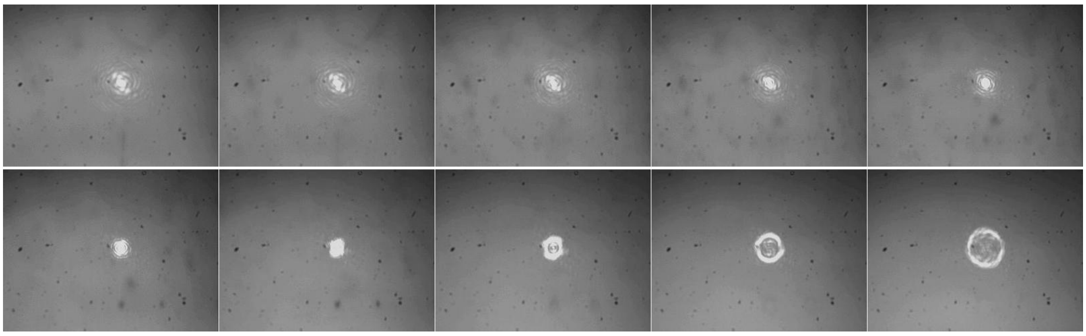

**Figure 30** ***Variation of the position of the spot depending on the voltage. From the left to right and from the top to the bottom each picture with the spot corresponds to several voltages, respectively : 4.5V, 4.6V, 4.7V, 4.8V, 4.9V, 5V, 5.1V, 5.2V, 5.3V, 5.4V.***

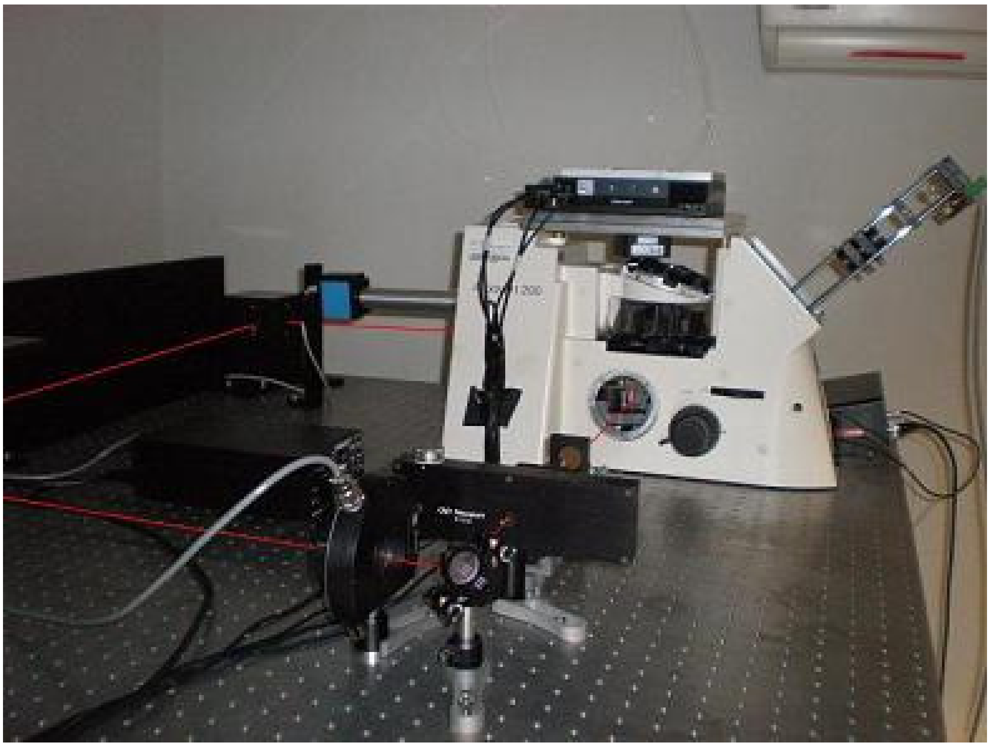

**Figure 31** ***Picture of the global setup.***

A picture of the global device is given in fig. 31. The setup includes a shutter (Uniblitz, USA) which is indirectly controlled by computer via the signals generated by the controller of the translation stage. Its exposure and delay interval range is adjustable from 1ms to 2.8 hours. The shutter has an opening and closing time of 50 ms typically for an aperture diameter of 20 mm.

# 4. Characterization of the laser beam for an optimal coupling into the device

To perform nanostructuring and to reach the ablation threshold of most materials with a very low average power laser source, it is necessary to control and optimize parameters as the quality of the laser beam, its profile, shape and its power of focusing as well as the different energy losses and pulse duration broadening throughout the several optics and more especially the focusing objective.

## 4.1. Spot size determination

Thanks to the beam analyzer, it has been possible to measure the size of the beam at different positions along the propagation axis after the focusing objective as illustrated in the fig. 32. From these measures we can deduce the divergence angle after the objective.

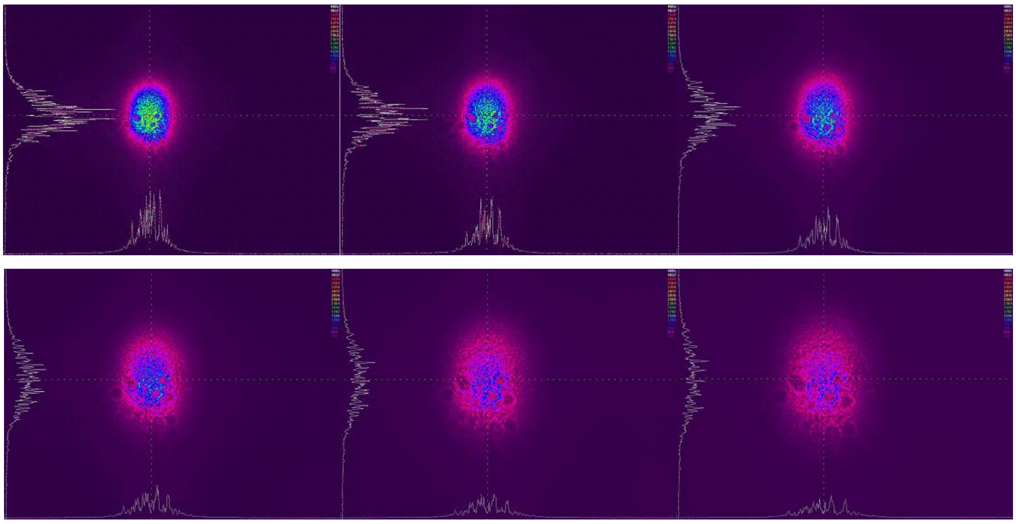

**Figure 32** ***Beam profiles for different positions of the detector after the focalisation of the beam by the objective.***

One can notice that the intensity decreases with the increase of the distance from the objective, due to the divergence of the beam. For each position the diameter of the beam has been measured at 1/e².

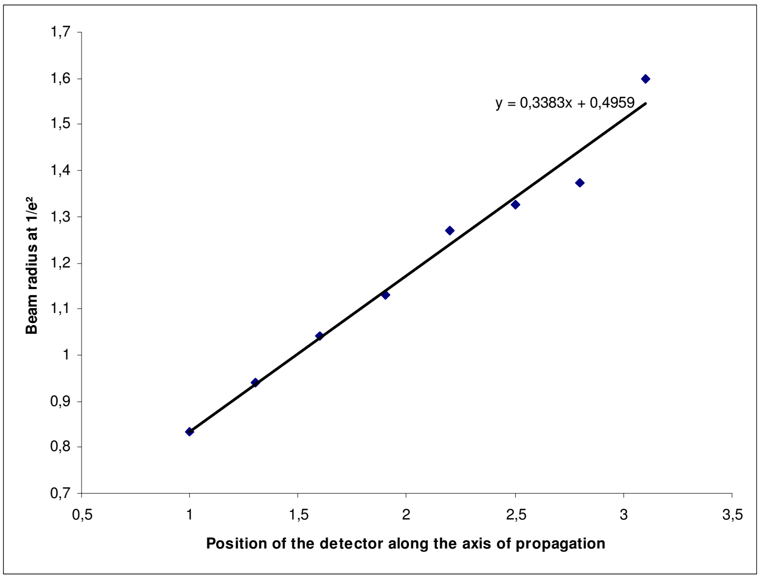

**Figure 33** ***Divergence of the beam after the objective according to the position.***

From the fig. 33 we can deduce the angle of divergence and therefore an estimation of the waist from the following formula. We find a waist of 800 nm.

$$\theta \cong \frac{\lambda}{\pi \omega_0} \qquad (2.1)$$

This size of the waist is estimation and corresponds to the case of a Gaussian beam shape. In the case of a Gaussian shaped spot, the radius of the beam (w0) is so given to be the distance between the center of the beam and the circle corresponding to 1/e² of the maximum intensity of the beam. The experimental diameter d of the laser spot obtained by this method is then $2 \times \omega_0$ i.e. 1.6 µm. The size of the laser spot is controlled thanks to the distance between the sample and the focusing objective. With such high focusing objective, we always work at the focus point. The working point corresponds to the position of the smallest size of the spot seen with the camera.

To know the size of the beam at the focus point, a series of impacts is necessary as shown in figure 34.(a). This method has already been described [87]. Indeed the fluence is not constant but depends on the distance r from the center of the beam. The fluence for a Gaussian beam is given by:

$$F(r) = F_{\max} \exp(-\frac{2r^2}{\omega_0^2}) \qquad (2.2)$$

There is an ablation of the material only if the fluence is greater than the fluence threshold. The fluence threshold Fth can be written as a function of the size of the impact $r_{th}$:

$$F_{th} = F_{\max} \exp(-\frac{2r_{th}^2}{\omega_0^2}) \qquad (2.3)$$

$r_{th}$ can be deduced as follow:

$$r_{th}^2 = \frac{\omega_0^2}{2}\left[\ln(F_{\max}) - \ln(F_{th})\right] = \frac{\omega_0^2}{2}\left[\ln(E_p) - \ln(E_{th})\right] \qquad (2.4)$$

Where $E_{th}$ is a constant representing the minimum energy per pulse necessary for ablating the material. We obtain a linear formula where the slope corresponds to the half of the squared radius of the beam. This method has the advantage of not depending on the material used.

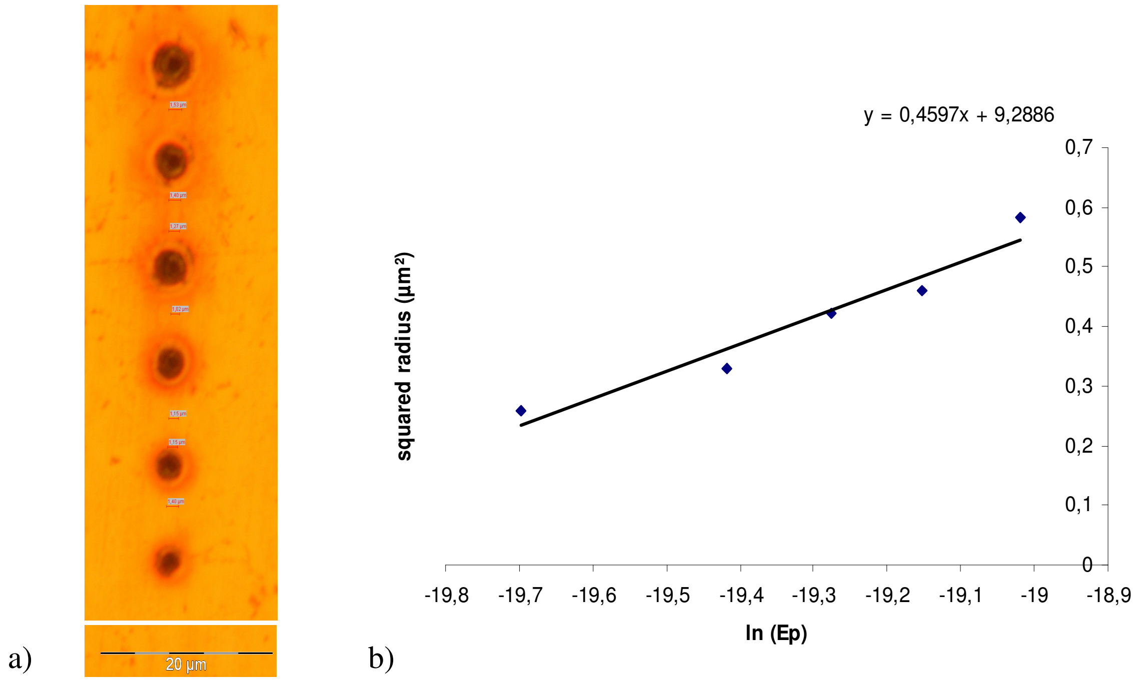

**Figure 34** ***A series of impacts done on the surface of a sample of copper for several energies per pulse. We can see the size varying with the energy per pulse (a). Plot of the squared radius as a function of ln(Ep) (b).***

The equation (2.4) describes the plot on the figure above (fig. 14 (b)). We can deduce the size of the spot from the slope of this plot. From a linear fit we can deduce the value of the waist:

$$\frac{\omega_0^2}{2} \approx 0.45 \rightarrow \omega_0 \approx 0,95\mu m$$

The experimental diameter deduced from this second method is then 2 x 0.95 = 1,9 µm which is quite in agreement with the first method presented above.

The theoretical minimum diameter obtainable is defined by the limit of diffraction:

$$d = 1,22\frac{\lambda}{NA} \qquad (2.5)$$

At 800 nm and with an objective with a NA of 1.3, the theoretical minimal diameter is calculated to be 750 nm.

The experimental results are then twice the value of the limit of diffraction. This could easily be expected because it is very dependent on the beam and objective quality. The theoretical estimation is provided for an ideal illumination. However, this limit of diffraction is obtained only with a uniform intensity illumination of the pupil. As a laser beam is always Gaussian shaped, this implies too much losses of power in order to get a uniform illumination. For example, in the case of a Gaussian beam two times larger than the aperture diameter of the objective, there are around 60% of losses. In order to be able to machine materials, it is necessary to have enough energy; this is why we illuminated the objective aperture with a beam quite smaller than the aperture as said above.

## 4.2. Fluence determination of a Gaussian shaped intensity profile

All experiments have been done at the focus point of the objective such as we have a Gaussian (Sech$^2$) shaped intensity profile. During experiments, it is necessary to control experimental conditions such as the fluence. The fluence is defined as a quantity of energy on a surface (J/cm²).

$$F = \frac{E_p}{S} \qquad (2.6)$$

With Ep the energy per pulse (J) and S the surface of the beam (cm²). It is also possible to describe this expression as a function of laser source characteristics.

$$F = \frac{P_{avg}}{kS} \qquad (2.7)$$

Where $P_{avg}$ is the average of the output power of the beam (in W) and $k$ the repetition rate of the laser (in Hz). In the following, the beam is considered to well fit with a Gaussian shape.

From the size of the beam, it is now possible to calculate the value of the fluence. The energy per pulse is applied on all the surface of the beam. But as said previously, the beam is Gaussian shaped, so that the energy is not distributed evenly on the surface of the beam. This implies that the fluence also follows a Gaussian distribution on the surface of the beam. Energy per pulse is equal to the sum of fluence spread over the surface of the beam, which can be expressed as follows:

$$E_p = \iint_{\infty} F_{\max} \exp(-2\frac{x^2+y^2}{\omega_0^2})dxdy \qquad (2.8)$$

The equation (2.8) gives the value of Ep. The values of fluence used in experiments rely on the determination method detailed in this paragraph and can be deduced from the equation above (2.10). The fluence has got different values along the spatial profile of the beam. The maximum fluence is located in the center of the beam. The calculation of $F_{\max}$ is described below. The axes x and y are not correlated, so the integral can be written as following:

$$E_p = F_{\max}\left[\int_{-\infty}^{+\infty}\exp\left(-\frac{x^2}{k^2}\right)dx \times \int_{-\infty}^{+\infty}\exp\left(-\frac{y^2}{k^2}\right)dy\right] \qquad (2.9)$$

By replacing variables with $k = \frac{\omega_0}{\sqrt{2}}$, we replaced variables $x$ and $y$ by $ku$ and by $kv$ respectively. We obtain the following expression:

$$E_p = F_{\max}\left[\int_{-\infty}^{+\infty}\exp\left(-\frac{k^2u^2}{k^2}\right)kdu \times \int_{-\infty}^{+\infty}\exp\left(-\frac{k^2v^2}{k^2}\right)kdv\right] \qquad (2.10)$$

$$E_p = F_{\max} \times k^2\left[\int_{-\infty}^{+\infty}\exp\left(-u^2\right)du \times \int_{-\infty}^{+\infty}\exp\left(-v^2\right)dv\right] = F_{\max} \times k^2 \times \pi$$

$$\Rightarrow F_{\max} = \frac{2E_p}{\pi\omega_0^2} \qquad (2.11)$$

## 4.3. Average power

We measured the power available at different locations of the setup. These measures have been made with the power meter PM10 (Coherent, USA). At the entrance of the microscope the laser beam power is 1,25 W and suffers no losses through the dichroïc. After the beam splitter the power decreases down to 1 W, this represents 80 % of the power left. Then after the objective, the power goes down to 710 mW. This represents 57 % of the incoming power into the system. The global path through optical components brings 43 % of losses. The biggest losses come from the objective, where the light crosses 4 cm thick glass. Other losses come from the beam splitter where the light loses 10 % more than the percentage said in the datasheet of this beam splitter.

## 4.4. Autocorrelation (at laser output and after objective)

Femtosecond laser pulses are stretched when they pass through an optical microscope objective used for laser machining. The question that must be answered is how much does the pulse stretch passing through the objective? Stretching of pulses would be more prominent in the case of ultrashort laser pulses. The laser intensity is strongly dependent on the pulse duration and can rapidly decreases when the pulse duration increases by a few amounts. This is critical in our case when using femtosecond laser source with very low average power, because transient TW/cm$^2$ laser intensities are needed to induce multiphoton ionization.

The pulse duration of the laser has been measured with an Autocorrelator MINI (APE GmbH, Germany). An external semiconductor detector can be added to the autocorrelator to measure pulse duration after the pulses go through an optical system as here at the focus of an optical microscope objective. Experimental autocorrelation profiles measured at the laser output and after the objective are given in the fig. 35.

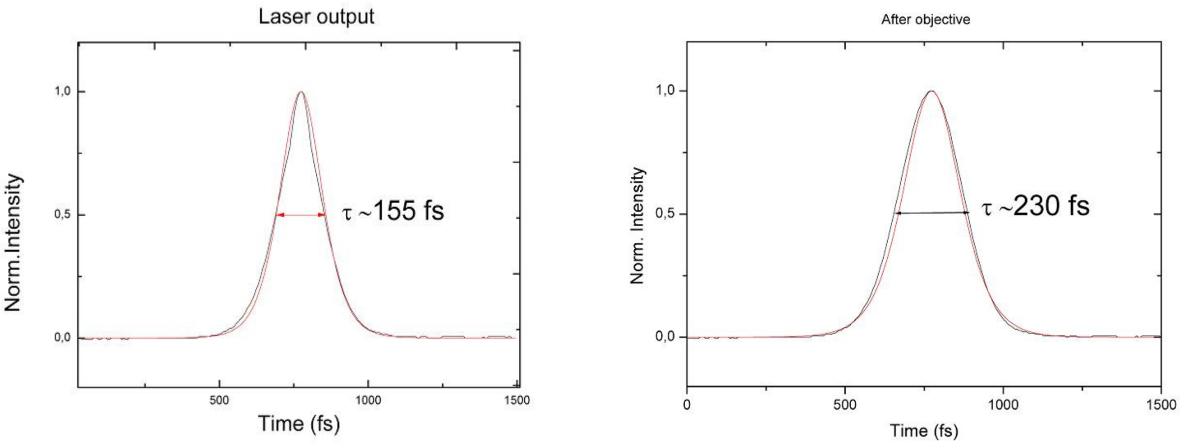

**Figure 35** ***Experimental autocorrelation profiles of pulses at the output laser (a) and after 40x 1.3 oil objective both fit with a squared hyperbolic secant (red).***

The pulse duration measured at the output of the laser and after the objective at full width at half maximum (FWHM) are respectively 155 fs and 200 fs. The intensity time profile is fit with a hyperbolic secant squared pulse (red). For hyperbolic secant squared shaped pulses, the autocorrelation width is 1.54 times longer than the real width of the pulse, but this conversion factor depends on the pulse shape. Therefore, in our case the real pulse duration is defined by:

$$\tau_{real} = \tau_{measured} \times 0.65 \qquad (2.12)$$

Thus the real pulse durations at the output of the laser and after the objective respectively are 100 fs and 150 fs.

The difference of the pulse duration before and after of the objective is 30 fs which is not negligible but not critical to reach sufficient intensities to overcome the ablation threshold of most of materials. If the stretching was more pronounced it would have been necessary to add a negative pre-chirp in the laser path to reduce the dispersion of the pulses. The optical index of a transparent material is not the same for all wavelengths. Thus, the speed of the light is not the same inside a transparent material and depends on the wavelength. This involves a phase difference. This phenomenon is known as Group Velocity Dispersion (GVD). The term can also be used as a precisely defined quantity, namely the derivative of the inverse group velocity with respect to the angular frequency (or sometimes the wavelength):

$$\mathrm{GVD} = \frac{\partial}{\partial \omega}\frac{1}{\upsilon_g} = \frac{\partial}{\partial \omega}\left(\frac{\partial k}{\partial \omega}\right) = \frac{\partial^2 k}{\partial \omega^2} \qquad (2.13)$$

The group velocity dispersion is the group delay dispersion per unit length. The basic units are $s^2$/m. For example, the group velocity dispersion of silica is + 35 $fs^2$/mm at 800 nm. After passing through a transparent medium, the pulse duration in relation to the input pulse duration is given by:

$$\frac{\tau_{out}}{\tau_{in}} = \sqrt{1 + \left( \frac{D_\omega L}{\tau_{in}^2} 16(\ln 2)^2 \right)^2} \qquad (2.14)$$

Where $D_\omega$ is the Group Velocity Dispersion in fs²/mm, and $L$ is the length of the medium in mm. From this equation it is possible to calculate the Group Delay Dispersion (GDD), also sometimes called the second-order dispersion, given by:

$$GDD = D_\omega L = \frac{\sqrt{\tau_{in}^2 \tau_{out}^2 - \tau_{in}^4}}{16(\ln 2)^2} \qquad (2.15)$$

It measures the rate at which a pulse centered at the reference frequency will increase in duration upon propagation through the system. It is specified in units of [fs$^2$]. In our case GDD is found to be 1262 fs$^2$ which is not critical.

# 5. Development of an autofocus method

The configuration of the system allows the establishment of an autofocus by coupling the position along the z axis with the camera. For each position of the objective along the z axis, the size of the spot changes depending on the distance between the objective and the sample. The purpose of this system is to place automatically the sample in the focus plane of the objective.

## 5.1. Principle

The feedback needed for the autofocus system is provided by pictures from the camera. First we ensure that the spot is at the center of the image. Each picture taken by the camera is kept inside a memory buffer and used for the autofocus positioning calculation. The longitudinal position is controlled thanks to the z piezo stage as described above. In order to reduce calculating time, the algorithm deals with a smaller part of the picture of 512 x 512 pixels². This part is in the center of the picture where the spot is.

## 5.2. The algorithm

The algorithm used is based on the calculation of the standard deviation of grey levels from an image of the surface to find the focal point of the objective. This standard deviation is used as the feedback signal for autofocusing. When the standard deviation is at the maximum it corresponds to the best focus position of the objective. In order to get this position, the algorithm should always try to find a larger standard deviation until it reaches the maximum. Pictures saved in the buffer are composed of 256 grey levels. Assuming that the $i$th pixel has a grey level of $G_i$, it is possible to calculate the mean grey level from the equation :

$$\mu = \sum_{i=1}^{n} \frac{G_i}{n} \tag{2.16}$$

The standard deviation $SD$ is then defined as following:

$$SD = \left[ \sum_{i=1}^{n} \frac{(G_i - \mu)^2}{n} \right]^{\frac{1}{2}} \tag{2.17}$$

At the beginning the system is out of focus, it is necessary to know which direction (up or down) the z piezo stage should move to come closer to the best focus position. To find this direction automatically, the program lets the objective move just one step, up or down randomly. It calculates standard deviation for each position before moving ($SD_1$) and after moving ($SD_2$) and compares them. If $SD_2 - SD_1 > 0$ then the objective can moves in the same direction for the next step. Otherwise, if $SD_2 - SD_1 < 0$ the objective moves in the opposite direction for the next step.

This algorithm has been approved in the case of creating a focusing feedback signal in compact disc drives from the image itself [88]. This method has the advantage that the calculation of the standard deviation is easy and fast.

By calculating the standard deviation for several positions, we find a maximum depending on the position in micrometers as illustrated by fig. 36.

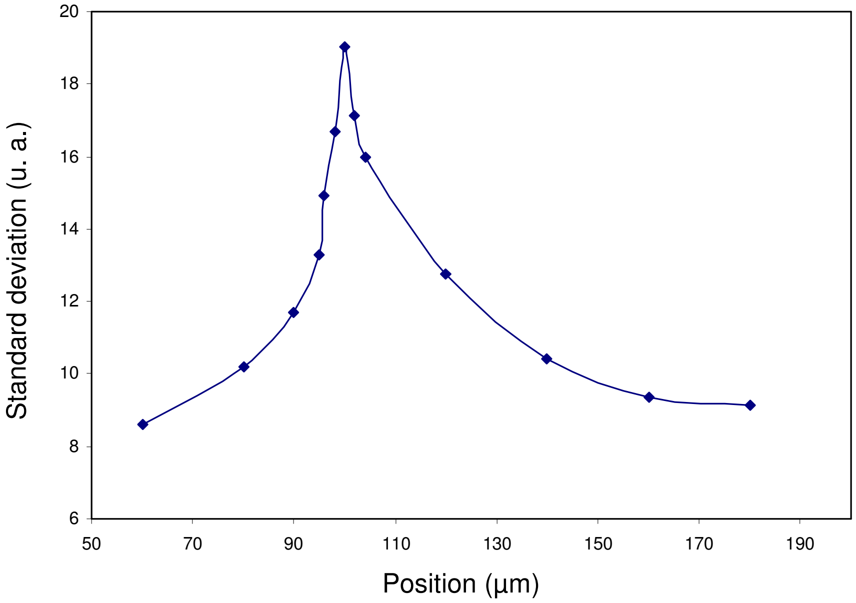

**Figure 36** ***Standard deviation depending on the position of the objective. We see clearly a maximum for the position of 100 µm which corresponds to the focus position.***

However the method developed has been demonstrated to be operable, it is quite slow. It takes around 2s from one step to the next one. In order to reduce time calculation, several algorithms have been developed. but it is still not fast enough for a real time autofocus during nanoprocessing displacement. This mainly comes from the acquisition time of the camera to put the picture into a buffer under LabVIEW, this has to be improved.

# 6. Control and software development

Hardware and software developments have been intensively performed for a convivial, open and powerful nanomachining control. As said above, the global software has been developed under LabVIEW using different ActiveX to control stages, image acquisition, piezoelectric z stage, shutter, autofocus, etc. This program is divided into several parts:

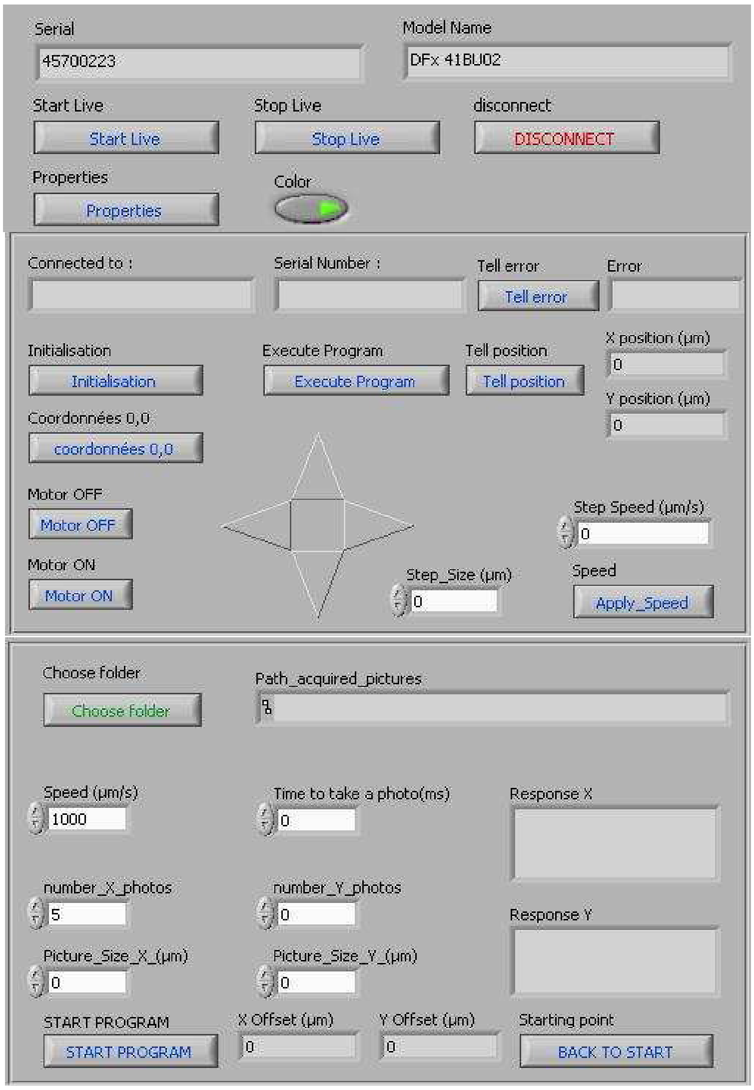

Serial: 45700223
Model Name: DFx 41BU02
X position (µm): 0
Y position (µm): 0
Step Speed (µm/s): 0
Step_Size (µm): 0
Speed (µm/s): 1000
Time to take a photo(ms): 0
number_X_photos: 5
number_Y_photos: 0
Picture_Size_X_(µm): 0
Picture_Size_Y_(µm): 0
X Offset (µm): 0
Y Offset (µm): 0

Figure 37 *Global interface of the labview software.*

## 6.1. The Camera control

The panel of the fig. 38 displays the serial number and the model name of the camera used. If these cases are empty, it means that the camera is not well detected by the computer. Two buttons allow starting and stopping the live display. It is also possible to get access to properties of the camera like contrast, exposure, brightness, … and change them manually. The button „Color“ allows to save 24-bit colour pictures or 8-bit grey level pictures.

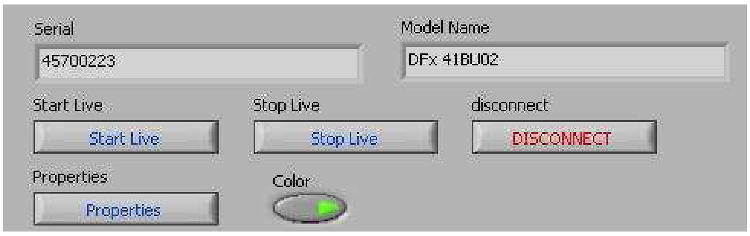

Serial: 45700223

Model Name: DFx 41BU02

**Figure 38** ***Front panel of the camera control.***

## 6.2. x,y translation stage control

The panel of the fig. 39 displays the serial number and the model name of the controller of the x,y translation stage. If boxes are empty, it means that the controller is not detected by the computer. Many buttons are used to control and get information from the x,y translation stage. First, an initialization of the stage has to be performed one time after switching on the controller. Initialization procedure consists on downloading a specific program into the controller and run it.

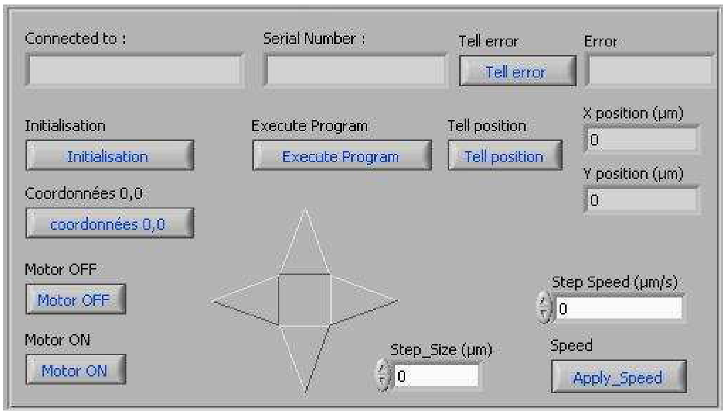

**Figure 39** ***Front panel of translation stages control.***

Then to execute a program we have to select it. All programs sent to the controller must have been programmed in G language with special Extension. From this panel, it is possible to put back stages to the center (coordinates X=0, Y=0). We can know the position from the center and the position error of motors. Two buttons are used to activate or deactivate motors. Four arrows have been placed in order to move manually stages until a desired position. It is possible to adjust the size and the speed of each step.

## 6.3. Scanning area control

The panel of the fig. 40 allows controlling stages and camera in a synchronised way. First, we have to select in which directory we want to save these pictures. The size of pictures taken by the camera must be calibrated. Pictures have a resolution of 1280 x 960 pixels. It is possible to change the size of the area by replacing the imaging lens before the CCD camera in the tube by a lens with another focal length. For a focal length of 250 mm, the size of the area is 70 x 90 µm.

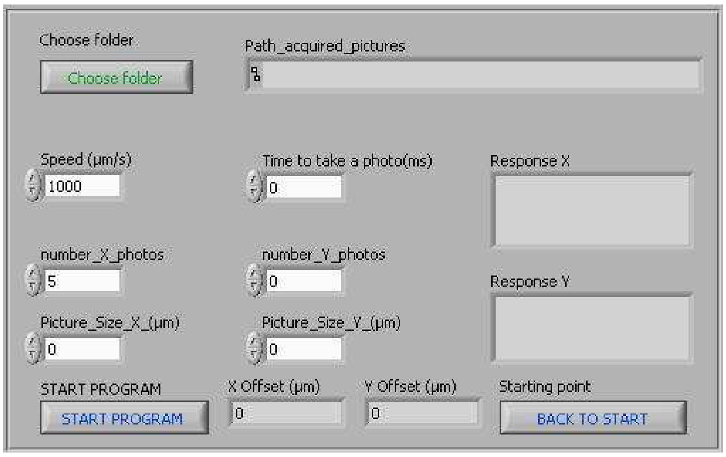

Speed (µm/s) 1000
Time to take a photo(ms) 0
number_X_photos 5
number_Y_photos 0
Picture_Size_X_(µm) 0
Picture_Size_Y_(µm) 0
X Offset (µm) 0
Y Offset (µm) 0

**Figure 40** ***Front panel of the scanning area control.***

The program takes pictures along X and Y directions of translation stages. We choose the number of pictures that we want to take in each direction. We put in values X and Y dimensions of the picture defined before. The X dimension corresponds to the travel distance of the stages. The Y dimension corresponds to the distance between two lines. By this way it is possible to take high resolution pictures of a big area. When the scan occurs, all pictures are saved in the „.bmp“ format. Scheme of the concept of an image reconstruction is given in figure 41.

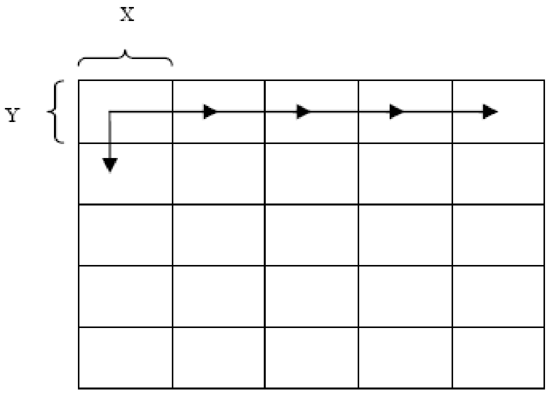

**Figure 41** ***Schematic representation of area mapping.***

All pictures saved are joined automatically together to build a matrix of pictures. Each picture has a name corresponding to its position in the matrix, for instance “11.bmp” corresponds to the first position in the matrix. This part takes into account the number of pictures wanted in the scanning area control along the X and Y axis. A dividing coefficient can be applied, number of pixels can be controlled in order to reduce the size of the picture.

# 7. CAD drawing to nanomachining

To approach industrial standards of machining, a CAD to G language software converter has also been added and developed in the Labview software to generate automatically a program of CAD files which allow performing laser structuring from drawing supports.

## 7.1. Size control

As mentioned previously, you can download programs with “.DMC” format executable by the controller. 2D drawings can be made with any software that saves files in DXF format. These files are then converted to DMC via specific software which is named CAD2DMC (GALIL Motion Control, USA). In order that the drawing can be interpreted by the controller, some rules have to be respected. First of all, the design must be decomposed into a series of continuous lines. Each drawing must include a starting point and ending point, marked on the drawing itself, respectively by the words "FIRST" and "LAST". Some features may be added through the use of macros which have to be inserted directly on the drawing, such as scale to control the size of patterns desired, or the opening and closing of a shutter. Fig. 40, shows an example of conversion.

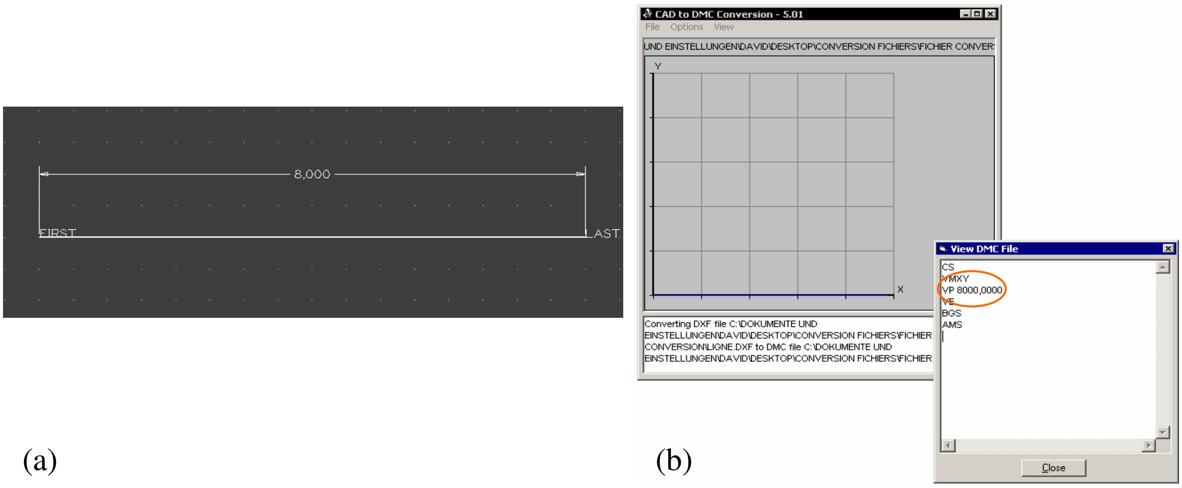

```
UND EINSTELLUNGEN\DAVID\DESKTOP\CONVERSION FICHIERS\FICHIER CONVER:
```

```
Converting DXF file C:\DOKUMENTE UND
EINSTELLUNGEN\DAVID\DESKTOP\CONVERSION FICHIERS\FICHIER
CONVERSION\LIGNE.DXF to DMC file C:\DOKUMENTE UND
EINSTELLUNGEN\DAVID\DESKTOP\CONVERSION FICHIERS\FICHIER
```

```
CS
VMXY
VP 8000,0000
VE
BGS
AMS
```

(a) (b)

**Figure 42** ***Picture of a line drawn with CAD software for a standard scale of 1000 (a) and the ".dmc" corresponding file (b).***

The corresponding distance is calculated from the resolution of translation stages which is 5nm/count. If we apply on the drawing a value of the scale of 1000, a drawn line which has a length of 8000 counts will correspond to a length of 40µm on the sample. In the case of a scale value of 2000, the length will be multiplied by two. This system provides a good and easy control with a very good precision.

## 7.2. Shutter control

Shutter control is also achieved through the use of macros included in the drawing itself. The use of macros allows you to enable or disable one bit or more among the eight output bits on the controller output port. The output signal is TTL (0V - +5V). This signal is then amplified before being sent to the shutter. Shutter control gives the possibility to make patterns with interruptions. Fig. 43 illustrates an example of drawing including macros for the control of the shutter. The opening of the shutter occurs each time it is written "ON" on the drawing, the command line "SB1" is sent to the controller, which sets the bit 1 to the value 1 (corresponding to the voltage +5V). The closing of the shutter occurs each time it is written "OFF" on the drawing, the command line "CB1" is sent to the controller, which sets the bit 1 to the value 0 (corresponding to the voltage 0V).

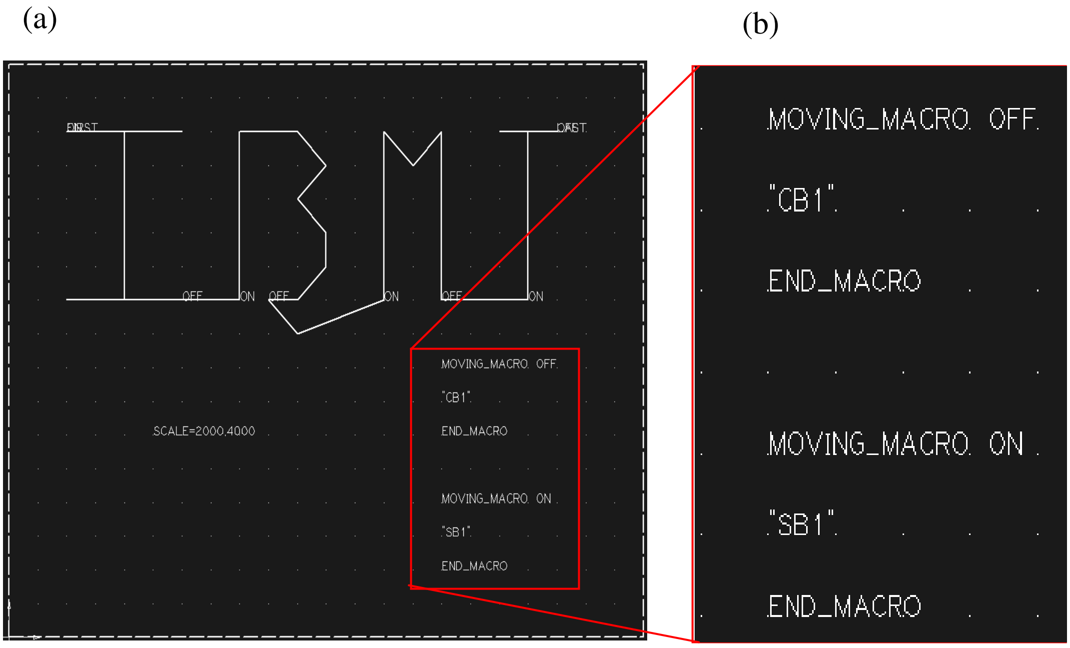

```
MOVING_MACRO. OFF.
"CB1".
END_MACRO

MOVING_MACRO. ON
"SB1".
END_MACRO
```

**Figure 43** ***IBMT logo drawn with CAD software (a). Illustration of the Corresponding macro used to control the shutter (b).***

This drawing defines the pattern, the corresponding size and where the laser has to be cut or not. Once the DXF drawing has been converted into DMC file, it is integrated into a broader program with a starting part containing PID (Proportional, Integrate, Derivative) constants for the stages control. It is also necessary to include a part containing loops of voltage control for the control of speed. Moreover, we have to set the speed and the number of reiterations. The insertion of all these part is done under LabVIEW. The following diagram (Fig. 44) summarizes the whole insertion operation.

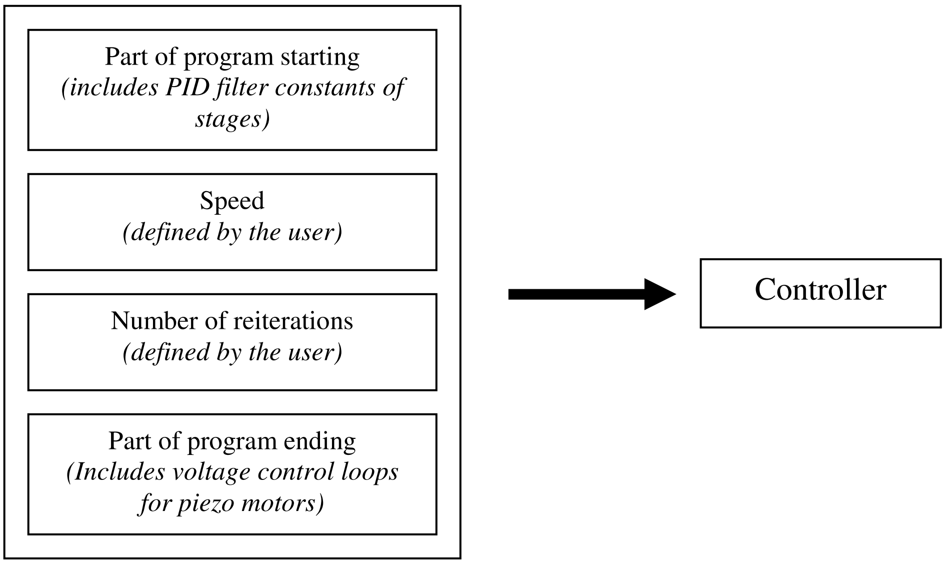

**Figure 44** ***Schematic representation of all parts of the program assembled before sending to the controller***

Once all the parts are assembled, the whole program is saved under the name of the drawing. The extension "_CAD2DMC" is added to this name of file. For each change done inside the program, the previous file is overwritten.

## 7.3. 3D structuring

The z-positionning piezo control has been integrated into the program developed under LabVIEW which allow 3D processing. The z-positionning piezo is controlled independently of the programming of x-y-translation stages. This allows repetitive execution along the z axis of a program with a step size selected by the user. The initial position is the focal point of the laser beam on the sample. Any program executed on several plans along z axis can then start from this position as the 0 position for the z positioning piezo stage. The global execution of a repetitive program along z axis is represented in a simple diagram (Fig.45).

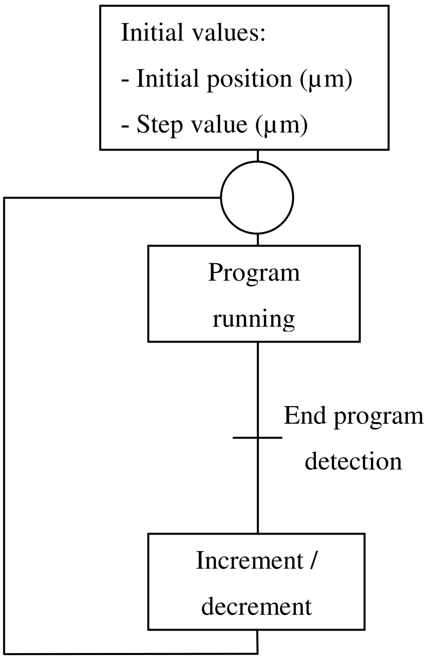

**Figure 45** ***Diagram of a repetitive program execution on several plans along z axis.***

# 8. Conclusion

Here we have demonstrated the development of an efficient, accurate and powerful nanoprocessing apparatus. The device is multifunctional, high flexible with a strong hardware and software environment which allow a high range of applications and performances.The development of this tool opens the door to many applications using low average power femtosecond laser pulses.

The workstation is compact and designed to be coupled with low average power laser systems which are more cost-effective and reliable compared to amplified laser systems (µJ or mJ/pulse).

However some questions concerning effects of the repetition rate laser pulses on the matter need more investigations. This is the topic of the next chapter.

# Chapter III

# Effects of high repetition rate femtosecond pulses on metals

# 1. Introduction

In this chapter we investigate the processing time of metals with femtosecond laser systems. Indeed, ultrafast laser pulses are becoming more and more interesting for industrial applications, so the processing time becomes an important factor in order to evaluate the economical interest of femtosecond processing. Moreover, a study of the influence of the repetition rate on the processing time puts in evidence a linear relation. These results are based on ablation rates obtained for repetition rates in the range of kilohertz. The following of this chapter is devoted to a study of the interaction between high repetition rate laser pulses and the matter in order to obtain ablation rates in the megahertz repetition rate range. A part consists of a discussion of effects of this interaction from results observed in the literature concerning dielectrics, metals and semi-conductors. Then an analysis of a dedicated experiment of interaction with copper is presented. Observations are discussed and a qualitative explanation is suggested.

## 1.1. Processing time

High precision machining with femtosecond pulses can be very time consuming due to the small amount of material removed per pulse. As ultra-short laser pulses have a growing interest for industrial applications, the processing time becomes a key factor to evaluate the economical interest of femtosecond processing. An efficient ablation rate can be determined for each material, in a corresponding fluence range [97][98][99][100][101].

### 1.1.1. Analytical method of processing time calculation

In order to calculate the processing time, it is necessary to know the number of pulses arriving at a point on the target. From the ablation rate of removal, it is possible to estimate the minimum time process laser cutting or machining.

The number of pulses ($N_p$) needed to cut through a sample of thickness (e) can be easily deduced, knowing the ablation rate per pulse ($L_a$):

$$N_p = \frac{e}{L_a} \qquad (3.1)$$

The number of pulses also depends on machining parameters: the sample translation speed (V), the size (ω) of the beam waist and the intensity profile (Gaussian shaped spot and a top-hat shaped spot). During the machining, laser spots on the material are spaced by a distance (d) (eq. 3.2), depending on the sample translation speed (V), and divided by the repetition rate of the laser (f).

$$d = \frac{V}{f} \tag{3.2}$$

This distance must be shorter than the spot diameter; otherwise some no machined areas will appear. Let us define $N_{pulses}$ as the number of pulses which overlap on the spot diameter distance D. In the case of a top-hat profile, the total number of pulses is expressed as:

$$N_{pulses} = \frac{D}{d} = \frac{D.f}{V} \tag{3.3}$$

Figure 46 gives a representation of how pulses are stacked on the material in the case of a top-hat shaped intensity profile. For a given point, the number of pulses is an integer. We can have a different value in the whole affected area. However, (eq. 3.3) gives decimal results since this equation takes into account the movement of the sample, so the result corresponds to the average number of pulses which reach the surface along the groove.

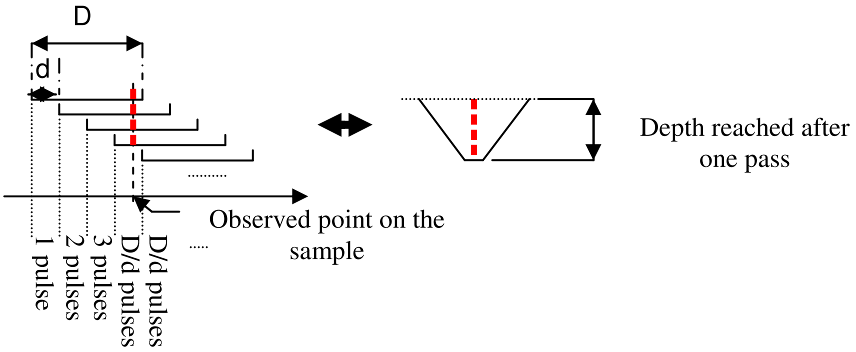

**Figure 46** ***Schematic representation of stacked pulses in the case of top-hat shape.***

In the case of the Gaussian profile, non-integer values are obtained as total number of pulses. Although (eq. 3.2) can still be used to calculate the distance between each spot, the Gaussian shape has to be taken into account in the stacking procedure (Fig. 47). Hence, the total number of pulses on the material becomes:

$$N_{pulses} = \sum_{i=-\infty}^{\infty} \exp(-2(\frac{i.d}{\omega_0})^2) \qquad (3.4)$$

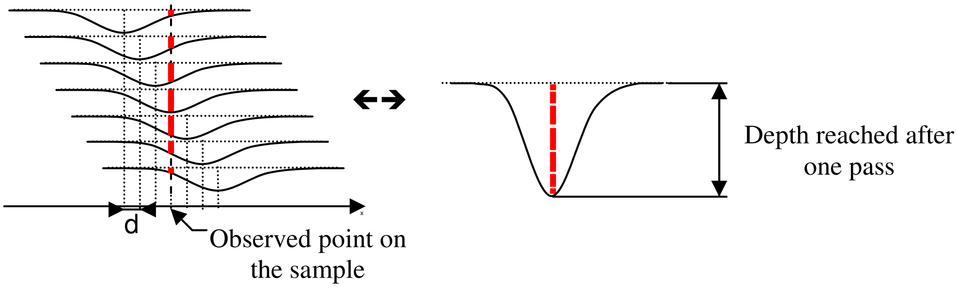

**Figure 47** ***Schematic representation of stacked pulse in the case of a gaussian shaped intensity profile***

In order to determine the processing time, the number of passes (n) needed to reach the desired depth (e) has to be taken into account. In the case of a top-hat profile, this number of passes can be simply obtained by dividing (eq. 3.1) by (eq. 3.3):

$$n = \frac{V.e}{D.f.L_a} \qquad (3.5)$$

In the case of a Gaussian profile, the number of passes is obtained by dividing (eq. 3.1) by (eq. 3.4):

$$n = \frac{\frac{e}{L_a}}{\sum_{i=-\infty}^{\infty} \exp(-2(\frac{i.d}{\omega_0})^2)} \qquad (3.6)$$

Finally, the processing time depends on the length of the groove (l), the number of pass and the speed (V)

$$t = \frac{l.n}{V} \qquad (3.7)$$

From equations (eq. 3.5), (eq. 3.6) and (eq. 3.7) processing time for a top-hat (eq. 3.8) and Gaussian intensity profile (eq. 3.9) can be expressed as:

$$t = \frac{l.n}{V} = \frac{l.e}{D.f.L_a} \qquad (3.8)$$

$$t = \frac{l.n}{V} = \frac{l.e}{V.L_a.\sum_{i=-\infty}^{\infty}\exp(-2(\frac{i.d}{\omega_0})^2)} \qquad (3.9)$$

Obviously these times correspond to “physical” times since there are deduced from the ablation rates. They correspond to the minimal value that can be observed during machining.

### 1.1.2. Results and discussion

Two laser sources have been used. A 1 to 5 KHz commercial laser with a pulse width of 120 fs, an average power of 2 W, corresponding to a maximum of 400 µJ per pulse at 5 kHz and a 1 to 10-kHz-repetition rate prototype laser system (Thales laser, France) which is based on a single and non-cryogenic regenerative amplifier [102]. This latter has a pulse energy of 350µJ at a 10 kHz with a 60 fs pulsewidth. By overclocking the pump it is possible to reach a 15 kHz repetition rate.

The laser beam is focused through a lens with a focal length of 50 or 200 mm. A polarizer and a half-wave plate are placed in the laser beam path in order to control the laser power. In this experiment two beam shapes are used. The Gaussian profile of the laser and a filtered beam using an adjustable diaphragm in order to obtain a controllable top-hat shaped spot at the image plane of the diaphragm. The size of the top-hat shaped spot is experimentally controlled by measuring the diameter of the impacts with an optical microscope.

The metal samples, copper (Goodfellow, purity: 99 %,) and stainless steel (Goodfellow 316L) have a thickness of 25 µm and/or 50 µm. The samples were mounted on an accurate microprocessing workstation composed of x,y,z motorized translation stages. The accuracy of translation stages is given to be +/- 3 µm with a repeatability of 0.1 µm, with speeds up to 500 mm/s.

Processing time measurements have been performed on copper and stainless steel samples in the case of a very simple machined pattern which consists on drilling a 3 mm radius disc at 9 mm/s until the disc drop down. The purpose is here to have direct access to “physical” times since other potential contributions to machining times (computing, mechanical) can be neglected considering such simple pattern. Measurements are performed using a 5 kHz laser repetition rate, and a fluence of 2.5 J/cm². This fluence has not been chosen haphazard. As already mentioned in the introduction, there is an optimal fluence for which good quality and high ablation speed can be obtained [97]. To investigate on the pertinence of the processing time analytical solution compared to measurements, drilling with a top-hat shape was tested on copper and with a Gaussian shape on stainless steel.

### a) *Case of copper*

Thanks to the calculations of Colombier *et al* [97], the ablation rate corresponding to the optimal fluence of 2.5 J/cm$^2$ is given to be 100 nm/pulse. This value was taken for the processing time calculation. Two samples of copper have been machined, one with a thickness of 25 µm, and the other of 50 µm. The machining was performed through the whole thickness of the sample. The spot diameter for the top-hat profile was 100 µm. We found that for the 25 µm thick copper sample, the experimental processing time is 9s, in good agreement with a calculated time of 9.4s. In the case of 50 µm thick copper sample the experimental and calculated processing times were 19s and 18.8s respectively.

Obviously, the calculated processing time is critically dependent on the chosen ablation rate value. The theoretical value of 100 nm/pulse taken is in good agreement with experimental results found in the literature [97][98][99][100][97]. Processing times calculated with these experimental values are shown in table 1.

| Experimental ablation rate (nm/pulse) | Experimental laser conditions | Calculated processing time for experimental ablation rates at 2.5 J/cm$^2$ (thickness = 25µm) (s) | Difference with measured experimental processing time (%) |
|---|---|---|---|
| 120 [97] | 10 Hz, 800 nm, 150 fs | 7,8 | -13 |
| 115 [98] | 1 khz, 800 nm, 120 fs | 8,2 | -9 |
| 120 [99] | 1 khz, 800 nm, 100 fs | 8 | -11 |
| 90 [100] | 100 Hz, 775 nm, 150 fs | 10,4 | +15 |
| 100 [97] | 20 Hz, 800 nm, 70 fs | 9,4 | +4 |

**Table 1** ***Comparison of calculated processing time with experimental ablation rates from literature at 2.5 J/cm$^2$ for copper.***

### *b) Case of stainless steel*

#### i. Processing time

For stainless steel, theoretical values of ablation rate are difficult to obtain since it is an alloy. Ablation rate has been experimentally deduced. Results are reported on the fig. 48 with also results from the literature [98][97][105]. As a remark, one can observe that for low fluences, values are in reasonable agreement but it has to be noticed that rather different values are obtained at higher fluence above 8 J/cm². For fluences around 2.5 J/cm² the averaged value of the ablation rate is taken to be 40 nm/pulse. This value has been used for the calculation of the processing time. Measurements and experiments have both been made with a Gaussian beam profile at 1 KHz, with a waist $\omega_0$ of 15µm on a sample with a thickness of 50 µm.

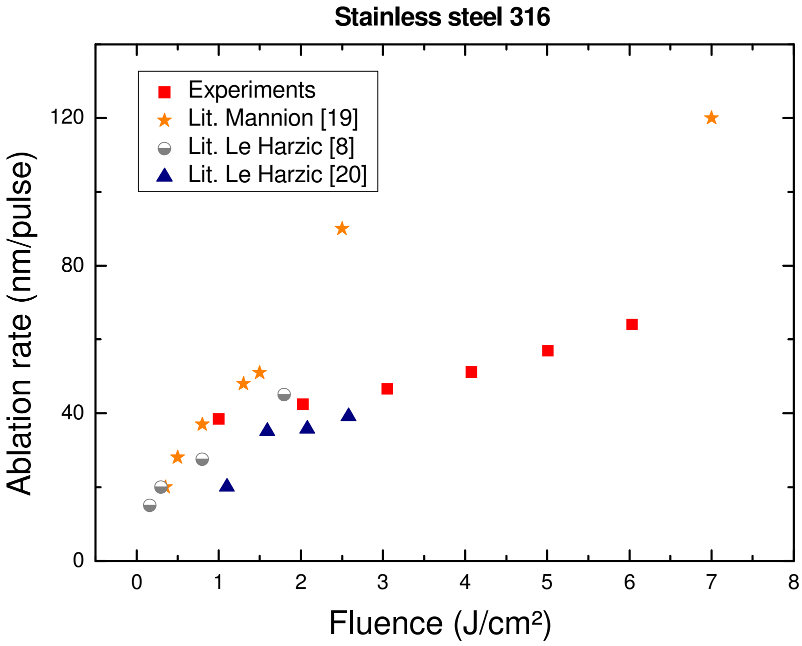

**Figure 48** ***Ablation rates in literature of stainless steel depending on the fluence.***

The experimental and calculated processing times were found to be 258 s and 250 s respectively. Experimental measurements are in quite good agreement with calculated processing times.

Both analytical solutions we proposed, i.e. for a top-hat and a Gaussian beam profile configuration, seem to be pertinent at the optimal fluence range. For the top-hat shaped spot in the case of copper, the difference between the calculated and the measured processing time is less than 1%. For stainless steel, with a Gaussian shaped beam the difference is around 3%.

### ii. Influence of the repetition rate

A study of the influence of the repetition rate on the ablation rate has been performed here. Micromachining of grooves has been done using various laser repetition rates of 1,5,10 and 15 kHz and varying proportionally the translation stage speed. Experimental ablation rates versus fluence are given in fig.49 for the four repetition rates. At 1 and 5 kHz results are comparable. It is not adequate to give an interpretation to slight observed variations of the ablation rates, but it seems reasonable to conclude that the ablation rates remain in the same range of value around 50 nm/pulse not far from the average experimental ablation rate obtained at 1 kHz (fig.48). So we can assume that the ablation rate is mainly constant from 1 kHz to 15 kHz. As a consequence, up to 15 kHz, the processing time reduction is proportional to the increase of the repetition rate. Thus a reduction of the processing time can be expected in a quite linearly manner by increasing the repetition rate. This result opens the way to shorter manufacturing times with higher repetition rates, with of course the same quality.

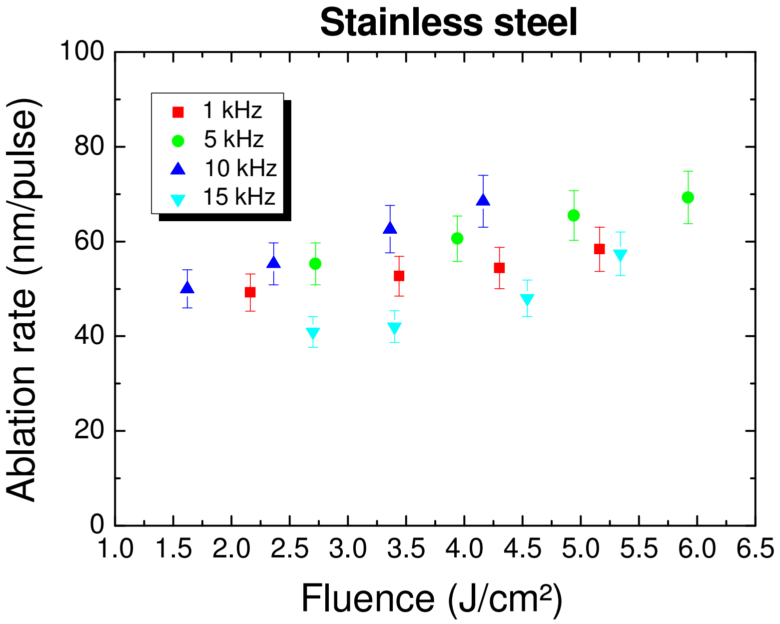

**Figure 49** ***Ablation rates of stainless steel depending on the fluence for 1, 5 10 and 15 kHz.***

## 2. Overview of high repetition rate pulses effects on matter

### 2.1. Case of dielectrics

Heat accumulation effects are well known to induce structural changes in the bulk of dielectrics. One of the most famous applications is the writing of waveguides inside the bulk of dielectrics. The refractive index changes produced open the door to three dimensions optical devices fabrication. Among possible applications we can cite three dimensional binary data storage [89][90][91], the direct writing of single and multi-mode optical waveguides (fig. 50) [92][93][94][95], optical splitters [96][106] and waveguide amplifier [107].

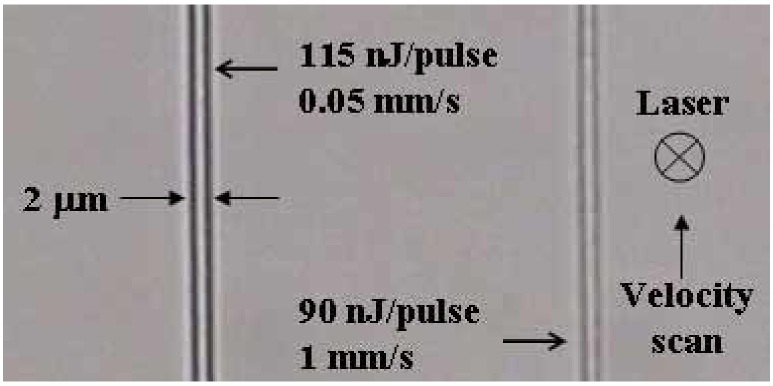

**Figure 50** ***Exemple of waveguides written into fused silica with a 522 nm femtosecond laser at a repetition rate of 1 MHz [108].***

By focusing femtosecond laser pulse inside a transparent material, the intensity reached in the focal volume can be high enough to make non-linear absorption occurring. In most cases multiphoton ionization provides seed electrons for avalanche ionization which leads to the formation of an optically dense plasma [109]. If sufficient energy is deposited by this nonlinear absorption, permanent structural changes are produced. The mechanism explaining these permanent induced changes have not been firmly established yet. One of proposed mechanisms for creating small refractive index changes is thermal. The material is melt by the energy deposited by the laser, and the subsequent resolidification dynamics lead to modify the density in the focal volume [111].

### 2.1.1. Heat accumulation phenomenon

In femtosecond lasers, we have to distinguish amplified femtosecond lasers and oscillators' femtosecond lasers only. Micromachining using one or the other is different. The difference comes from repetition rates. Amplified femtosescond laser system provides pulses spaced in time by milliseconds. This delay is much bigger than the time needed for heat to diffuse out of the focal volume. For fused silica, the heat is diffused out after 1µs for 1µm$^3$. The temperature of this volume gets back to the room temperature before the arrival of the next pulse. Consequently structural changes occur only in the focal volume. As we can see on the fig. 51 the number of pulses has therefore no impact on the heat accumulation.

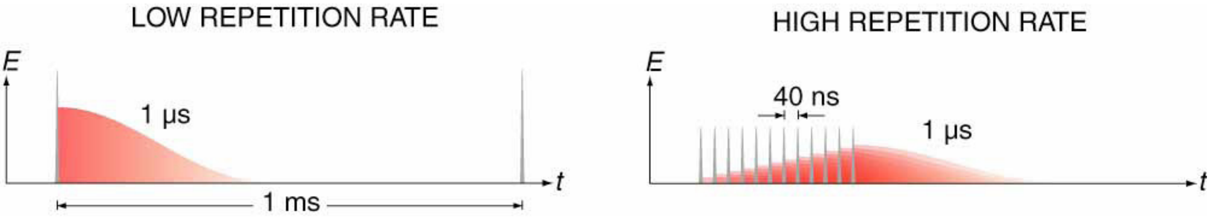

**Figure 51** ***Energy deposition in a material with low and high repetition rates. In the first case, the energy deposited by each pulse diffuses out of the focal volume before the next pulse arrives. In the case of high repetition rate, the energy deposited by one pulse can not diffuse out before the next pulse arrives. This energy accumulates with the energy of following pulses [112].***

Contrary to amplified systems, pulses from an oscillator system are separated by tens of nanoseconds. This time is much shorter than the time needed by heat to diffuse out, consequently the temperature can not decrease until the room temperature. So when the next pulse arrives, its energy is stored up at the focal volume, inside the bulk of the material. More pulses arrive at the focal volume, higher the temperature is, and larger the affected area is. If the temperature exceeds the melting point of the material, structural changes occur. It has already been demonstrated melting and resolidification of the material up to a radius of 50 µm from a laser spot size of 1 µm [94][110] [111]. This underlines that it is possible to control micromachined features size by simply varying the number of pulses. Fig. 52 shows results of experiments obtained with a femtosecond laser at 1045 nm and 450 nJ per pulse in AF45 borosilicate glass [113]. We clearly see the dependence of the size with repetition rates, number of pulses and fluence. The size of features obtained is much bigger than the spot size. This puts in evidence that heat accumulation effect is significant.

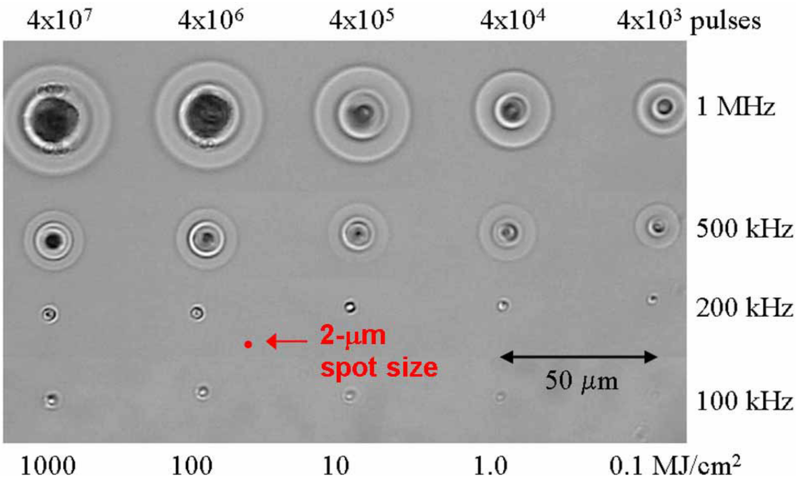

**Figure 52** ***Optical picture showing the dependence of the size of features depending on repetitions rates, fluence and number of pulses. Impacts were performed with a 1045 nm femtosecond laser and with 450 nJ per pulse in AF45 glass [113].***

Repetition rate is another parameter which can influence the size of features. We could expect that N pulses at the same energy deposit the same energy than one pulse contained the sum of energy brought by all pulses. But the energy of several pulses is not deposited in the same way than a single pulse [112]. Indeed for the same energy per pulse, the time between two pulses will be significant on how heat accumulation occurs. A calculation has been done at a distance of 2 µm from the center of the beam. An example of calculation is given which has been done for different repetition rates of 0.1, 0.5 and 1 MHz. Results have been represented on the fig 53 [113].

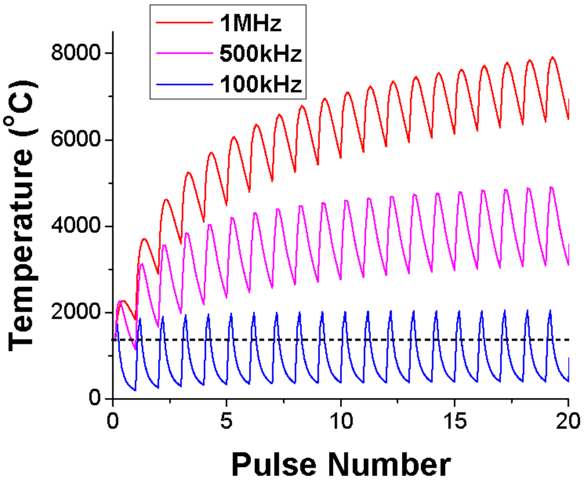

**Figure 53** ***Comparison of heat accumulation for different repetition rates of 100 kHz, 0,5 MHz and 1 MHz. These results were obtained thanks to a finite-difference model of glass temperature at a radial position of 2 µm from the center of the laser beam [113].***

The horizontal dashed line represents the 1225 °C working point of AF45 glass. For the lowest repetition rate of 100 kHz the temperature decreases below the working point before the arrival of the next pulse. Consequently the heat accumulation is not significant. For higher repetition rates of 0.5 and 1 MHz, we clearly see heat accumulation. This increase of the temperature leads to a melted volume which increases with the increase of the pulse number and the repetition rate.

### 2.1.2. Hillocks phenomenon

We have to notice that thermal effects with very small energies per pulse can induce strange features formations. For example, formations of hillock shaped damages have been observed. These features have been obtained with specific parameters using a single pulse for machining fused silica and borosilicate glass, with pulse energy of 5 nJ and a spot size of 0.7 µm. For higher pulse energies, crater-like ablation sites including debris deposition were observed. This hillock formation at a damage site is consistent with the mechanism of Coulomb explosion driving the ablation. This mechanism has been confirmed for crystalline dielectrics such as Al2O3, NaCl, and BaF2 [114][115][116].

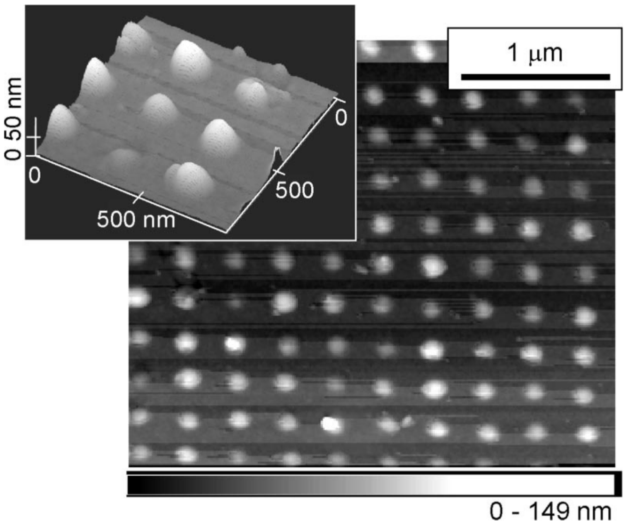

**Figure 54** ***AFM image of bumps obtained on glass surface with a single pulse of 180 fs and 5 nJ energy [117].***

The formation of hillocks occurs without melting neither crater pitting. It seems that the material starts to leave before melting or vaporizing occurs. The fig. 54 illustrates bumps obtained on the glass surface by a single pulse of 180 fs with energy of 5 nJ [117]. The bumps are estimated to be 40-70 nm high. Lateral dimensions of the damage site were 4 to 6 times smaller than the spot size on the sample. These dimensions put in evidence that a multiphoton phenomenon induced this mechanism. Indeed, inside a transparent material, as one photon of visible light has not enough energy to excite an electron from the valence to the conduction band, so a transparent material does not absorb the laser light linearly. In order to excite an electron over this gap, several simultaneous photons are necessary so that the total energy of all photons equal or greater than the band gap of the material. This multiphoton effect is achievable with focused high intensity laser pulses, especially in the centre of the beam where the intensity is the highest.

## 2.2. Case of metals

Due to high concentration of free electrons, metals have a very good conductivity. Metals are good electric and heat conductors. As said in chapter I, fabrication of nanostructures is possible by direct ablation with tightly focused femtosecond laser pulses with a resolution down to some hundreds of nm. However, due to specific interactions between metals and femtosecond laser pulses, other phenomena appear like porosity. Submicrometer structures fabrication with femtosecond laser pulses can be dominated by solidified flow dynamics in molten material [118]. Two phenomenons are presented here which differ from ablation and machining of holes or grooves.

In literature, the hillock phenomenon has been observed on metals. In the case of metals, results were obtained with pulses of 130 fs and a repetition rate from 1 Hz to 1 kHz on chromium film of 80 nm thick deposited on a quartz substrate. In these experiments, formations of microcolumns were observed after cumulative pulses with energy close to the ablation threshold [119]. Fig. 55 illustrates result observed with AFM. We see clearly that microcolumns protrude from the surface. From the profile of this formation, it has been possible to measure the height which is more than 100 nm and corresponds approximately to the original thickness of the metallic film. According to the authors, this mechanism of microcolumns formation consists of porosity. This porosity occurs

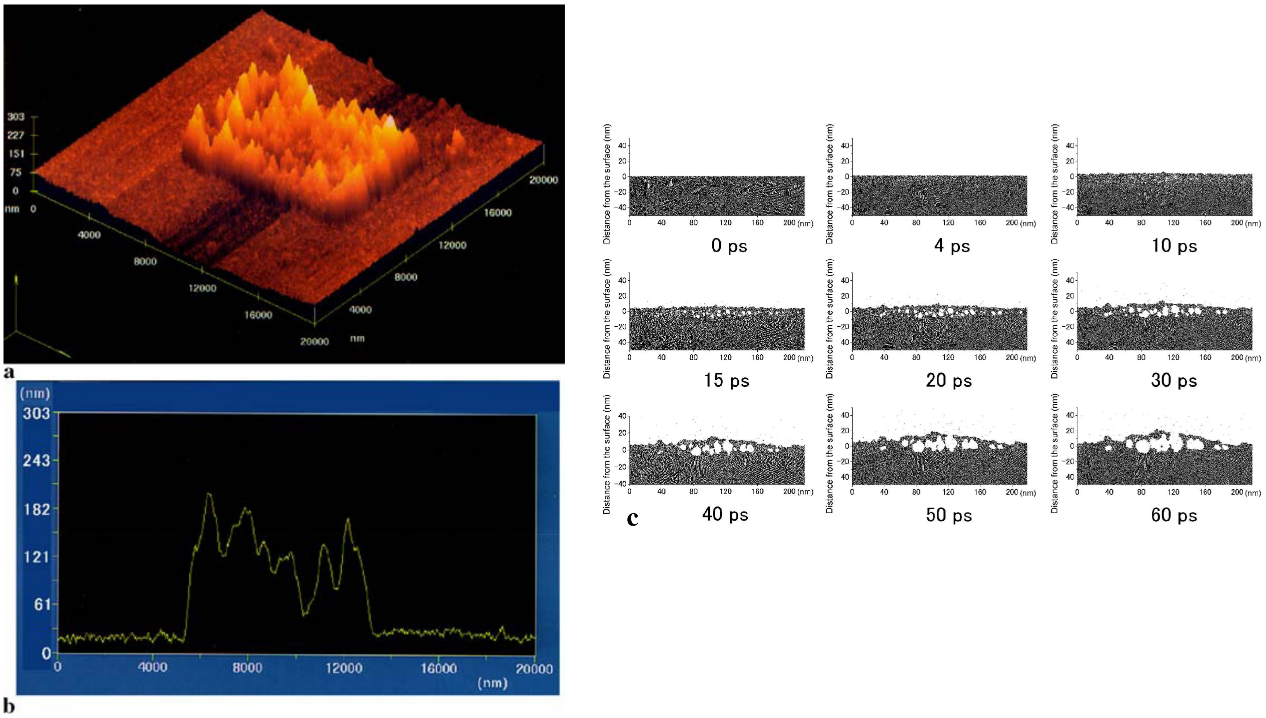

**Figure 55** ***AFM pictures of microcolumns obtained after 500 pulses on 80 nm thick chromium film. (a) 3D profile of microcolumns, (b) line profile. (c) Snap shots from MD simulation of the surface instability. We can clearly see the formation of the porosity [119].***

From a MD (molecular dynamics) simulation, they have been able to get snap shots (figure 55 (c)) of an irradiated surface by pulses energies close to the ablation threshold and put in evidence the effect of the porosity which evolves depending on the cumulative pulses. Even if pulse width is of the femtosecond order, surface instability occurs in picosecond order and results from the absorption process on the principle of a relaxation function. If porosity evolves by repetitive irradiation, the surface would rise higher and higher. This porosity formation is caused by insufficient energy to remove the material from the surface.

As said in chapter I, femtosecond laser pulses induce in metals a strong thermal non-equilibrium between electrons and lattice of ions. The relaxation of this non-equilibrium occurs after the laser pulse and depends on several materials properties. A slow increase of the temperature of the lattice results in a longer existence of the molten phase, in consequence this increase influences ablation results. High repetition rates might lead to melting and increased heat affected zones. The fig. 56 shows an example of molten stainless steel obtained at higher repetition rate by Ancona *et al.* [120]

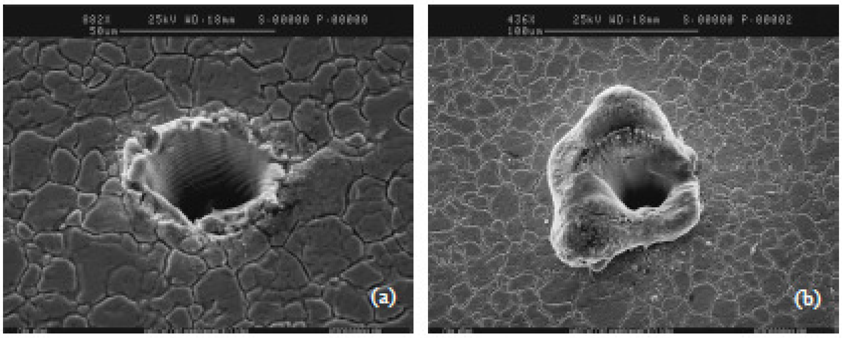

**Figure 56** ***SEM pictures of holes obtained with percussion drilling technique with energy of 30 µJ at (a) 100 kHz and (b) at 400 kHz[120] .***

Both of these holes have been performed with the same pulse energy of 30 µJ but with different repetition rates. In the first case (fig. 56 (a)), the hole has been drilled at 100 kHz. In the case of 400 kHz (fig. 56 (b)), we can clearly see a big bump of molten material all around the hole. This indicates that at a repetition rate higher than 100 kHz, heat accumulation has to be taken into account and can influence the size and the shape of machined structures. The same kind of phenomenon has been observed on thin film of gold by Koch *et al.* [118]. The fig- 57 illustrates results obtained on gold and chromium 100 nm thick films performed by one pulse. We can see a strong melting dynamic whereas no visible melt material in the case of chromium. The pulse fluence used is 1.5 times the ablation threshold fluence. According to the authors, metals ablation occurs out of the molten phase for weak electron-phonon coupling of metals like gold whereas for metals with strong electron-phonon coupling like chromium, ablation occurs almost without melting [121], indeed, the energy transfer depends on the electron-phonon coupling as predicted by the two temperature model.

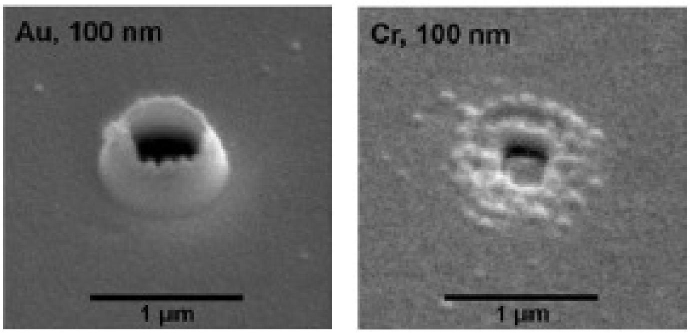

**Figure 57** ***SEM pictures of single pulse ablation of gold and chromium 100 nm thick films [118].***

As shown by [118] melting dynamics can be a way to fabricate sub micrometer metal structures by using complex processes occurring at the same time than ablation. The authors demonstrate the possibility to fabricate nanojets (fig. 58) on thin gold films. Nanojets always appear after a formation of a bump-like structure. This process induced by a femtosecond laser pulse in a molten gold layer is not yet fully understood.

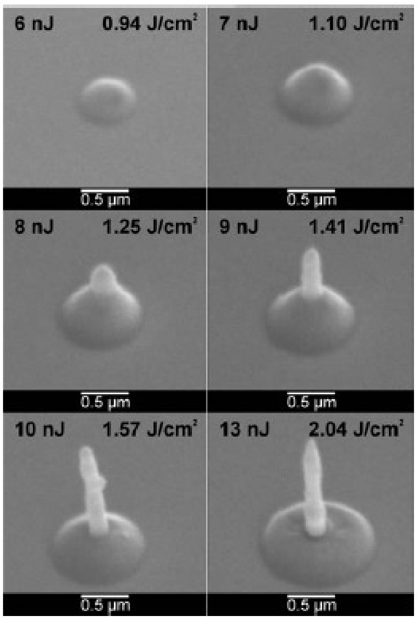

**Figure 58** ***SEM pictures of sub-wavelength surface structures produced in 60 nm thick gold film by focused femtosecond laser pulses with different pulse energies [118].***

## 2.3. Case of semiconductors

This phenomenon can also induce structures on semiconductors. In literature, embossed lines have been observed on silicon [122]. Authors observed three different regimes depending on the fluence and the scanning speed (fig. 59). At low fluence and high speed, they observed a slight modification with a colour-change but without breakdown of the material. With a higher fluence and a scanning speed adjusted in order to have a heat accumulation which reaches a constant temperature in the oxidation range temperature, embossed lines were created, until hundred of nanometers above the surface. Then, by adjusting fluence and scanning speed parameters in order to reach a temperature over the oxidation range temperatures, they observed material removal, and ablation occurs.

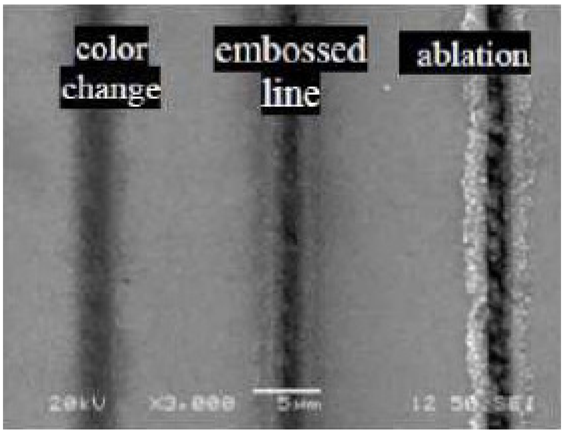

*Figure 59 Lines on silicon surface irradiated by femtosecond laser pulses at 1W and for several repetition rates, from left to right respectively : 8, 13 and 26 MHz[122].*

Authors do a proceeding description of the cooling cycle after irradiation. They start from a finite absorption and temperature-independent material parameters with a gaussian shaped beam. They use a single temporal-rectangular pulse. They approximate the analytical expression of the temperature cooling ([123]) in the laser irradiated point by:

$$\Delta T = \frac{I_a w_0^2 \tau_l}{4kt\sqrt{\pi D t}} \qquad (3.10)$$

where $I_a$ is the absorbed laser-light intensity, $w_0$ the radius of the laser focal spot, $\tau_l$ the pulse duration, $k$ the thermal conductivity, $D$ the heat diffusivity and $t = \frac{1}{f}$ pulse interval ($f$ is the repetition rate of the laser).

By taking into account laser parameters such as the intensity of the laser light on the sample, the repetition rate, the wavelength and properties of the material such as the reflectivity at 800 nm [124], authors demonstrate that it is possible to deduce the equation giving the temperature at the end of $N^{th}$ pulse irradiation and for a given energy per pulse:

$$T = N\frac{K(1-R)\times E_P \times f}{4k\sqrt{\pi^2 D t}} \qquad (3.11)$$

Recent simulations using various thermal models have shown that thermal oxidation of silicon takes place at temperatures in the range of 700~1300 °C [125][126][127][128][129] . In the following analysis, it is assumed that if the temperature of the silicon surface is brought up and kept in the range of 700~1300°C (1000~1600 K), oxidization occurs (let take 1400 K as average value). To reach the average oxidation temperature and to keep it more or less constant, one need $N_{P\text{-}T\approx 1400K}$= 15442 pulses to overlap at a constant scan speed of 4 mm/s.

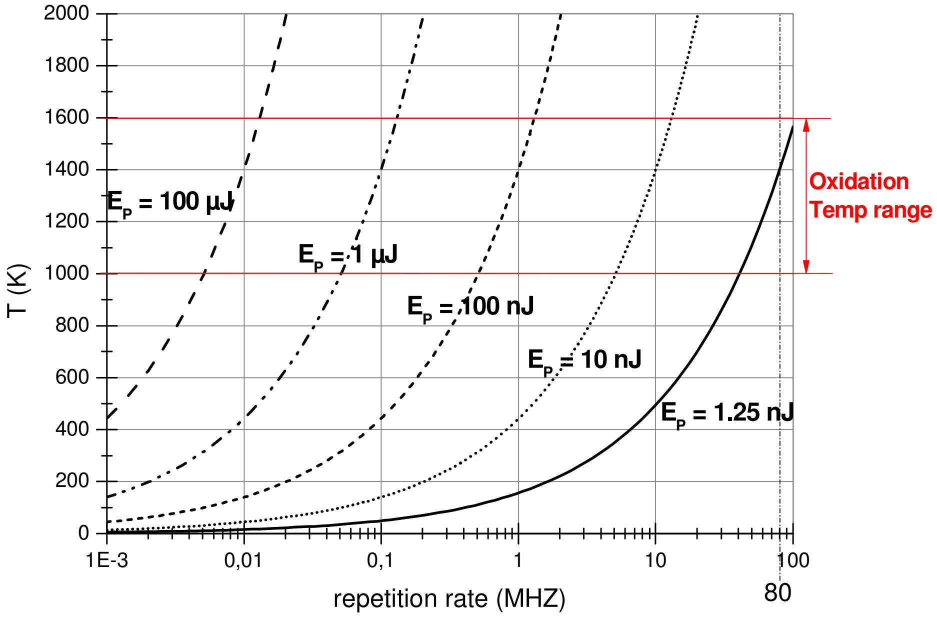

**Figure 60** ***Temperature reached after accumulation effects for different repetitions rates in the case of silicon.***

On fig. 60, we can see that for low repetition rates at very low energy per pulse (1.25 nJ) in the kilohertz range, it is not possible to reach the melting temperature, no heat accumulation is observed. However, every laser pulse deposits its energy in the irradiated region. One part of this energy is required for the plasma generation and bond breaking and an additional part is carried away by the ablation particles. However, a significant fraction remains in the irradiated region, which is diffusing into the surrounding material. For high repetition rates the time between successive pulses may not be long enough for the heat to diffuse out of the focal volume before the next pulse arrives. Consequently, the energy from successive pulses accumulates in and around the focal volume. Accordingly, the temperature of the substrate increases from pulse to pulse. Due to the increased substrate temperature a lower ablation threshold per pulse can be anticipated. Even more significant changes concerning the ablation efficiency can be expected once the temperature has reached the melting threshold. However, the heat accumulation is detrimental to the quality since a large amount of molten material is generated.

To conclude we can say that by using high repetition rates we see thermal effects due to heat accumulation, although laser matter interaction using femtosecond laser pulses is considered as athermal. The heat accumulation influences the formation of such protrudes of matter above the surface.

# 3. Experimental conditions and parameters

Experimental studies focus on effects of femtosecond laser pulses at high repetition rate on metallic samples, effects such as thermal accumulation. As said above, we use high repetition rate of 80 MHz, that means that each pulse is separated to the following pulse by a time delay of 12,5 ns. So short time delay should make thermal effects significant.

Studies have been made on copper. Very pure samples of copper are used (Goodfellow 99,9%). Experiments have been executed thanks to the device developed and described in chapter II. The use of oil immersion objective implies to take into account the modification and/or ablation threshold of oil. By focusing the laser into the oil, bubble formation occurs. The threshold of bubble formation is lower than the threshold sample. There is also bubble formation when the ablation of the material occurs. The optical index of these bubbles is different than the optical index of oil, so the laser beam is deviated and does not focus on the surface sample. So the ablation occurs in a blinking way. In order to avoid this problem while keeping the same numerical aperture, we use a glass microscope plate between the oil and the sample. This glass has an optical index close to the oil (1,5), and an ablation threshold much higher than the sample. Due to the thickness of the plate (170µm), the laser beam passing through the oil, before has not high enough intensity to reach bubble formation. This technique avoids the deviation of the laser beam when the ablation occurs. The fig. 61 illustrates the setup at the output of the objective.

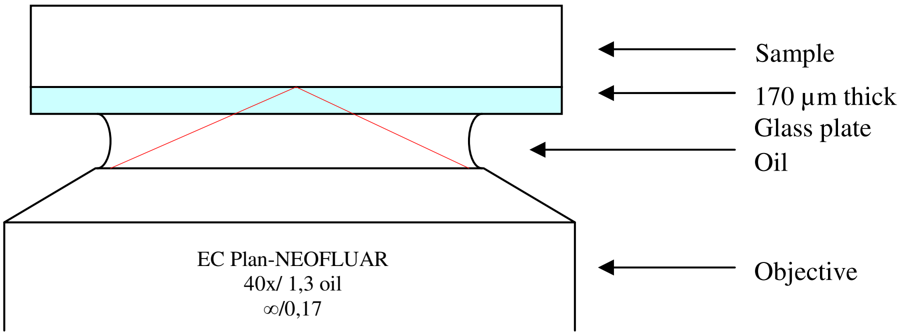

**Figure 61** ***Oil immersion setup at the output of the objective.***

Samples have been machined with a Gaussian shaped spot with a diameter of about 1.9 µm at 1/e² (see chap II). The power range investigated for this machining is 410 mW down to 0 mW. According to the fluence calculation method demonstrated in chapter II, the corresponding fluence range is 0.36 J/cm² down to 0. Machining pattern consists in doing groups of lines. Each group corresponds to a fixed fluence. In one group lines are spaced by 10 µm. Each group of lines are spaced by 30 µm. The number of passes by line in each group is 1, 2, 5, 10 and 20 passes. A long line is machined at the beginning of all lines in order to have a reference. The fig. 62 illustrates the pattern machined.

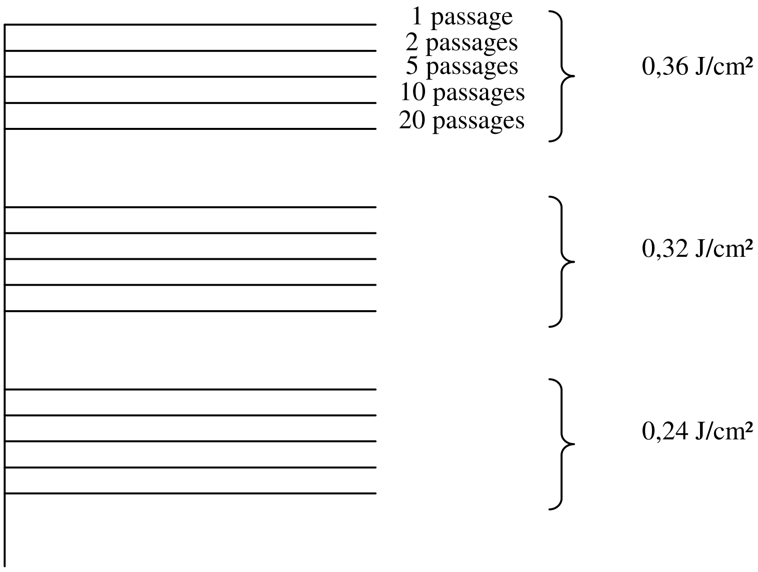

**Figure 62** ***Description of the pattern machined with different parameters.***

Experiments have been performed on copper. Three samples of each metal have been used. For each sample, one speed has been fixed: 10 µm/s, 50 µm/s and 100 µm/s. For cases of 50 and 100 µm/s, the number of passes follows the following scheduling: 1, 2, 4, 6, 8, 10 and 20 passes, but the pattern stays the same than previous. Results obtained on copper are presented in the following for each speed used and for three different fluences in order to give an overview.

## 3.1. Results

The fig. 63 illustrates structures obtained after cleaning with ultrasonic bath. Fig. 64 illustrates a 3D enlargement of AFM picture of grown matter.

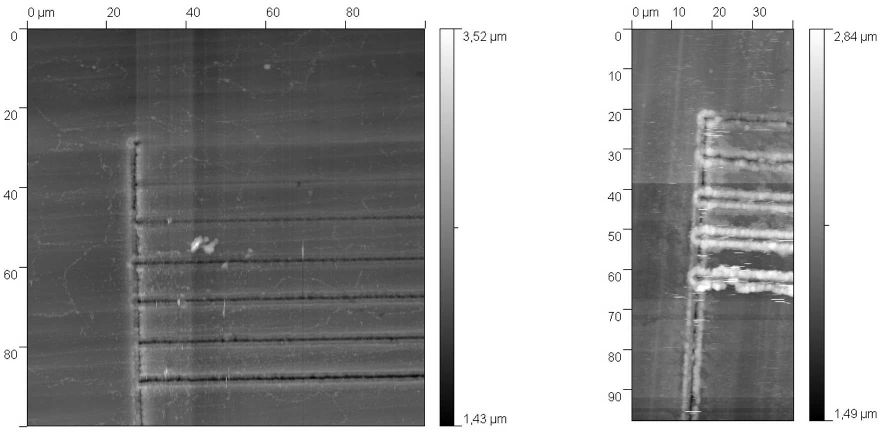

a) b)

**Figure 63** ***AFM pictures of structures obtained for 1, 2, 5, 10 and 20 passes for a fluence of 0.36J/cm² at (a) 100 µm/s and (b) 10 µm/s.***

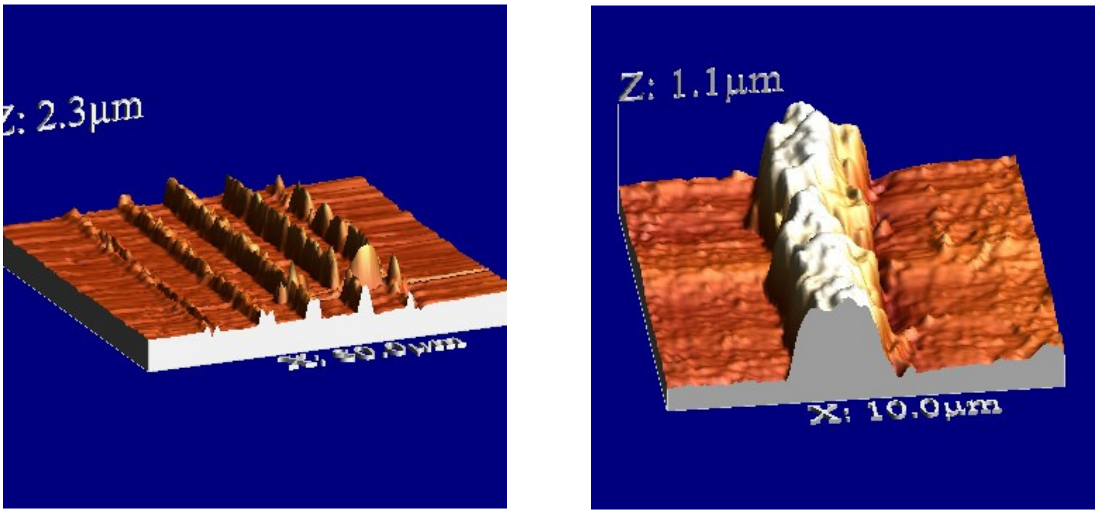

a) b)

**Figure 64** ***3D AFM pictures of growth matter for a speed of 10 µm/s at 024 J/cm²(a) and an enlargement of the line of grown matter after 10 passes(b).***

We see on these results many differences observed for different speeds in the case of copper. Each sample has been cleaned up in an ultrasonic bath of acetone. Two kinds of results appear. When the speed is high, the ablation seems to be the predominant phenomenon, we can see well-marked grooves, whereas for low speed, structures emerge above the surface thus it indicates that. another phenomenon seems to compete with the ablation.

Structures obtained at 10 µm/s seem to have a lot of molten material all along machined lines whereas for 100 µm/s, grooves are almost free of such phenomenon. Under certain conditions, we can see grooves at the top of “walls” of grown matter. In the following we present profiles for different cases. Characteristics of machined and grown matter are discussed.

AFM pictures have been taken both with the AFM of the Fraunhofer institute and also with the AFM of the LTDS of Lyon. Profiles presented in the following have been taken with a specific and powerful AFM imaging analysis freeware called Gwyddion 2.14. In order to have a good representation of such phenomenon along structures done, each profile line presented corresponds to an average of 30 profiles. Other figures of profiles are presented in appendix A. Hence, the height or the depth of structures can locally be even higher or deeper. We can see that we don't have only grooves, but we obtain structures like bumps, or walls which protrude from the surface. The height of these "walls" of matter is in the order of few hundred of nanometers (until 600 nm). All experiments have been done in the same optical conditions (same spot size and same range of power).

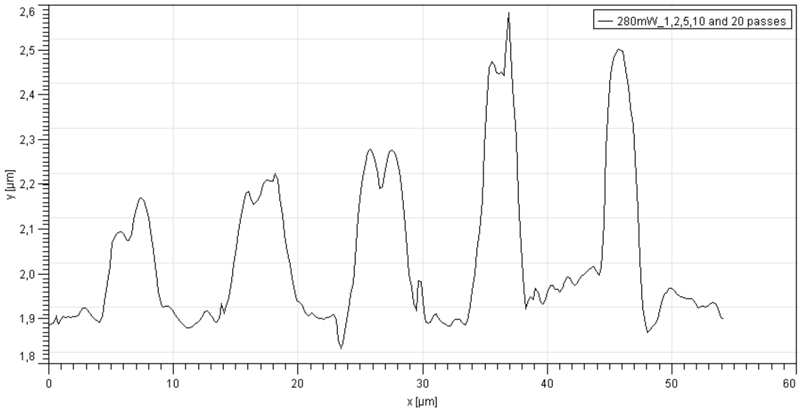

**Figure 65** ***Results on copper at 10µm/s at the fluence of 0.24 J/cm², and different number of passes, respectively from the left to right 1, 2, 5, 10, 20 passes.***

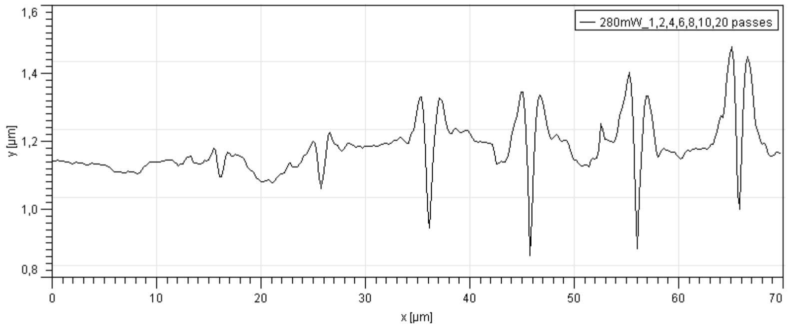

**Figure 66** ***Results on copper at 50µm/s at the fluence of 0.24 J/cm², and different number of passes, respectively from the left to right 1, 2, 4, 6, 8, 10, 20 passes.***

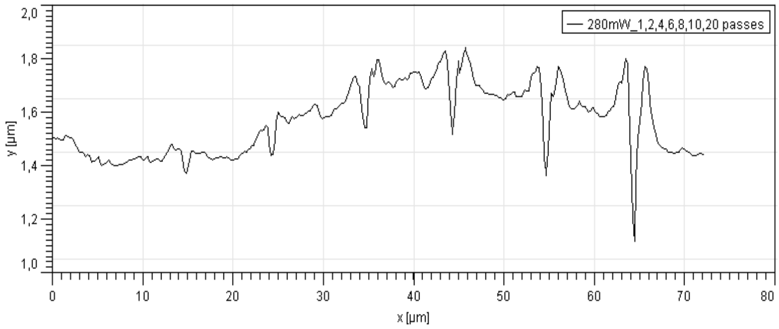

**Figure 67** ***Results on copper at 100µm/s at the fluence of 0.24 J/cm², and different number of passes, respectively from the left to right 1, 2, 4, 6, 8, 10, 20 passes.***

## 3.2. Discussion:

A quick analysis put in evidence the difference between results corresponding to different number of pulses. In the case of the speed of 10 µm/s, we obtain “bumps” or “walls” of molten matter whereas for 100 µm/s we obtained grooves with much less molten matter on the edge of grooves, which does not protrude so height from the surface. At the speed of 50 µm/s we obtained features which seem to be intermediate between structures obtained at 10 µm/s and structures obtained at 100 µm/s.

### 3.2.1. Heat accumulation effect on ablation rate

For 10 µm/s no groove are detectable so ablation rate has been studied only in cases of 50 µm/s and 100 µm/s. The depth of each groove has been measured. In order to avoid wrong values due to the size of the AFM tip, values which are the same than measured just before are not taken into account. Indeed, identical maximum values mean that the tip can’t go to bottom of the groove. For all lines and for each fluence, the depth has been averaged to one pass. Depth has been measured from the bottom of each groove to the surface level around the groove analysed.

| Fluence | 0.075 | 0.15 | 0.24 | 0.32 | 0.36 |
|---|---|---|---|---|---|
| Ablation rate (nm/pass) | 21 | 25 | 37 | 62 | 66 |

**Table 2** ***Ablation rate in nm/pass obtained for different fluence at 50 µm/s.***

| Fluence | 0.24 | 0.32 | 0.36 |
|---|---|---|---|
| ablation rate (nm/pass) | 26 | 29 | 30 |

**Table 3** ***Ablation rate in nm/pass obtained for different fluence at 100 µm/s.***

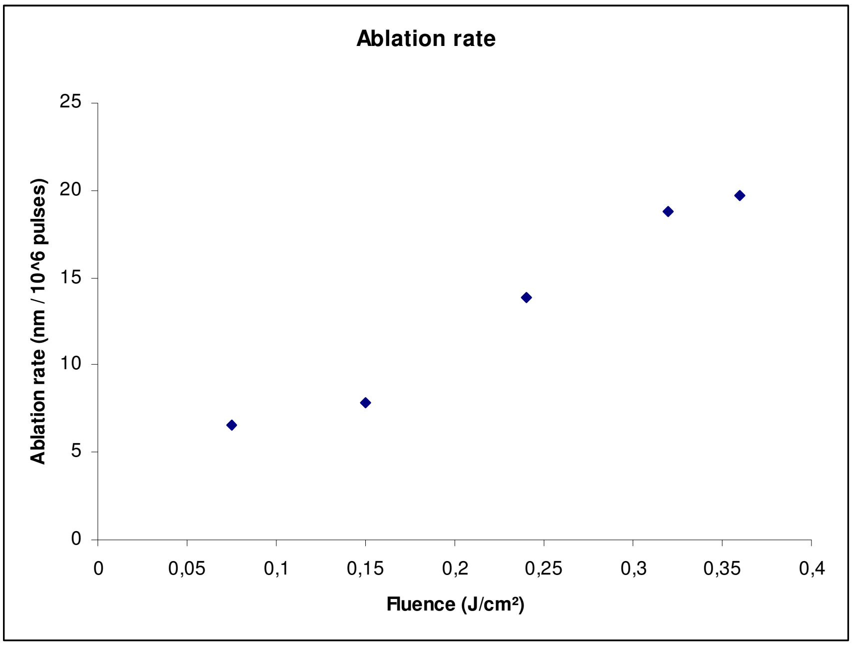

**Figure 68** ***Evolution of the ablation rate expressed in nm/10^6 pulses depending on the fluence.***

According to the literature, the ablation threshold of copper is estimated to be around 0.18 J/cm² [130] or 0.35 J/cm² [131]. The difference between these two values mainly comes from a difference between the methods for calculating the fluence. In the first case, the fluence is calculated in relation to the surface of the spot at 1/e² of the Gaussian beam, using the formula: $F = \frac{E_P}{\pi\omega_0^2}$, whereas in the second case, the fluence has been determined at the top of the Gaussian beam using the formula : $F = \frac{2E_P}{\pi\omega_0^2}$ as demonstrated in the chapter II. So there is thus a factor two between the two results. If we take into consideration the first value of threshold and we multiply it by two in order to get the value at the top of the Gaussian used, the threshold fluence value becomes 0.36 J/cm². In our experiment, this value corresponds to the maximal fluence used. However, at this fluence we see that ablation occurs, and even for fluences down to 0.075 J/cm², which is lower than reported in literature. This can be explained by the heat accumulation effect which occurs for high repetition rates. This effect enables machining of metals even with very low fluences. Ablation rates obtained are expressed for a very high number of pulses. Indeed, in this case, the ablation rate expressed for one pulse is so small, with a dimension of $10^{-6}$ nm/pulse, that would not be significant, moreover this ablation is due to an accumulation of many pulses.

### 3.2.2. Influence of speed and fluence on the height of protrudes

As illustrated on figures 65,66 and 67, two phenomena occur : ablation and growth of matter. The phenomenon of growth of matter is predominant for very low speeds. There are 10 times more pulses in the case of bumps than in the case of grooves. There are $16.10^6$ pulses per point, $32.10^5$ and $16x10^5$ for 10 µm/s, 50 µm/s and 100µm/s respectively. We can also see that there is a difference of height depending on the number of passes. For a given speed, more important the number of passes is, more high “walls” of molten matter are. This observation confirms the idea of the number of pulses as a factor of “walls” growing. The average growth has been calculated for each pass of the laser from the height of protrudes. Height is measured from the surface level around the protrude analysed up to the maximum of it. Values are reported in the table 4. The figure 69 illustrates the relation between the number of pulses and the growth of matter depending on the fluence.

| Fluence (J/cm²) | | 0.075 | 0.15 | 0.24 | 0.32 | 0.36 |
|---|---|---|---|---|---|---|
| growth (nm/pass) | 10 µm/s | 49 | - | 111 | 116 | 138 |
| | 50 µm/s | 21 | 22 | 25 | 25 | 24 |
| | 100 µm/s | - | - | 14 | 16 | 15 |

**Table 4** ***Growth of protrudes for each pass of the laser for (a) 10 µm/s, (b) 50 µm/s, (c) 100 µm/s.***

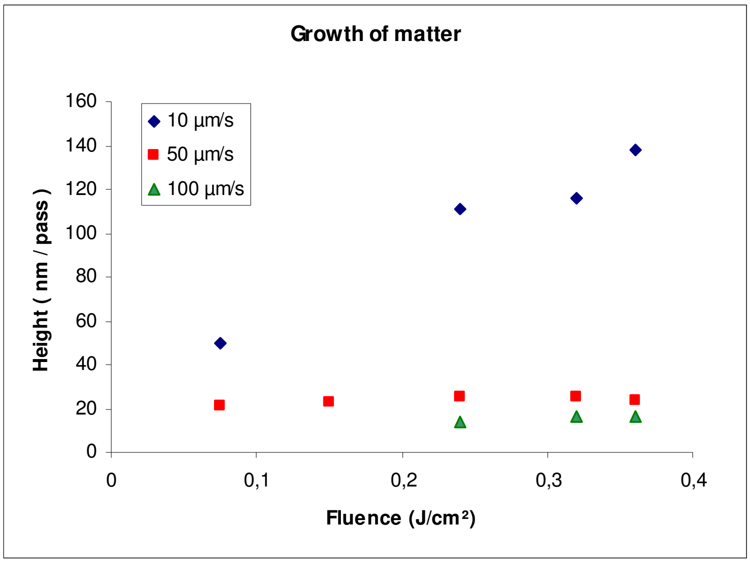

**Figure 69** ***Growth of the matter depending on the fluence for 10, 50 and 100 µm/s, the corresponding number of pulses are 16.10$^{6}$, 32.10$^{5}$ and 16.10$^{5}$ pulses respectively.***

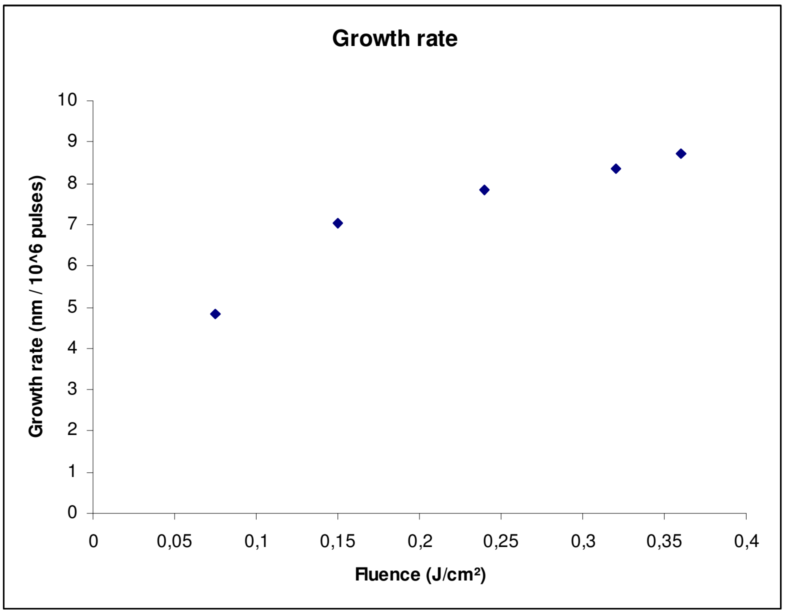

**Figure 70** ***"Growth rate" (in nm per 10$^{6}$ pulses) of the copper depending on the fluence.***

The figure 69 illustrates the average height of grown matter for each pass of the laser beam on the sample. We can see clearly that the dependence of the grown matter on the fluence is very significant only for a high number of pulses. Indeed, for speeds of 50 µm/s and 100 µm/s, the height of grown matter does not exceed 25 nm even for a high fluence whereas height reaches 138 nm at 10 µm/s. However, we can see that matter is slightly higher in the case of 50µm/s with a maximum of 25 nm, than in the case of 100µm/s where the maximum reaches 16 nm only. From this analysis we deduce a “growth rate” for many pulses as shown on figure 70.

We can see that the growth rate increases with the fluence. However, for highest fluences we can see on profiles that grooves inside protrudes appear. That shows that for high fluences, the ablation occurs and tends to get the upper hand. It suggests that for higher fluences the growth rate should present a kind of cut off value of fluence after which the ablation is the dominant process.

As said at the beginning of the chapter, a same kind of phenomenon has already been observed. At such repetition rate (80 MHz) and with a so high number of pulses a heat accumulation effect occurs. As we have seen using simulation results, the evolution of the temperature inside the material, even limited to four pulses, heat accumulation effect occurs. In the case of much higher number of pulses, the heat accumulation occurring should be thus much more important. We think that phenomenon is linked and/or of the same order than which occurred during growing of nanojets on gold film observed by [118]. As seen with simulations in chapter one, for an amount of constant energy, the temperature goes deeper and deeper inside the material depending on the number of pulses. If this hypothesis of the depth propagation of the temperature is verified, so we can say that with 10 µm/s the temperature increase on more important depths than with 100 µm/s. At this speed of 10 µm/s, there are $16.10^6$ pulses arriving on the material in 0.2s on a diameter of 2 µm. We think that the diffusion of the heat takes more time than the heat accumulation. The diffusion is constrained by the small volume where the heat accumulation occurs.

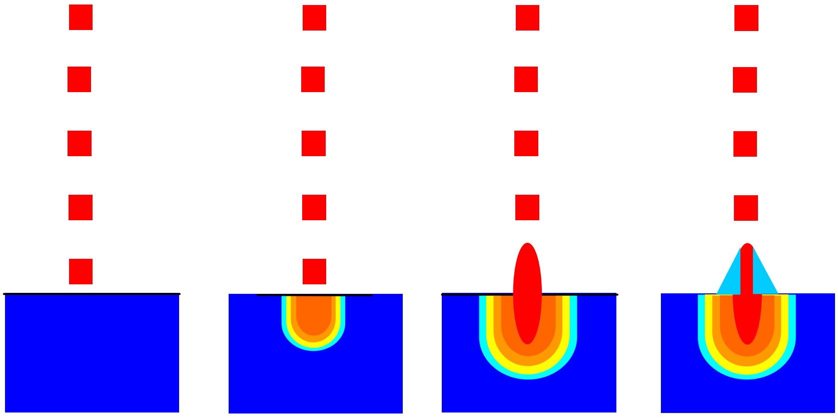

**Figure 71** ***Schematic representation of the presumed phenomenon of growth matter broken up in four steps. High repetition rate femtosecond pulses arrive on the material, then heat accumulation effect occurs inside the material until reaching the melting temperature and expands over the surface of the sample. Then solidification of the molten matter occurs.***

As we can see on profiles, for low fluences the growth of matter has a better appearance without machining effects inside. It suggests that a smoother heat accumulation effect tends to melt the material instead of ablate it. Once the temperature of fusion is reached, the material melts into the liquid state and so its volume is expanding. We can imagine that we have a cylinder under the surface of the material in which the temperature is higher than in the area surrounding. As the molten material is constrained by the solid colder material surrounding, the only possible outcome is at the surface of the material directly followed by a solidification of the material. The figure 71 gives a schematic representation in several steps.

# 4. Conclusion

The interaction of high repetition rate laser pulses on the matter induces phenomena which do not appear with lower repetition rate lasers. Indeed, the time delay between two pulses is so small that the energy stacked into the volume irradiated can not escape before the arrival of next pulses. Hence, an accumulation phenomenon of the energy occurs inside the material. This slow accumulation of small amounts of energy modifies the kind of ablation. Molten matter has been observed. It seems to grow up depending on the strength of the heat accumulation effect. Indeed, highest structures have been observed for the highest number of pulses interacting with the material. This new phenomenon depends on laser parameters. This implies that size and height of structures can be controlled. This open the way to a new field of applications using high repetition rate femtosecond laser pulses.

# Chapter IV

# Results and applications in biotechnologies

# 1. Introduction

Lasers have become irreplaceable tools in modern medicine, spanning a wide spectrum of applications from laser surgery [132] to optical imaging [133]. Laser ablation, which has the great advantage of precise material removal, is a promising method in processing and treatment of biological tissues [134][135][136], biodegradable polymers [137][138], dental implants [139], etc. In this chapter the potential of the multifunctional tool presented in chapter 2 for different applications in biotechnology is shown. Results on large area multiphoton imaging as well as nanoprocessing of biological tissue and various materials are presented.

## 2. Mapping of micro area

As describe in the chapter 2 in the section 5.3, the setup developed allows imaging a large area of a sample with high resolution. The field of view of a 40×/1.3 NA objective lens is of 0.625 mm. The magnification has been furthermore increased by a factor of about 10 x to obtain high detailed images through the focusing setup of variable lenses inserted before the CCD camera. After calibration, the final field of view is of 57x76 $\mu m^2$ and 70x90 $\mu m^2$ when using a lens of 300 mm and 250 mm focal length respectively. Two-dimensional matrix of images is captured and stitched in software to create a mosaic that displays a large field of view. As already said in chapter 2, the matrix of images is acquired with a continuous step-and-capture routine while translating the sample with the pizo-driven linear XY stages. Due to the high resolution translation stages, junctions of pictures are very fine with non significant overlapping. The software developed is high flexible, it allows to capture a undefined number of images in X and Y, with desired resolution and at any desired location. To minimize possible illumination vignetting effects, shading bands at the edges between pairs of neighbouring, images were corrected by brightness averaging. All images and the complete mapping are saved in bmp format. Processing routine and time of individual image capture, transferring, archiving and complete mosaic have been optimized to be relatively fast. Of course, it depends on the number and the resolution of individual images. The number of pixels of individual image can be selected in the software in order to find compromise between resolution and time processing. In the fig. 72, an example of a mosaic of 5 x 5 images of blood cells (standard size: 6-8 µm) is given.

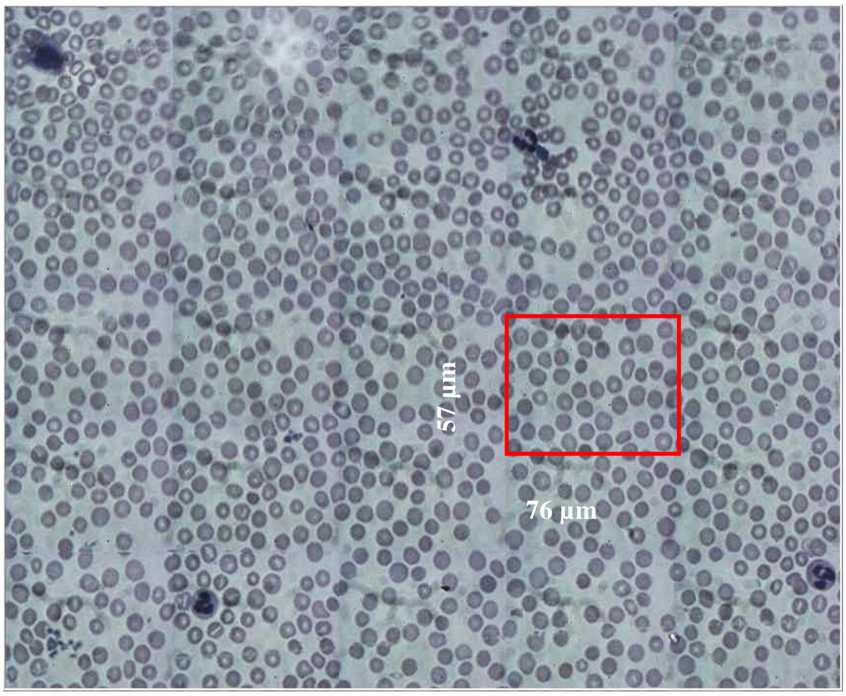

**Figure 72** ***Schematic representation of area mapping of blood cells.***

Each image consist of 1280 × 960 pixels, is 24-bit greyscale and requires 4,6 MB of memory. Thus, a mosaic of 5 × 5 images at full resolution consists of 6400 × 4800 pixels and requires about 115 MB of memory. For acquisition of a mosaic, a continuous step-and-capture routine requires around 30 s for 5 × 5 images. Transferring and archiving images followed by processing to create a mosaic requires another 60 s on a PC with a Pentium 2.2-GHz processor. Thus, total time to create a mosaic is 90 s. One can observe the high overlapping quality and the good illumination uniformity at the edges.

Such an image reconstruction allows high control and inspection of small features. Various examples are presented in the fig. 73: A large area mosaic of a 6 × 6 (a) and 12 × 12 (b) grid pattern performed on Su8 photoresist under lithography, a 5 × 5 mosaic of bird feather (c).

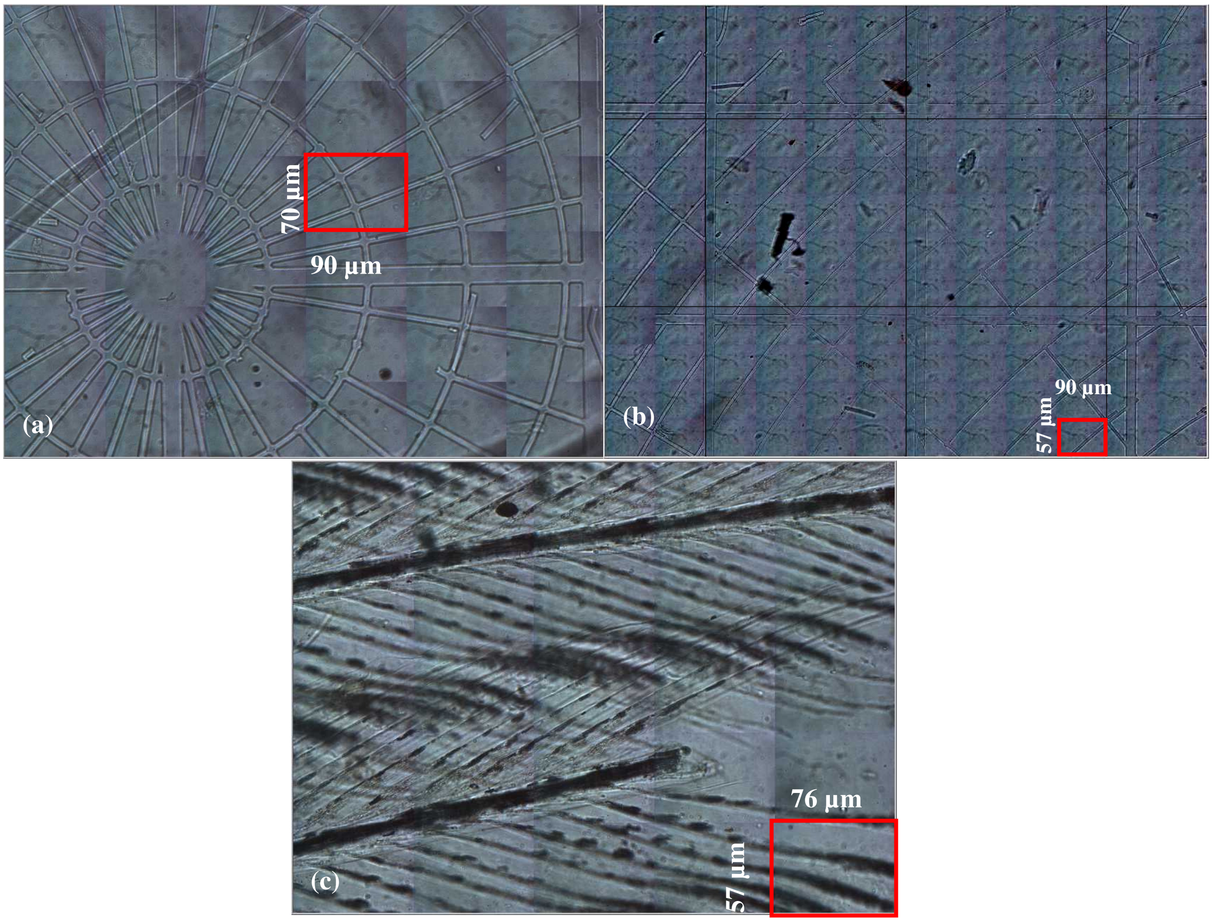

**Figure 73** *Mapping of 6 × 6 (a) and 12 × 12 (b) images of a grid pattern performed on Su8 photoresist under lithography, (b) 5 × 5 mosaic of a bird feather.*

The mosaicing system is also suitable for other kind of microscopy imaging as confocal or two photon laser scanning microscopy. Confocal microscopy is a technique for obtaining high-resolution optical images with depth selectivity [140]. Two-photon microscopy is a fluorescence imaging technique that allows imaging living tissue up to a depth of one millimetre [141]. For very thin objects such as isolated cells, single-photon (confocal) microscopes can produce images with higher optical resolution due to their shorter excitation wavelengths. In scattering tissue, on the other hand, the superior optical sectioning and light detection capabilities of the two-photon microscope result in better performance Two-photon excitation can be a superior alternative to confocal microscopy due to its deeper tissue penetration, efficient light detection and reduced phototoxicity. Nowadays, multiphoton microscopy typically uses sources like Ti:sapphire lasers with high repetition rate like 70 - 80 MHz and pulses duration shorter than 150 fs.

The large area mapping system has been coupled and tested with a commercial two-photon laser scanning microscope (TauMap, JenLab GmbH, Germany). The system is based on a conventional fluorescence microscope equipped with a high numerical aperture (1.3) objective, a special compact scanning module and a photomultiplier detector attached to the microscope ports. The laser “Mai Tai” used has already been depicted in the chapter 2. Single high resolution two photon images are performed by the scanner. The scan field of each image is limited to a maximal area of 350 × 350 µm² due to the high numerical aperture objective and the request resolution.

A sample composed of fluorescent sphere (beads) with different sizes has been mapped (fig. 74). The mosaic of 3 × 2 images has a dimension of 624 × 384 µm² (the size of each image is 192 × 208 µm²). Each individual image has a resolution of 512 x 512 pixels ant thus 1,5x$10^6$ pixels for the full mapping.

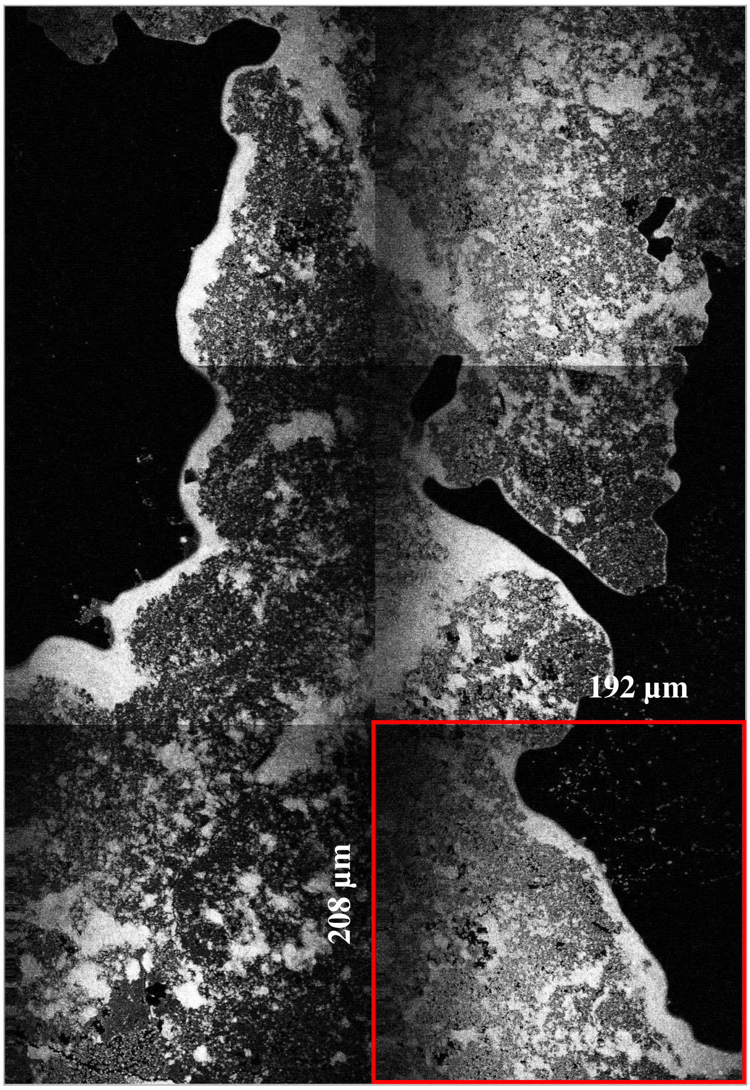

**Figure 74** ***Two-photon fluorescence large image assembly of a sample composed of different fluorescent beads.***

# 3. Targeting and nanodissection

Tissue processing with femtosecond laser pulses has been of growing interest since its high precision was demonstrated on a variety of different tissue types [142]. Due to its sub $\mu$m precision, it is possible to perform for example surgical procedures like refractive surgery inside the human eye [143]. Near-infrared (NIR) femtosecond laser pulses with low average power are novel tools for ultraprecise intracellular and intratissue surgery, cell isolation, tissue engineering, stem cell research, gene therapy, the production of DNA vaccines for examples. Multiphoton ablation can be achieved with low nanojoule energy laser pulses when using focusing optics of high numerical aperture. The high peak powers at a moderate average power provided by the pulsed laser in combination with high numerical aperture optics leads to photon fluxes of more than $10^{27}$ photons $s^{-1}$ $cm^{-2}$ and therefore high light intensities in the $TW/cm^2$ region at the target material. NIR light at such high intensities results in multi-photon absorption which leads via multi-photon ionization and avalanche ionization to an optical breakdown and the formation of a spatially confined micro-plasma [144][145]. It has been shown that processing of biological with a spatial resolution in the order of some hundred nanometer and lower is possible [146][147][148][149][150][151][152][153]. Nanodissection with ultra short laser pulses opens new horizons for scientists, who are primarily interested in investigation of cells, and tissues processes. High accurate, compact and flexible workstations as the one developed in this work are needed.

The mapping presented in the previous paragraph can be a useful tool to locate a precise position on a large area for enabling laser processing as for example cell perforation or applications for cell transfection, cell sorting, cell killing, etc. An option has been developed in the software which allows to select the point of laser impact directly by clicking on the mouse on the desired target everywhere on the area. The operation can be repeated as many times as request. The programmed software allows bringing back the position of the mouse dragged over the map. When clicking with the mouse, mouse pointer coordinates are recovered. Dimensions of the map are known thanks to the beforehand calibration. The initial position (0,0) of translation stages in their own referential corresponds to the center of the first picture taken. From this characteristic, pointer coordinates can be calculated and transposed to a micrometric coordinate system, and also in the translation stages coordinate system. It is therefore possible that for each click done on the map, to precisely move translation stages at the position on the sample corresponding to the position selected on the map. Then it is possible to perform static and non static machining as the cutting of lines or more complex patterns. Fig. 75 (a) shows a large histological image of a skin biopsy composed of the mapping of 5 × 5 individual images. The different layers and junctions of the skin are easily observable: the epidermis with the cells of the stratum corneum and the stratum spinosum, the stratum basale which define the barrier between the epidermis and the dermis, the stratum papillare in the dermis with observable collagen fibers. On this image, a schematic representation of the expected position of the laser impact which has been assigned by the mouse is represented before laser perforation. The fig. 75 (b) is the same image but with the effective laser impact (see arrow). Fig. 75 (c) and (d) are two other examples of laser perforation of respectively a blood cell and a micro-pattern performed in SU-8 photoresist, a biocompatible polymer.

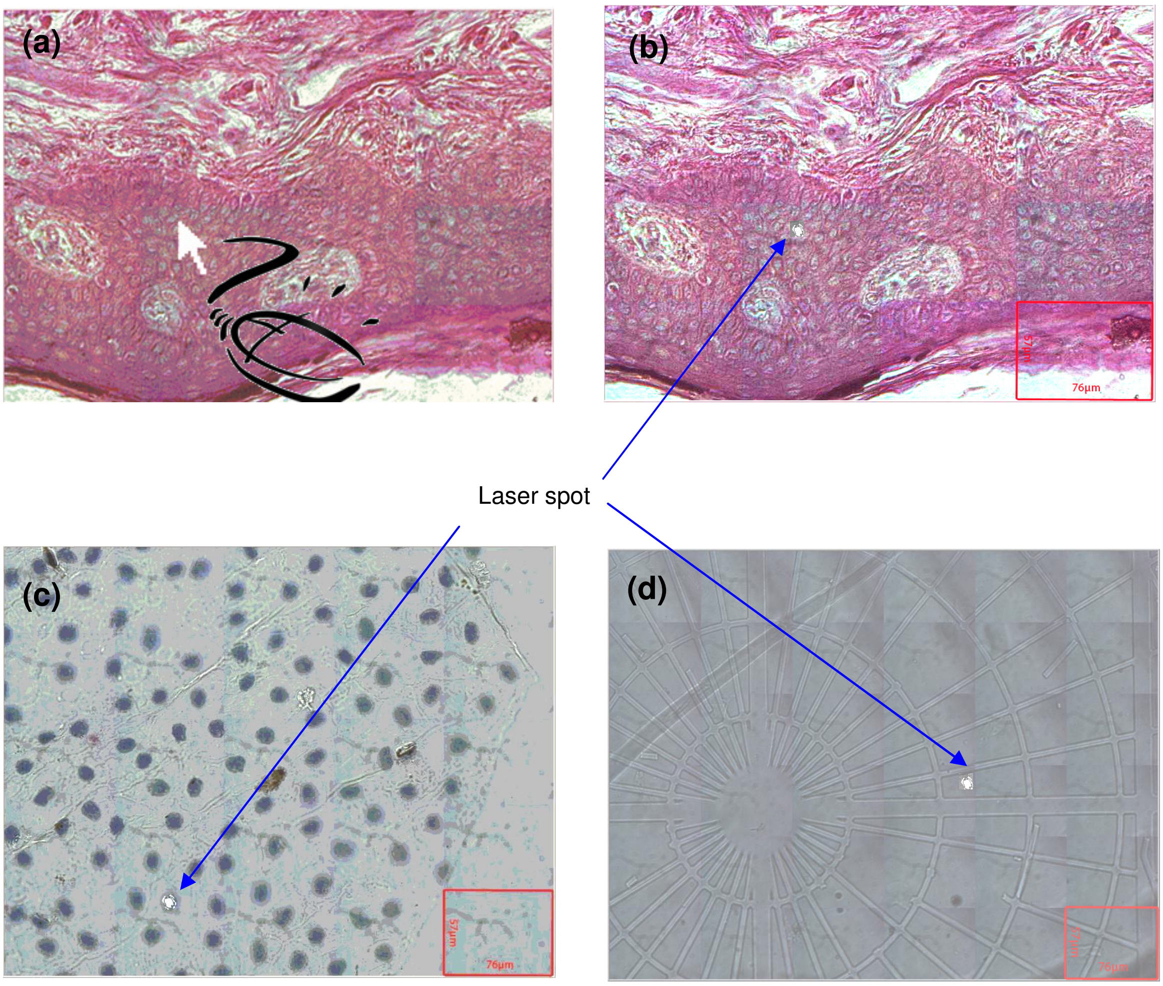

**Figure 75** ***Large histological image of skin biopsy composed of the mapping of 5 x 5 individual images before (a) and after (b) laser perforation. Further examples of laser perforation of a blood cell (c) and in a micro-pattern performed in a polymer (d).***

Nanodissection and perforation of living mouse fibroblasts cells are presented in fig. 76. The mapping is composed of 3 x 4 individual images. White lines and circles represent the location of the programmed dissection and perforation before laser processing in the fig. 76 (a). Fig. 76 (b) gives the results after laser processing. Cutting lines have been performed at a speed of 20 µm/s and an energy of 0.5 nJ. A cost and time saving benefit of the tool presented here is the ability to slice different biological tissues in their native states. Extensive and time consuming sample preparation techniques are not required. In particular, the nanoprocessing device is an optimal solution for sectioning tissue which is sensitive to chemical fixation. The gentle and contact-free cutting method prevents tissue damage and contamination. Even sectioning of hard tissues such as bone and tooth is feasible without decalcification.

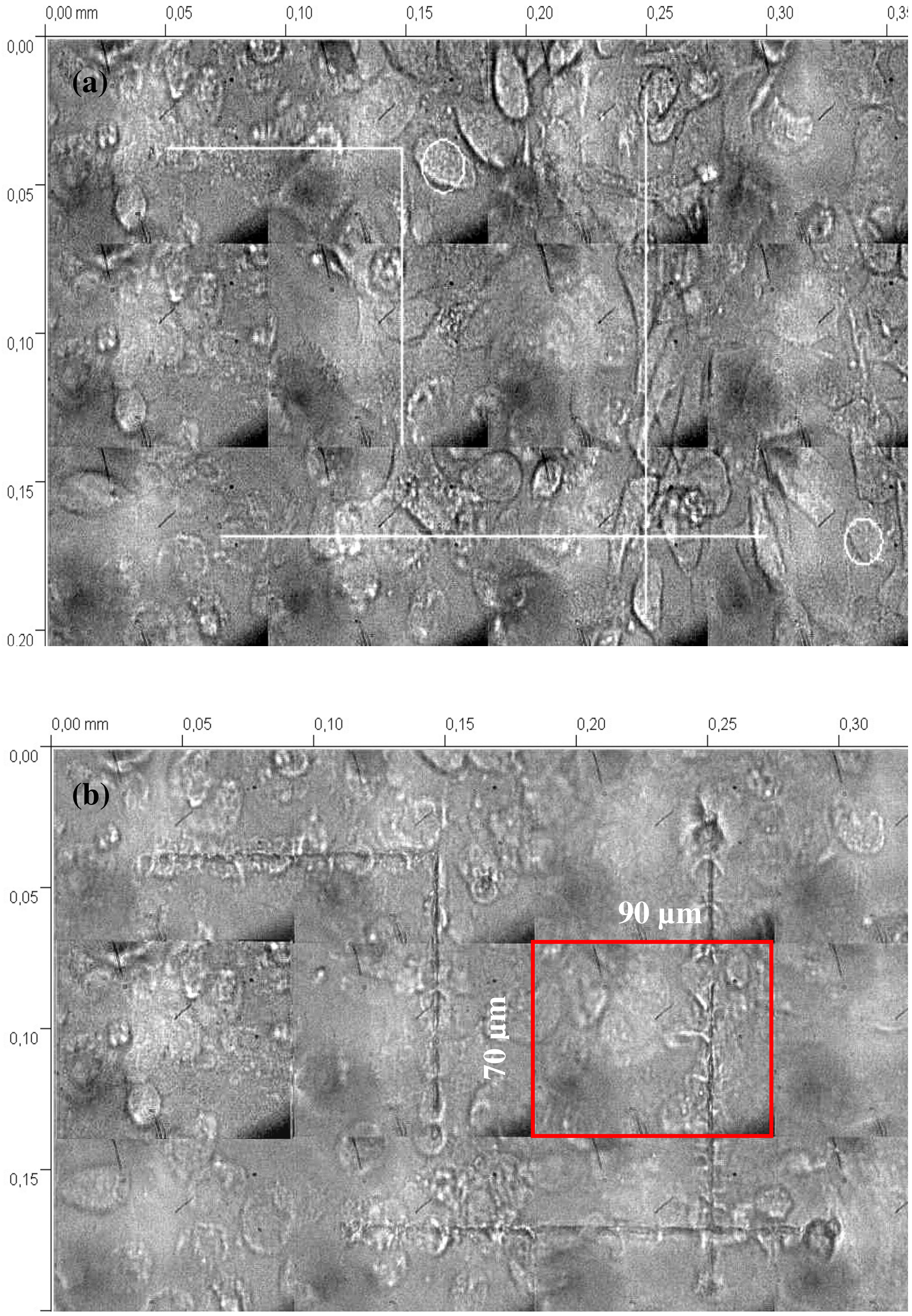

**Figure 76** ***Cutting and perforation of living mouse fibroblasts cells, before (a) (the white lines and circles indicate the programmed desired position) and after processing (b).***

Another example of Atomic Force Microscopy (AFM) analyses of laser nanoprocessing of human metaphase chromosomes prepared from peripheral blood by standard methods is given in fig. 77. Nanocuts have been performed at a speed of 100 µm/s and at a very low energy of 0.25 nJ. The width of the dissection is in a range of 500 nm - 1 µm as shown in the profil example (fig. 77 c).

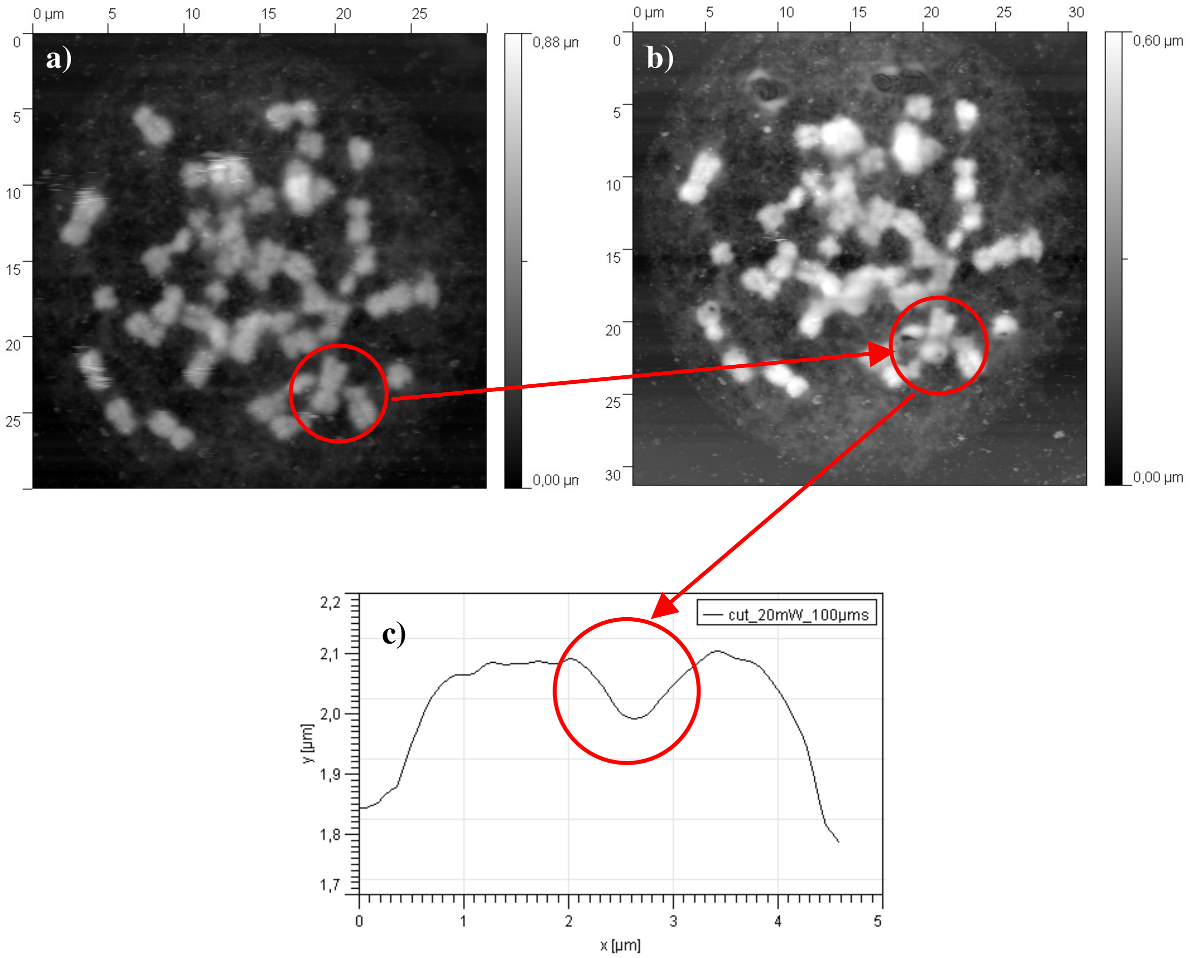

**Figure 77** ***AFM picture of the two photon nanodissection of a human chromosome before processing (a) and after processing (b). the width of the cut is in a range of 500 to 1µm (c).***

# 4. Micro-nano-processing of complex patterns

Marking is of prime importance in the field of biomaterials to allow the identification of surgical tools as well as prostheses. Nowadays, marking is often achieved by means of laser beam, which may modify the characteristics of the treated surfaces. The use of laser devices delivering nanosecond pulses is known to induce dramatic corrosion degradations during sterilization or decontamination processes of the biomaterials. Studies have demonstrated the ability of femtosecond laser treatments to avoid preferential corrosion processes of the marked areas, in order to extend the durability and the reliability of biomaterials and surgical instruments for example [154][155]. Non thermal sub-µm engraving and nano-patterning can find applications in medicine, pharmaceutics, cosmetics for traceability and against counterfeiting [156][157].

Thanks to the CAD option developed in the device, it is possible to perform machining using drawing supports as CAD files allowing the possibility to realize complex patterns with reducing time as request in the industry. Some examples of complex nano structuring are given in the following figures. fig. 78 illustrates an example of engraving the letters LHC (Laboratoire Hubert Curien) on a human hair of a diameter of about 50 µm. The width of grooves is around 1-2 µm.

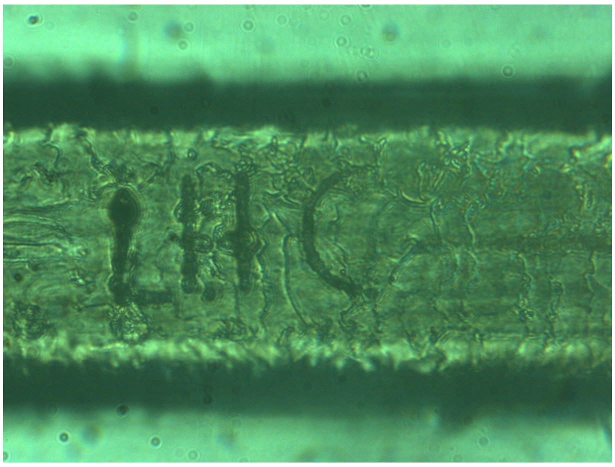

**Figure 78** ***LHC letters engraved on a human hair. Letters have been drawn with a CAD program.***

Fig. 79 shows a representation of the logo design of the Laboratoire Hubet curien performed with the CAD option of the developed device. Sub 1µm width has been measured.

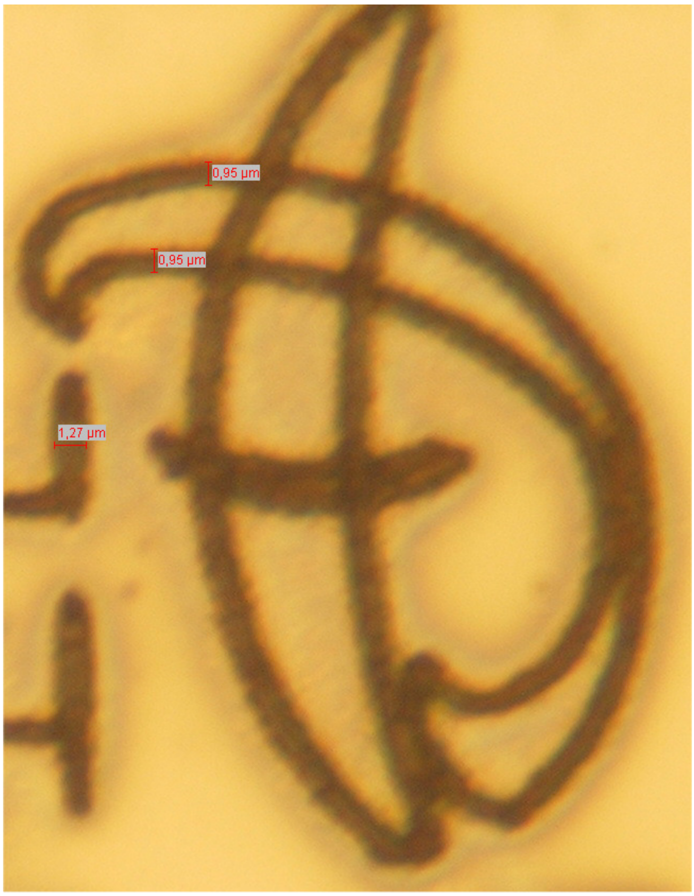

**Figure 79*****: Nanoprocessing of the Hubert Curien Laboratoire logo performed by the use of CAD support.***

The Fraunhofer IBMT logo has also been patterned on a silicon wafer as depicted in fig. 80.

The average line width is less than 1 µm.

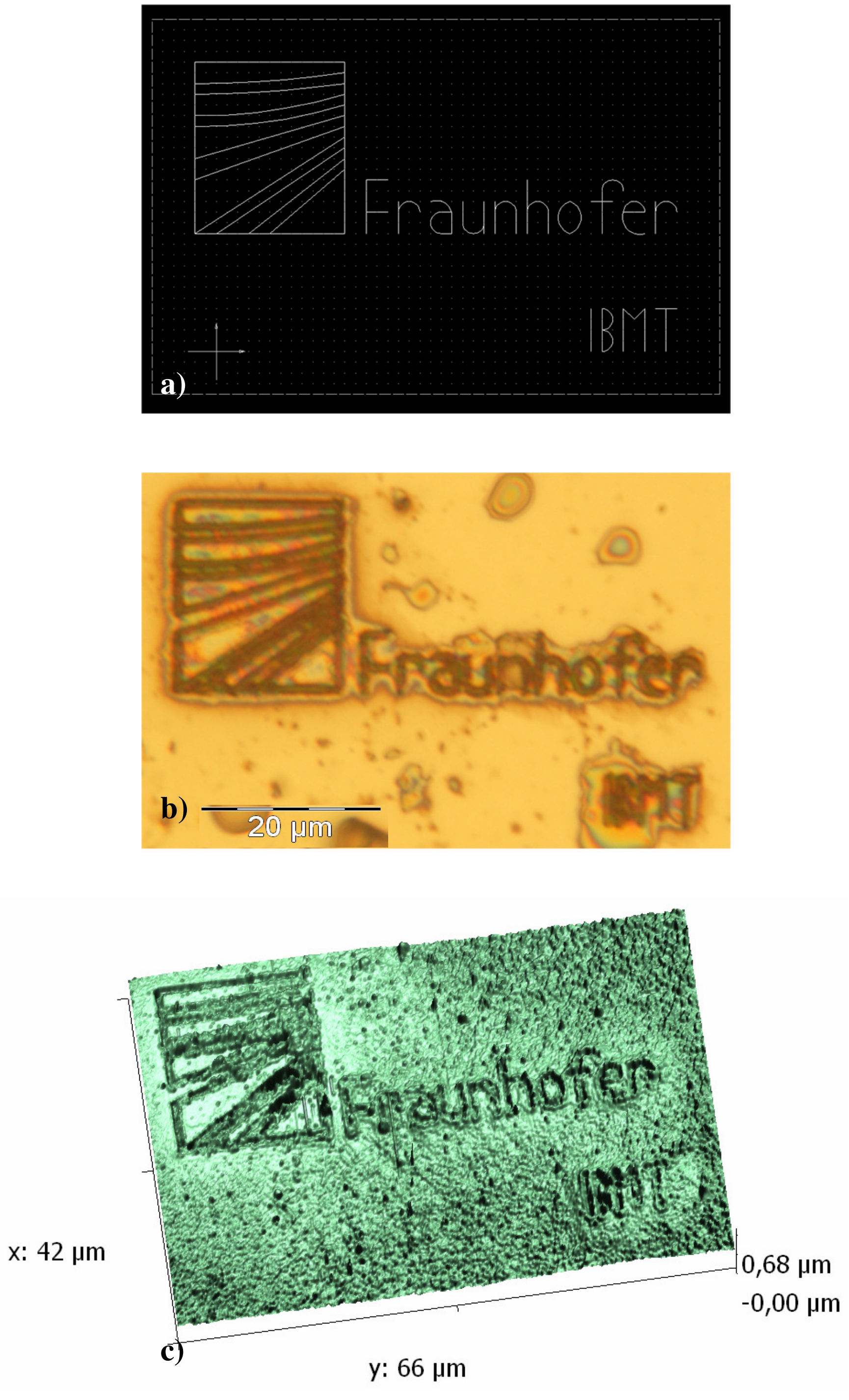

**Figure 80***: Nanoprocessing of the Fraunhofer IBMT logo performed by the use of CAD support. (a) drawing made under a CAD software, (b) optical image, (c) AFM image.*

Laser micro-nano-patterning could be also applied in surface texturing to fabricate superhydrophobic surfaces, phenomenon known as the “Lotus effect”. In nature, lotus leaf and other plants have superhydrophobic surface with self-cleaning effect. Water drop does not adhere to lotus leaf and completely rolls off the leaf, carrying away undesirable particles [158][159]. The influence of material topography on cellular behaviour has shown that different structures such as pores, grooves and pits in micrometer and nanometer dimensions affect cell morphology, orientation, adhesion, and proliferation of cells. Material hydrophilic / hydrophobic character depends on nano- and microscale surface topography. Furthermore, it has been demonstrated that hydrophilic/hydrophobic materials influence cellular adhesion and cytoskeletal organization. The hydrophobic properties of femtosecond laser fabricated structures and their effects on cell proliferation shows interesting results [160]. Often hard implants undergo detachment from the host tissue due to inadequate biocompatibility and poor osteointegration. Changing surface chemistry and physical topography of the surface influences biocompatibility. Potential of nano-patterning of implant and prosthesis with femtosecond laser pulses on materials such as Titanium have been shown [161][162].

# 5. Two-photon polymerization

It has been shown that nonlinear optical lithography based on two-photon polymerization (2PP) of photosensitive resins allows the fabrication of true 3D nanostructures and therefore of 3D photonic crystals [163][164][165][166][167][168]. When tightly focused into the volume of a photosensitive resin, the polymerization process can be initiated by nonlinear absorption of femtosecond laser pulses within the focal volume. By moving the laser focus three-dimensionally through the resin any 3D nanostructure with a resolution down to 100 nm can be fabricated. There are many well known applications for single-photon polymerization (1-PP) like UV-photolithography or stereolithography, where a single UV-photon is needed to initiate the polymerization process on the surface of a photosensitive resin. Depending on the concentration of photo-initiators and of added absorber molecules, UV light is absorbed within the first few µm. Therefore, single-photon polymerization is a planar process restricted to the surface of the resin.

However, the photosensitive resins used are transparent to near-infrared light, so it is possible to focus near-infrared femtosecond pulses into the volume of the resin. If the photon density reaches the threshold value, two-photon absorption occurs within the focal volume, initiating the polymerization process. If the laser focus is moved three-dimensionally through the volume of the resin, the polymerization process is initiated along the track of the focus, allowing the fabrication of any 3D microstructure. There are several advantages of the two-photon polymerization compared to one-photon polymerization. The most important is that polymerization can be initiated into the volume of the resin, that is to say the 2-PP is a true 3D process whereas 1-PP is a planar process. 1-PP allows making of 3D structures but only layer by layer. A new approach to photolithography in which multiphoton absorption of pulsed 800-nanometer (nm) light is used to initiate cross-linking in a polymer photoresist and one-photon absorption of continuous-wave 800-nm light is used simultaneously to deactivate the photopolymerization allow to achieve λ/20 (40 nm) structures [169].

Patterns in photoresist SU-8 2000 using the 3D structuring system have been tested. SU-8 2000 is a high contrast, epoxy based photoresist designed for micromachining and applications, where a thick, chemically and thermally stable image is desired. SU-8 2000 is an improved formulation of SU-8, which has been widely used by MEMS producers for many years. Photoresist is most commonly exposed with conventional UV radiation, from 350 to 400 nm, although 365 nm is the recommended wavelength. SU-8 2000 may also be exposed with e-beam or x-ray radiation. It is also possible to expose SU-8 2000 with femtosecond laser emitting at a wavelength of 800 nm. Indeed, due to typical very high peak power, several photons of smaller energy together can produce the same absorption effect than normally produced by the absorption of a single photon of higher energy.

Thanks to the 3D option developed as presented in the chapter 2, features have been performed in the volume of SU-8 as shown in fig. 81. The pattern is made of 2 rows of 6 tubes each with a diameter of 15 µm imbricated into each other. The structure is 30 µm high which was the thickness of the SU-8 film.

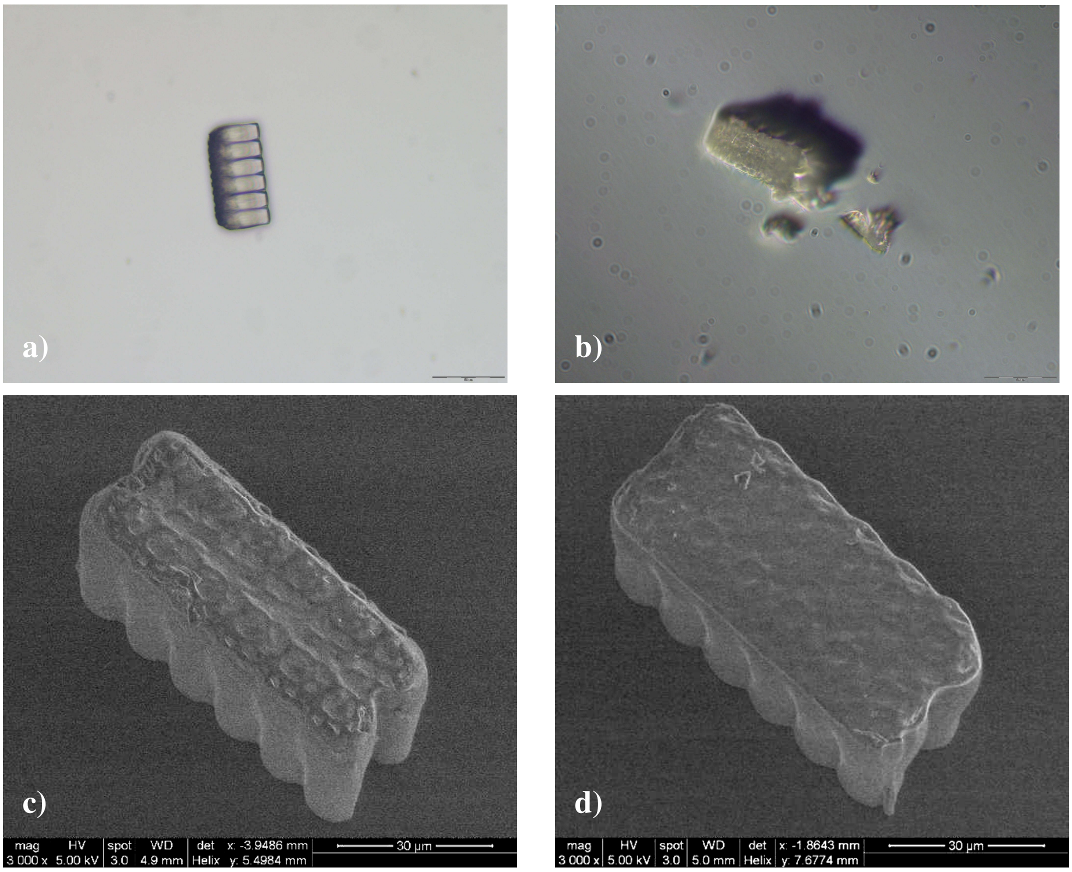

**Figure 81** ***Optical (a, b) and SEM (c, d) images of 3D structures performed in SU-8 photoresist by two photon polymerization.***

Applications such as in micro nano fluidics with complex pattern are conceivable or also ideal for the fabrication of drug delivery systems as well as for micro- nano-structuring of scaffolds for tissue engineering and regenerative medicine [170][171].

# 6. Conclusion

Here we have demonstrated the development of an efficient and powerful nanoprocessing apparatus for biotechnological applications. The device is high flexible and adaptable with a strong hardware and software environment which allow a high range of applications and performances for medicine, biology, pharmaceutics, cosmetics, etc. Such a device is also potentially useful for materials nanoprocessing in a general manner as the manufacture of waveguides, gratings, micro fluidic devices, nanocontainers, data storage, nanolithography, nanomarking, etc. Of course one of the limitation is the processing speed for high-volume and high-rate nanomanufacturing.

# Conclusion

Miniaturization is an attribute of today's photonic industry, determining an intense and global effort in micro- and nano-technology, and in this context, materials micro/nano structuring has become the backbone of rapidly expanding application areas in emerging technologies. Further progress in telecommunications, optics, electronics, biomaterials, medicine, and transport strongly depends on the availability of reliable and rapid processing techniques. Laser-based micro technology holds great promises and the evolution will be dictated by the development of inexpensive yet precise processing tools that can develop and structure materials with a high degree of controllability, accuracy, and reduced residual damage.

New processes are presented as well as for micro machining as for nano machining ranges. Due to deterministic behaviour of femtosecond laser pulses, it has been possible to develop an innovative method to calculate processing time for micro machining process. This method enables the calculation of the time when the ablation of the material is active. This enables to evaluate time processing due to external reasons such as mechanical or computing which is full of interest for industries. Indeed, that gives concrete information and to what extent improvements are possible.

In this work we have demonstrated the feasibility to take advantage of the interaction of femtosecond laser pulses with matter and this by having developed a compact and flexible apparatus. This device is of great interest and covers wide research fields such as nanoprocessing of biological samples, nanostructuring of different type of materials, hence is of great interest for many applications in material science, nanobiotechnology and nanomedicine. This workstation enables the mapping of a large area with a very high resolution, as well as transmission and reflexion imaging than two photons imaging. This allows targeting a precise location on a large area of a sample and makes possible the nanodissection of biological samples, cells, chromosomes …

The use of high numerical aperture focusing objective enables to reach very high intensities in a very small volume. This can initiate a two photon effect due to high peak power reached at the focus point. Two photon of the same energy can produce the same absorption effect than the absorption of one photon which has two times more energy. This effect occurs in a smaller volume than on photon and so is huge of interest for real 3D nanostructuring using photopolymerization of resins such as SU-8.

The whole device is controlled with a software developed to be easy to learn and easy to work for a final customer. Moreover, the workstation is designed to be coupled with a low average power femtosecond oscillator laser systems which are more cost-effective and more reliable compared to amplified lasers.

However, there are still open questions concerning physical comprehension of phenomenon of growing matter and heat accumulation effects on matter. Analysis put in evidence a dependency between experimental parameters and the high and shape of protrudes of matter. However, more investigations are still necessary to well understand this phenomenon. The control of such phenomenon open a new way for nanostructuring and could have many applications in fields such as cell adhesion or cell growth, tribology, electronics …

# List of figures

## Chapter I: Overview of nanostructuring techniques

# Bibliography

[1] Yong Chen, Anne Pépin, Electrophoresis, Nanofabrication : *conventional and nonconventional methods,* 22,187-207 (2001)

[2] Y. Ochiai, M. Ishida, J. Fujita, T. Ogura, J. Momoda, and E. Ohshima, MNE ’02, Lugano Switzerland, 17–19 September (2002)

[3] M. J. Word, Ilesanmi Adesida, Paul R. Berger, *Nanometer-period gratings in hydrogen silsesquioxane fabricated by electron beam lithography*, J. Vac. Technol. B, 21 (2003)

[4] M. A. McCord and R. F. W. Pease, *Lift-off metallization using poly(methylmethacrylate) exposed with a scanning tunnelling microscope* J. Vac. Sci. Technol. B 6, 293 (1988)

[5] E. A. Dobisz and C. R. K. Marrian, *Sub-30 nm lithography in a neative electron beam resist with a vacuum scanning tunnelling microscope,* Appl. Phys. Lett. 58, 22 (1991)

[6] J. A. Dagata, J. Schneir, H. H. Haray, C. J. Evans, M. T. Postek, and J. Bennett, *Modification of hydrogen-passivated silicon by a scanning tunnelling microscope operating in air,* Appl. Phys. Lett. 56, 2003 (1990)

[7] E. S. Snow and P. M. Campbell,*Fabrication of Si nanostructures with an atomic force microscope,* Appl. Phys. Lett. 64, 1932 (1994)

[8] I.-W. Lyo and Ph. Avouris, Science 253, 173 (1991)

[9] H. J. Mamin, P. H. Guenther, and D. Rugar, *Atomic emission from a gold scanning-tunneling-microscope tip,* Phys. Rev. Lett. 65, 2418 (1990)

[10] H. J. Mamin and D. Rugar, *Thermomechanical writing with an atomic force microscope tip,* Appl. Phys. Lett. 61, 1003 (1992)

[11] L. A. Nagahara, T. Thundat, and S. M. Lindsay, *Nanolithography on semiconductor surfaces under an etching solution,* Appl. Phys. Lett. 57, 270 (1990)

[12] Gwyn, C. W., Stulen, R., Sweeney, D., Attwood, D., J. Vac. Sci. Technol. (1998), B16, 3142-3149

[13] Cardinale G. F., Henderson C. C., Goldsmith J. E. M., Mangat P. J. S., Cobb J., Hector S. D. , J. Vac. Sci. Technol. 1999, B17, 2970-2974

[14] Viswanathan R., Seeger D., Bright A., Bucelot T., Pomerene A., Petrillo K., Blauner P., Agnello P., Warlaumont J., Conway J., Patel D., *Fabrication of high performance 512K static-random access memories in 0.25 μm complementary metal-oxide semiconductor technology using x-ray lithography,* J. Vac. Sci. Technol. , B 11, 2910 (1993)

[15] Deguchi K., Miyoshi K., Oda M., Matsuda T., *Extendibility of synchrotron radiation lithography to the sub-100 nm region,* J.Vac. Sci. Technol., B 14, 4294 (1996)

[16] Silverman J. P., *Challenges and progress in w-ray lithography,* J. Vac. Sci. Technol., B 16, 3137 (1998)

[17] A. Kumar and G. M. Whitesides, *Features of gold having micrometer to centimetre dimensions can be formed through a combination of stamping with an elastomeric stamp and an alkanethiol "ink" followed by chemical etching,* Appl. Phys. Lett. 63, 2002 (1993)

[18] Y.-L. Loo, R. L. Willett, K. W. Baldwin, and J. A. Rogers, *Additive, nanoscale patterning of metal films with a stamp and a surface chemistry mediated transfer process: Applications in plastic electronic,* Appl. Phys. Lett. 81, 562 (2002)

[19] J. Haisma, M. Verheijen, and K. van den Heuvel, *Mold-assisted nanolithography: A process for reliable pattern replication,* J. Vac. Sci. Technol. B 14, 4124 (1996)

[20] T. Bailey, B. J. Choi, M. Colburn, M. Meissl, S. Shaya, J. G. Ekerdt, S. V. Sreenivasan, and C. G. Wilson, *ibid.* 18, 3572 (2000)

[21] D.J. Resnick, W.J. Dauksher, D. Mancini, K.J. Nordquist, T.C. Bailey, S. Johnson, N. Stacey, J.G. Ekerdt, C.G. Willson, S.V. Sreenivasan, and N. Schumaker, Microlithography 2003, proc. Spie 5037, 12 (2003)

[22] Chou S. Y., Krauss P. R., Renstrom P. J., Appl. Phys.Lett. 76, 3114 (1995)

[23] Chou S. Y., Krauss P. R., Zhang W., Guo L., Zhang L., *Sub-10 nm imprint lithigraphy and applications,* J. Vac. Sci. Technol., B 15, 2897 (1997)

[24] M. Okai, S. Tsuji, N. Chinone, and T. Harada, *Novel method to fabricate corrugation for a λ/4-shifted distributed feedback laser using a grating photomask,* Appl. Phys. Lett. 55, 415 (1989)

[25] M.N. Cooke, J.P. Fisher, D. Dean, C. Rimnac, A.G. Mikos, *Use of stereolithography to manufacture critical-sized 3D biodegradable scaffolds for bone ingrowth,* J. Biomed. Mater Res. Part B: Appl Biomater. 64B, 65– 69 (2002)

[26] T. Matsuda, M. Mizutani, S.C. Arnold, *Molecular design of photocurable liquid bidegradable copolymers. 1.Synthesis and photocuring characteristics*, Macromolecules 33, 795–800 (2000)

[27] M. H. Hong, Q. Xie, K. S. Tiaw, and T. C. Chong, *Laser singulationof thin wafers & difficult processed substrates: A niche area over saw dicing,* J. Laser Micro/Nanoeng. 1, 84 (2006)

[28] E. Baubeau, *Etude et réalisation d'une chaîne laser femtoseconde haute cadence et de haute puissance moyenne. Applications au micro-usinage,* PhD thesis. Universite Paris XI Orsay, (2002)

[29] B.C. Stuart, M. D. Feit, S. Herman, A. M. Rubenchik, B. W. Shore, M. D. Perry, *Optical ablation by high-power short-pulse lasers,* J. Opt. Soc. Am. B 13, 459 (1996),

[30] B.C. Stuart, *Laser-induced damage in dielectrics with nanosecond to subpicoseond pulses,* Phys. Rev. Lett. 74, 2248 (1995)

[31] J.H. Campbell, *Laser-induces damage in optical materials,* SPIE 1441, 444 (1990)

[32] B.C. Stuart, M.D. Feit, S. Herman, A.M. Rubenchik, B.W.Shore, and M.D. Perry, *Optical ablation by high-power short pulses lasers,* J. Opt. Soc. Am. B 13, 459 (1996).

[33] E.G. Gamaly, A.V. Rode, B. Luther-Davies, and V.T. Tikhonchuk, *Ablation of solids by femtosecond laser: ablation mechanism and ablation thresholds for metals and dielectrics,* Phys. of Plasmas 949 (2002).

[34] B.C. Stuart, M.D. Feit, A.M. Rubenchik, B.W.Shore, and M.D. Perry, *Laser-induced damage in dielectrics with nanosecond to subpicosecond pulses,* Phys. Rev. Lett. 74, 2248 (1995).

[35] J.F. Ready, *LIA Handbook of laser materials processing*, Magnolia Publ. Inc. (2001)

[36] J. Meijer, *Laser beam machining (LBM) state of the art and new opportunities* Journal of Materials Processing Technology, 149 (2004), 2-17

[37] Bloembergen, N. (1974) *IEEE J. Quantum Electron*. QE-10, 375–386

[38] Ajit P. Joglekar, Hsiao-hua Liu, Edgar Meyhöfer, Gerard Mourou, and Alan J. Hunt, *Optics at critical intensity: Applications to nanomorphing,* PNAS, (2004)

[39] A.P. Joglekar, H. Liu, G.J. Spooner, E. Meyhöfer, G. Mourou, A.J. Hunt, *A study of the deterministic character of optical damage by femtosecond laser pulses and applications to nanomachining,* Appl. Phys. B, 77, 25 (2003)

[40] X. Liu, D. Du, G. Mourou, *Laser ablation and micromachining with ultrashort laser pulses,* IEEE J. Quantum Electron QE-33, 1706 (1997)

[41] D. Du, J. Squier, R. Kurtz, V. Elner, X. Liu, G. Gutmann, G. Mourou, ed. By P.F. Barbara P. 254, Springer, New York (1995)

[42] P. Pronko, S. Dutta, J. Squier, J. Rudd, D. Du, G. Mourou, *Machining of sub-micron holes using a femtosecond laser at 800 nm,* opt. Commun. 114,106 (1995)

[43] K. Venkatakrishnan, B. Tran, P. Stanley, N. Sivakumar, *The effect of polarization of ultrashort pulsed laser ablation of thin metal films,* J. Appl. Phys. 92,1604 (2002)

[44] Bo Tan, Narayanswamy, R. Sivakumar and KrishnanVenkatakrishnan, *Direct grating writing using femtosecond laser interference fringes formed at the focal point,* J. Opt. A: Pure and Applied Optics 7, 169 (2005)

[45] K. Kawamura, N. Sarujura and M. Hirano, Appl. Phys. B, 71 119-21, (2001)

[46] K. Kawamura, N. Sarujura, M. Hirano and H. Hosono, *Holographic encoding of permanent gratings embedded in diamond by two beam interference of a single femtosecond near-infrared laser pulse,* Japan J. Appl. Phys. 39, L767 (2000)

[47] A. Karsanov, A. Kiselev, A. Stepanov and N. Polushkin, J. Appl. Phys., 94, 10 (2003)

[48] A. Chimmalgi, T. Y. Choi, C. P. Grigoropoulos and K. Komvopoulos, *Femtosecond laser aperturless near-field nanomachining of metals assistedby scanning probe microscopy,* Appl. Phys. Lett., 82, 1146 (2003)

[49] J. Jersh and K. Dickmann, *Nanostructure fabrication using laser field enhancement in the near field of a scanning tunnelling microscope tip,* Appl. Phys. Lett. 68, 868 (1996)

[50] A. A. Gorbunov and W. Pompe, *Thin film nanoprocessing by laser/STM Combination,* Phys.Status Solidi A 145, 333 (1994)

[51] R. Huber, M. Koch and J. Feldmann, *Laser-induced thermal expansion of a scanning tunneling microscope tip measured with an atomic force microscope,* Appl. Phys. Lett. 73, 2521 (1998)

[52] V.gerstuer, A. Thon and W. Pfeiffer, *Thermal effects in pulsed laser assisted scanning tunnelling microscopy,* J. Appl. Phys., 87, 2574 (2000)

[53] S. F. Ho, B. K. A. Ngoi, *Sub-microdrilling with ultrafast pulse laser interference,* Appl. Phys. B, 79, 99 (2004)

[54] M. Fanetti, L. Gavioli, M. Sancrotti, *Long-range-ordered, Molecular-induced nanofaceting,* Adv. Mater. 18, 2863 (2006)

[55] H. Brune, M. Giovannini, K. Bromann, K. Kern, *Self-organized growth of nanostructure arrays on strain-relief patterns,* Nature 394, 451, (1998)

[56] P. Soukiassian, F. Semond, A. Mayne, G. Dujardin, *Highly stable Si Atomic line formation on the β-SiC(100) surface,* Phys. Rev. Lett. 79, 2498 (1997)

[57] J. Lobo, E.G. Michel, A.R. Bachmann, S. Speller, J. Kuntze, J.E. Ortega, *Tuning the surface state dimensionality of Cu nanostripes,* Phys. Rev. Lett. 93, 137602 (2004)

[58] N. Sykaras, A.M. Iacopino, V.A. Marker, R.G. Triplett, R.D.Woody, *Femtosecond laser structuring of titanium implants,* Int. J. Oral Maxillofac. Implan. 15, 675 (2000).

[59] F. Pfeiffer, B. Herzog, D. Kern, L. Scheideler, J. Geis-Gerstorfer, H. Wolburg, *Cell reactions to microstructured implant surfaces,* Microelectron. Eng. 67/68, 913 (2003).

[60] X.D. Bai, E.G. Wang, P.X. Gao, Z.L. Wang, *Crystallographic orientation-aligned ZnO nanorods grown by a tin catalyst,* Nano Lett. 3, 1147 (2003)

[61] X.D. Bai, P.X. Gao, Z.L. Wang, E.G. Wang, Appl. *Dual-mode mechanical resonance of individual ZnO nanobelts,* Phys. Lett. 82 (2003) 4806.

[62] Z.L. Wang, J.H. Song, *Piezoelectric nanogenerators based on zinc oxide nanowire arrays,* Science 312 (2006) 242

[63] . Z.L. Wang, Materials today, 26–33 June (2004)

[64] C.X. Xu, X.W. Sun, Z.L. Dong, G.P. Zhu, Y.P. Cui, *Zinc oxide hexagram whiskers,* Appl. Phys. Lett. 88, 093101 (2006)

[65] M. Birnbaum, *Semiconductor surface damage produced by ruby lasers,* J. Appl. Phys. 36, 3688 (1965)

[66] J. E. Sipe, Jeff F. Young, J. S. Preston, H. M. van Driel, *Laser-induced periodic surface structure,* Phys. Rev. B 27, 1141 (1983)

[67] G. N. Maracas, G. L/ Harris, C. A. Lee, and R. A. McFarlane, *On the origin of periodic surface structure of laser-annealed semiconductors,* Appl. Phys. Lett. 33, 453 (1978)

[68] N. R. Isenor, *$CO_2$ laser-produced ripple patterns on $Ni_xP_{1-x}$ surfaces,* Appl. Phys. Lett. 31, 148 (1977)

[69] A. K. Jain, V. N. Kulkarni, D. K. Sood, and J. S. Uppal, *Periodic surface ripples in laser-treated aluminium and their use to determine absorbed power,* J. Appl. Phys. 52, 4882 (1981)

[70] P. A. Temple and M. J. Soileau, *Polarization charge model for laser-induced ripple patterns in dielectric materials,* IEEE J. Quant. Elec. QE-17, 2067 (1981)

[71] J. A. van Vechten, *Experimental tests for boson condensation and superconductivity in semiconductors during pulsed beam annealing,* Solid State Commun. 39, 1285 (1981)

[72] D. C. Emmony, R. P. Howson, and L. J. Willis, *Laser mirror damage in germanium at 10.6 $\mu m$,* Appl. Phys. Lett. 23, 598 (1973).

[73] M. Oron and G. Sorensen, *New experimental evidence of the periodic surface structure in laser annealing,* Appl. Phys. Lett. 35, 782 (1979)

[74] Her T.-H., Finlay R.J., Wu C. and E. Mazur, *Femtosecond laser-induced formation of spikes on silicon,* Appl. Phys. A, 70, 383 (2000)

[75] Henyk M., Vogel N., Wolfframm D., Tempel A. And Reif J., *Femtosecond laser ablation from dielectric materials: Comparison to arc discharge erosion,* Appl. Phys. A, 69, S355 (1999)

[76] J. Reif, F. Costache and M. Bestehorn, *Recent Advances in Laser Processing of Materials*. Ed. J Perière (2006)

[77] Bonse J., Baudach S., Kruger J., Kautek W. And Lenzner M., *Femtosecond laser ablation of silicon-modification thresholds and morphology,* Appl. Phys. A 74, 19 (2006)

[78] Coyne F., Magee J.P., Mannion P., O'Connor G.M. and Glynn T.J., *STEM (Scanning transmission electron microscopy) analysis of femtosecond laser pulse induced damage to bulk silicon,* Appl. Phys. A 81, 371 (2004)

[79] Costache F., Kouteva-Arguirova S. and Reif J., *Sub-damage-threshold femtosecond laser ablation from crystalline Si: surface nanostructures and phase transformation,* Appl. Phys. A. (2004)

[80] Bonse J., Wrobel J.M., Krüger J., and Kautek J., *Ultrashort-pulse laser ablation of indium phosphide in air,* Appl. Phys. A, 72, 89 (2001)

[81] Erlebacher J., Aziz M.J., Chason E., Sinclair M.B. and floro J.A., *Spontaneous pattern formation on Ion bombarded Si(001),* Phys. Rev. Lett., 82, 2330 (2000)

[82] Mayer T.M., Chason E. and Howard A.J., *Roughening instability and ion-induced viscous relaxation of $SiO_2$ surfaces,* J. Appl. Phys, 76,1633 (1993)

[83] Habenicht S., Lieb K.P., Koch J. And Wieck A.D., *Ripple formation and velocity dispersion on ion-beam-eroded silicon surfaces,* Phys. Rev. B, 65,115327 (2002)

[84] J.P. Colombier, P. Combis, F. Bonneau, R. Le Harzic, and E. Audouard, *Hydrodynamic simulations of metal ablation by femtosecond laser irradiation,* Physical Review B 71, 165406 (2005).

[85] J.P. Colombier, P. Combis, R. Stoian and E. Audouard, *High shock release in ultrafast laser irradiated metals: Scenario for material ejection,* Physical Review B 75, 104105 (2007).

[86] J.P. Colombier, *Théorie et simulation de l'interaction des impulsions laser ultracourtes à flux modéré avec un solide métallique*, PhD thesis, Université Jean Monnet de Saint-Etienne, 2005.

[87] J. M. Liu, *Simple technique for measurements of pulsed Gaussian-beam spot sizes,* Optics Letters 7, 5 (1982)

[88] Xiao Tang, Pierre L'Hostis and Yu Xiao, *An auto-focusing method in a microscopic testbed for optical discs,* J. Res. Natl. Inst. Stand. Technol. **105**, 565 (2000)

[89] E.N. Glezer, M. Milosavljevic, L. Huang, R.J. Finlay, T.H. Her, J.P. Callan, E. Mazur, *Three-dimensionaloptical storage inside transparent materials,* Opt. Lett. 21, 2023 (1996)

[90] M. Watanabe, H.B. Sun, S. Juodkazis, T. Takahashi, S. Matsuo, Y. Suzuki, J. Nishii, H. Misawa, *Three-dimensional optical data storages in vitreous silica,* Jpn. J. Appl. Phys. Part 2 37, L1527 (1998)

[91] K. Yamasaki, S. Juodkazis, M. Watanabe, H.B. Sun, S. Matsuo, H. Misawa, *Recording by microexplosion and two-photon reading of three-dimensional optical memory in polymethylmethacrylate films,* Appl. Phys. Lett. 76, 1000 (2000)

[92] K.M. Davis, K. Miura, N. Sugimoto, K. Hirao, *Writing waveguides in glass with a femtosecond laser,* Opt. Lett. 21, 1729 (1996)

[93] K. Miura, J.R. Qiu, H. Inouye, T. Mitsuyu, K. Hirao, *Photowritten optical waveguides in various glasses with ultrashort pulse laser,* Appl. Phys. Lett. 21, 3329 (1996)

[94] C.B. Schaffer, A. Brodeur, J.F. Garcia, E. Mazur, *Micromachining bulk glass by use of femtosecond laser pulses with nanojoule energy,* Opt. Lett. 26, 93 (2001)

[95] O.M. Efimov, L.B. Glebov, K.A. Richardson, E. Van Stryland, T. Cardinal, S.H. Park, M. Couzi, J.L. Bruneel, *Waveguide writing in chalcogenide glasses by a train of femtosecond laser pulses,* Opt. Mater. 17,379 (2001)

[96] D. Homoelle, S. Wielandy, A.L. Gaeta, N.F. Borrelli, C. Smith, *Infrared photosensitivity in silica glasses exposed to femtosecond laser pulses,* Opt. Lett. 24, 1311 (1999)

[97] C. Momma, B. N. Chichkov, S. Nolte, F. von Alvensleben, A. Tunnermann, H. Welling, B. Wellegehausen, *Short-pulse laser ablation of solid targets*, Opt. Comm. 129 (1996) 134-142

[98] R. Le Harzic, D. Breitling, M. Weikert, S. Sommer, C. Foehl, S. Valette, C. Donnet, E. Audouard, F. Dausinger, *Pulse-width and energy influence on laser micromachining of metals in a range of 100 fs to 5 ps*, Appl. Surf. Sci. 249 (2005) 322-331

[99] S. Nöel, J. Hermann, T. Itina, *Investigation of nanoparticle generation during femtosecond laser ablation of metals*, Appl. Surf. Sci. 253 (2007) 6310-6315

[100] P. Mannion, J. Magee, E. Coyne, G. M. O'Connor, *Ablation thresholds in ultrafast laser micro-machining of common metals in air,* Proc. SPIE 4876 (2003) 470-478

[101] M. Hashida A. F. Semerok, O. Gobert, G. Petite, Y. Izawa, J. F-. Wagner, *Ablation threshold dependence on pulse duration for copper*, Appl. Surf. Sci, 197-198 (2002) 862-867

[102] G. Matras, N. Huot, E. Baubeau, E. Audouard, *10 kHz water-cooled Ti :Sapphire femtosecond laser*, Opt. Express 15 7528-7536 (2007)

[103] J.P. Colombier, P. Combis, F. Bonneau, R. Le Harzic, E. Audouard, *Hydrodynamic simulations of metal ablation by femtosecond laser irradiation*, Phys. Rev. B 71 (2005) 165406

[104] P.T. Mannion, J. Magee, E. Coyne, G.M. O'Connor, T.J. Glynn, *The effect of damage accumulation behaviour on ablation thresholds and damage morphology in ultrafast laser micro-machining of common metals in air*, App. Surf. Sci. 233 (2004) 275-287

[105] R. Le Harzic, *Study of laser processing for micro-machining with limited thermal effects*, PhD Thesis Université Jean-Monnet à Saint Etienne (2003)

[106] K. Minoshima, A.M. Kowalvicz, I. Hartl, E.P. Ippen, J.G. Fujimoto, *Photonic device fabrication in glass by use of nonlinear materials processing with a femtosecond laser oscillator,* Opt. Lett. 26, 1516 (2001)

[107] Y. Sikorski, A.A. Said, P. Bado, R. Maynard, C. Florea, K.A. Winick: *Optical waveguide amplifier in Nd-doped glass written with near-IR femtosecond laser pulses,* Electron. Lett. 36,226 (2000)

[108] L. Shah, A. Y. Arai, S. M. Eaton, P. R. Herman , *Waveguide writing in fused silica with a femtosecond fiber laser at 522 nm and 1 MHz repetition rate,* Optics Express, 13, 6 (2005)

[109] B.C. Stuart, M.D. Feit, A.M. Rubenchik, B.W. Shore, M.D. Perry, *Laser induced damage in dielectrics with nanosecond to subpicosecond pulses,* Phys. Rev. Lett. 74, 2248 (1995)

[110] M. Lenzner, J. Kruger, S. Sartania, Z. Cheng, C. Spielmann, G. Mourou, W. Kautek, F. Krausz, *Femtosecond optical breakdown in dielectrics,* Phys. Rev. Lett. 80, 4076 (1998)

[111] C.B. Schaffer, J.F. Garcia, E. Mazur, *Bulk heating of transparent maerials using a high-repetition-rate laser,* Appl. Phys. A 76, 351 (2003)

[112] R.R. Gattass, L.R. Cerami, E. Mazur, *Micromachining of bulk glass with bursts of femtosecond laser pules at variable repetition rates,* Optics Express 14, 12, 5279-5284 (2006)

[113] S. M. Eaton, H. Zhang, P. R. Herman, F. Yoshino, L. Shah, J. Bovatsek, A. Y. Arai, *Heat accumulation effects in femtosecond laser-written waveguides with variables repetition rate,* Optics Express, 13, 12, 4708-4716 (2005)

[114] M. Henyk, D. Wolfframm, and J. Reif, *Ultra short laser pulse induced charged particle emission from wide bandgap crystals,* Appl. Surf. Sci. 168, 263 (2000)

[115] M. Henyk, R. Mitzner, D. Wolfframm, and J. Reif, *Laser-induced emission from dielectrics,* Appl. Surf. Sci. 154-155, 249 (2000)

[116] M. Henyk, F. Costache, and J. Reif, *Femtosecond laser ablation from sodium chloride and barium fluoride,* Appl. Surf. Sci. 186, 381 (2002)

[117] E. Vanagas, I. Kudryashov, D. Tuzhilin, S. Juodkazis, S. Matsuo, H. Misawa, *Surface nanostructuring of borosilicate glass by femtosecond nJ energy pulses,* Appl. Phys. Lett. 82, 2901, (2003)

[118] J. Koch, F. Korte, T. Bauer, C. Fallnich, A. Ostendorf, B.N. Chichkov, *Nanotexturing of gold films by femtosecond laser-induced melt dynamics,* Appl. Phys. A , 81, 325 (2005)

[119] T. Okamoto, E. Ohmura, T. Sano, Y. Morishige, I. Miyamoto, *Analytical study on metal microstructures using femtosecond laser,* Appl. Phys. A, 81, 639-643 (2005)

[120] A. Ancona, F. Röser, K. Rademaker, J. Limpert, S. Nolte, A. Tünnermann, Optics Express, 16, 12 (2008)

[121] F. Korte, J. Koch, B.N. Chichkov, *Formation of microbumps and nanojets on gold targets by femtosecond laser pulses,* Appl. Phys A, 79, 879 (2004)

[122] Amirkianoosh Kiani, Krishnan Venkatakrishnan, Bo Tan, *Micro/nano scale amorphozation of silicon by femtosecond laser irradiation,* Optics Express, 18, 3 (2010)

[123] D. Bäuerle, *Laser Processing and Chemistry 2nd ed,* (Springer-Verlag Berlin, 1996), Chap. 7.

[124] J. Bonse, K. W. Brezinka, and A. J. Meixner, *Modifying single-crystalline silicon by femtosecond laser pulses : an analysis by micro Raman spectroscopy, scanning laser microscopy and atomic force microscopy,* Appl. Surf. Sci. 221(1-4), 215 (2004).

[125] B. E. Deal, and A. S. Grove, *General relationship for the thermal oxidation of silicon,* J. Appl. Phys. 36(12), 3770 (1965).

[126] J. Blanc, *A revised model for oxidation of Si by oxygen,* Appl. Phys. Lett. 33(5), 424 (1978).

[127] V. K. Samalam, *Theoretical model fort he oxidation of silicon,* Appl. Phys. Lett. 47(7), 736 (1985).

[128] A. Fargeix, and G. Ghibaudo, *Role of stress on the parabolic kinetic constant for dry silicon oxidation,* J. Appl. Phys. 56(2), 589 (1984).

[129] H. Z. Massoud, J. D. Plummer, and E. A. Irene, *Thermal oxidation of silicon indry oxygen: Growth-rate enhancement in the thin regime,* J. Electrochem. Soc. 132(11), 2693–2700 (1985).

[130] R. Le Harzic, D. Breitling, M. Weikert, S. Sommer, C. Föhl, S. Valette, C. Donnet, E. Audouard, F. Dausinger, *Pulse width and energy influence onlaser micromachining of metals in a range of 100 fs to 5 ps*, Appl. Surf. Sci. 249, 322-331 (2005)

[131] P. Mannion, J. Magee, E. Coyne, G. M. O'Connor, *Ablation thresholds in ultrafast laser micro-machining in common metals in air* Proc. Of SPIE 4876 (2003)

[132] Niemz M H 2003 *Laser–Tissue Interactions: Fundamentals and Applications* 3rd edn (Heidelberg: Springer)

[133] Guo Z, Wan S K, August D A, Ying J, Dunn S M and Semmlow J L 2006 *Optical imaging of breast tumor through temporal log-slope difference mappings Comput. Biol.* Med. 36, 209-223

[134] Niemz M H, Klancnik E G and Bille J F 1991 *Plasma-mediated ablation of corneal tissue at 1053 nm using a Nd : YLF oscillator/regenerative amplifier laser* Lasers Surg. Med. 11, 426–431

[135] Fischer J P, Dams J, Götz M H, Kerker E, Loesel F H, Messer C J, Suhm N, Niemz M H and Bille J F 1993 *Plasma-mediated ablation of brain tissue with picosecond laser pulses* Appl. Phys. *B* 58, 493–499

[136] Moss J P, Patel B C, Pearson G J, Arthur G and Lawes R A 1994 *Krypton fluoride excimer-laser ablation of tooth tissues: precision tissue machining* Biomaterials 15, 1013–1018

[137] Chen S C, Kancharla V and Lu Y 2003 *Laser-based microscale patterning of biodegradable polymers for biomedical applications* Int. J. Mater. Prod. Technol. 18, 457–68

[138] Aguilar C A, Lu Y, Mao S and Chen S 2005 *Direct micro-patterning of biodegradable polymers using ultraviolet and femtosecond lasers* Biomaterials 26, 7642–7649

[139] Hallgren C, Reimers H, Chakarov D, Gold J and Wennerberg A 2003 *An in vivo study of bone response to implants topographically modified by laser micromachining* Biomaterials 24, 701–710

[140] *Handbook of Biological Confocal Microscopy* (3rd Ed.). Berlin: Springer. Pawley JB (editor), 2006

[141] Denk W, Strickler J, Webb W (1990). *Two-photon laser scanning fluorescence microscopy*. *Science* 248 (4951): 73–6

[142] Lubatschowski H, Heisterkamp A, Will F, Singh A I, Serbin J, Ostendorf A, Kerani O, Heermann R, Welling H and Ertmer W 2003 *Medical applications of ultrafast laser pulses* RIKEN Review 50, 113-118

[143] Juhasz T, Loesel F H, Kurtz R M, Horvath C, Bille J F, Mourou G A 1999 *Corneal refractive surgery with femtosecond laser* IEEE J Quantum. Electron **5**, 902–909

[144] Vogel A and Venugopalan V 2003 *Mechanisms of Pulsed Laser Ablation of Biological Tissues* Chemical Reviews 103, 577-644

[145] Vogel A, Noack J, Huttman G, and Paltauf G 2005 *Mechanisms of femtosecond laser nanosurgery of cells and tissues* Appl. Phys. B 81, 1015-1047

[146] König K, Riemann I and Fritsche W 2001 *Nanodissection of human chromosomes* with *near-infrared femtosecond laser pulses* Opt. Lett. 26, 819-821

[147] König K, Riemann I, Stracke F and Le Harzic R 2005 *Nanoprocessing with nanojoule near-infrared femtosecond laser pulses* Med. Laser Appl. 20, 169-184

[148] Maxwell I, Chung S and Mazur E 2005 *Nanoprocessing of subcellular targets using femtosecond laser pulses* Med. Laser Appl. 20, 193-200

[149] Watanabe W, Arakawa N, Matsunaga S, Higashi T, Fukui K, Isobe K and Itoh K 2004 *Femtosecond laser disruption of subcellular organelles in a living cell* Opt. Express 12, 4203-4213

[150] Kohli V, Elezzabi A and Acker J P 2005 *Cell nanosurgery using ultrashort (femtosecond) laser pulses: applications to membrane surgery and cell isolation* Lasers Surg. Med. 37, 227-230

[151] Shen N, Datta D, Schaffer C B, Le Duc P, Ingber D E and Mazur E 2005 *Ablation of cytoskeletal filaments and mitochondria in live cells using a femtosecond laser microscissors* Mech Chem Biosyst 2,17–26

[152] Huang H and Guo Z 2009 *Human dermis separation via ultra-short pulsed laser plasma-mediated ablation* J. Phys. D:Appl. Phys. 42, 165204-165213

[153] Liu Y M, Sun S, Singha S, Cho M R and Gordon R J 2005 3D *femtosecond laser patterning of collagen for directed cell attachment* Biomaterials 26 4597–4605

[154] Valette S, Steyer P, Richard L, Forest B, Donnet C and Audouard E 2006 *Influence of femtosecond laser marking on the corrosion resistance of stainless steels* Appl. Surf. Scie 252 4696-4701

[155] Steyer P, Valette S, Forest B, Millet J P, Donnet C and Audouard E 2006 *Surface modification of martensitic stainless steels by laser marking and its consequences regarding corrosion resistance* Surf. Eng. 22 167-172

[156] Mottay E, Kupisiewicz A, Detroux G, Costet X, Simmons A, Vivarelli U, Lemaire P and Lopez J 2008 *Industrial ultrafast internal engraving laser system for anti-counterfeiting applications* Proc. SPIE 6881 66810H

[157] Le Harzic R, Sauer D, Riemann I and König K 2005 *Nanoprocessing of semiconductors and metals with nJ femtosecond laser pulses* Proc. SPIE **5990**, 189-198

[158] Groenendijk M 2008 *Fabrication of Super Hydrophobic Surfaces by fs Laser Pulses* Laser Technik Journal 5, 44-47

[159] Zorba V, Persano L, Pisignano D, Athanassiou A, Stratakis E, Cingolani R, Tzanetakis P and Fotakis C 2006 *Making silicon hydrophobic: wettability control by two-lengthscale simultaneous patterning with femtosecond laser irradiation* Nanotechnology 17, 3234

[160] Fadeeva E, Schlie S, Koch J, Ngezahayo A and Chichkov BN 2009 *The hydrophobic properties of femtosecond laser fabricated spike structures and their effects on cell proliferation* Phys. Status Solidi A 206, 1348-1351

[161] Vorobyev AY and Guo C 2007 *Femtosecond laser structuring of titanium implants* Appl. Surf. Scie. 253, 7272-7280

[162] Oliveira V, Ausset S and Vilar R 2009 *Surface micro/nanostructuring of titanium under stationary and non-stationary femtosecond laser irradiation* Appl. Surf. Scie. 255, 7556-7560

[163] Maruo S, Nakamura O and Kawata S 1997 *Three-Dimensional Microfabrication with Two-Photon-Absorbed Photopolymerization* Opt. Lett. 22, 132-134

[164] Cumpston BH, Ananthavel SP, Barlow S, Dyer DL, Ehrlich JE, Erskine LL, Heikal AA, Kuebler SM, Lee IYS, McCord-Maughon D, Qin J, Rockel H, Rumi M, Wu X L, Marder SR and Perry JW 1999 *Two-Photon Polymerization Initiators for Three-Dimensional Optical Data Storage and Microfabrication* Nature 398, 51-54

[165] Sun HB, Matsuo S and Misawa H 1999 *Three-dimensional photonic crystal structures achieved with twophoton- absorption photopolymerization of resin* Appl. Phys. Lett.74, 786-788

[166] Kawata S, Sun HB, Tanaka T and Takada K 2001 *Finer features for functional microdevices* Nature (London) 412, 697–698

[167] Serbin J, Egbert A, Ostendorf A, Chickov BN, Houbertz R, Domann G, Schulz J, Cronauer C, Fröhlich L and Popall M 2003 *Femtosecond laser-induced two-photon polymerization of inorganic-organic hybrid materials for applications in photonics* Opt. Lett. 28, 301-303

[168] Mizeikis V, Seet KK, Juodkazis S and Misawa H 2004 *Three-dimensional woodpile photonic crystal templates for the infrared spectral range* Opt. Lett. **29**, 2061-2063

[169] Li L, Gattass RR, Gershgoren E, Hwang H and Fourkas JT 2009 *Achieving λ/20 Resolution by One-Color Initiation and Deactivation of Polymerization* Science 324, 910 - 913

[170] Ovsianikov A, Ostendorf A and Chichkov B 2007 *Three-dimensional photofabrication with femtosecond lasers for applicationsin photonics and biomedicine* Appl. Surf. Sci. 253, 6599-6602

[171] Choi HW, Johnson JK, Nam J, Farson DF and Lannutti J 2007 *Structuring electrospun polycaprolactone nanofiber tissue scaffolds by femtosecond laser ablation* J. Laser Appl. 19, 225

# APPENDIX A

# 10 µm/s

410 mW  (0.36 J/cm²)

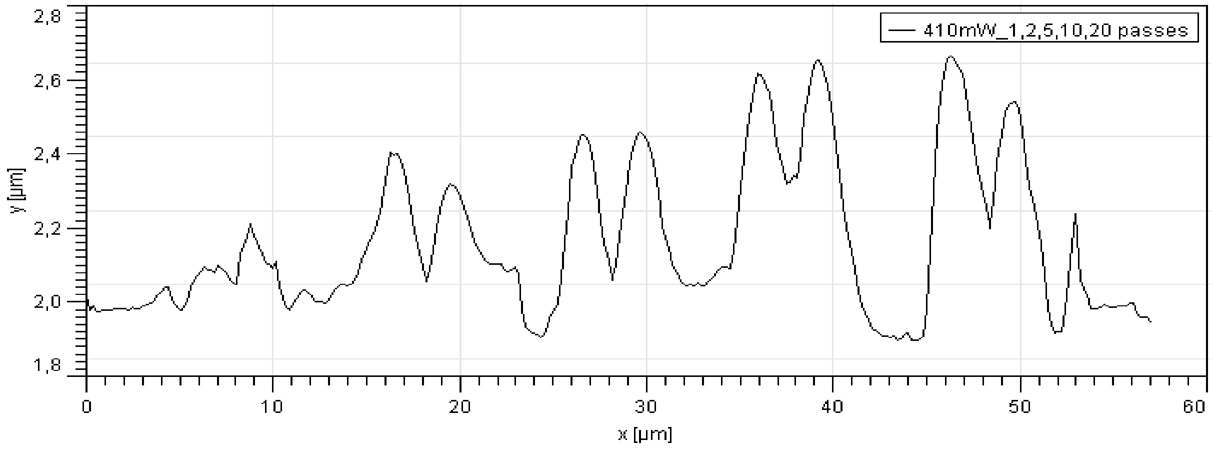

365 mW  (0.32 J/cm²)

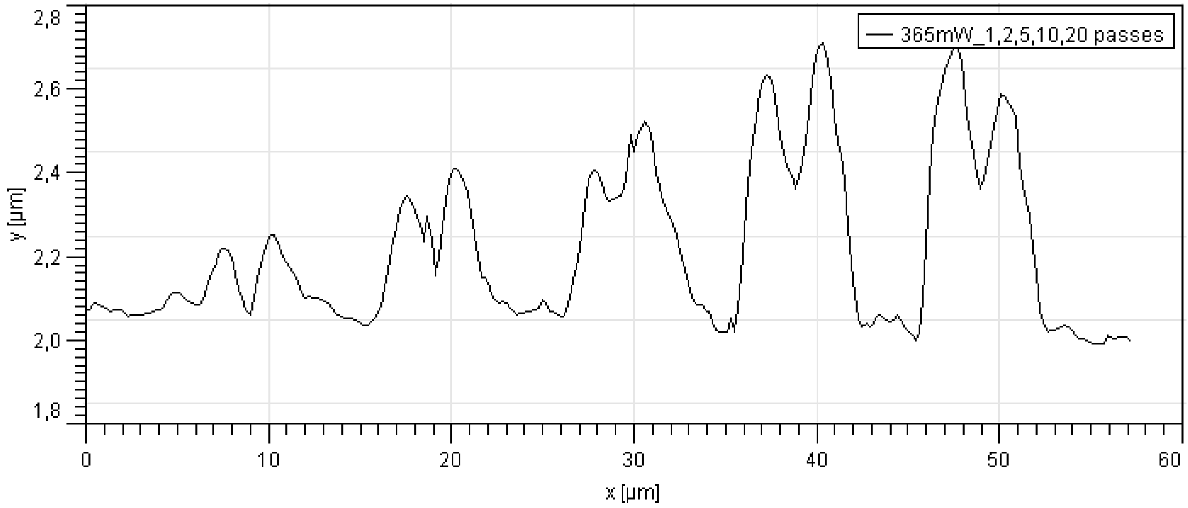

280 mW (0.24 J/cm²)

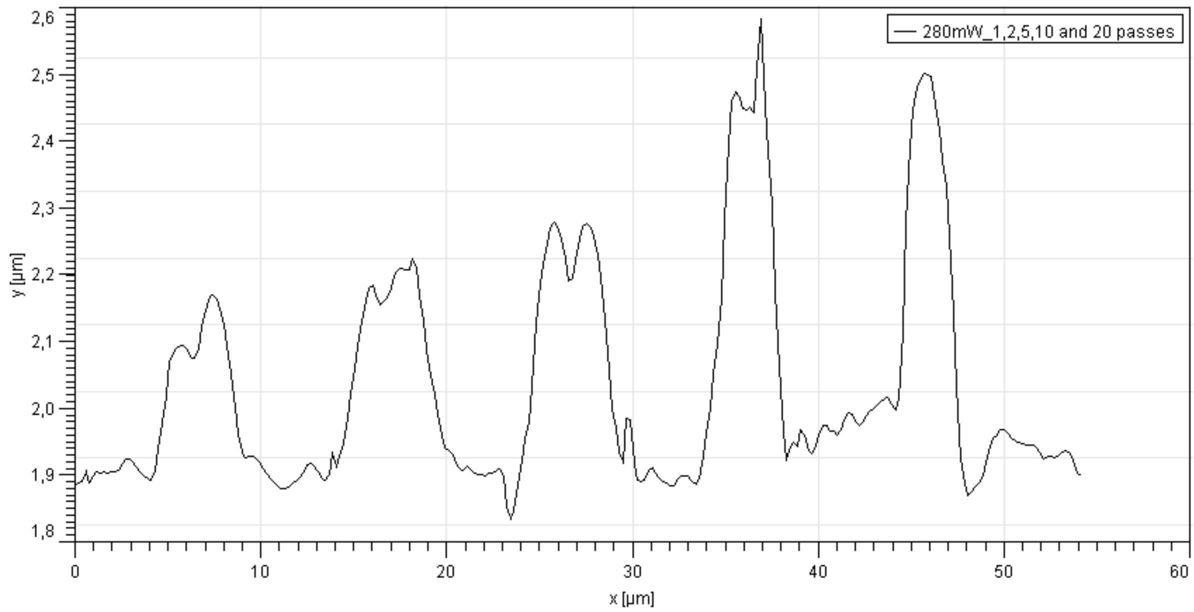

175 mW (0.15 J/cm²)

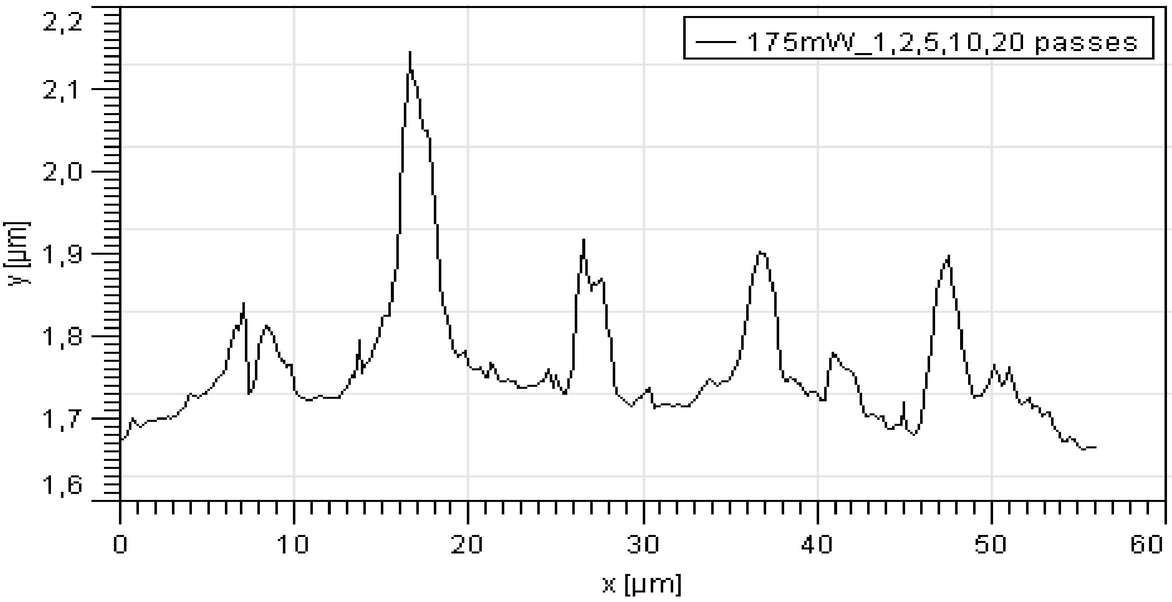

85 mW (0.075 J/cm²)

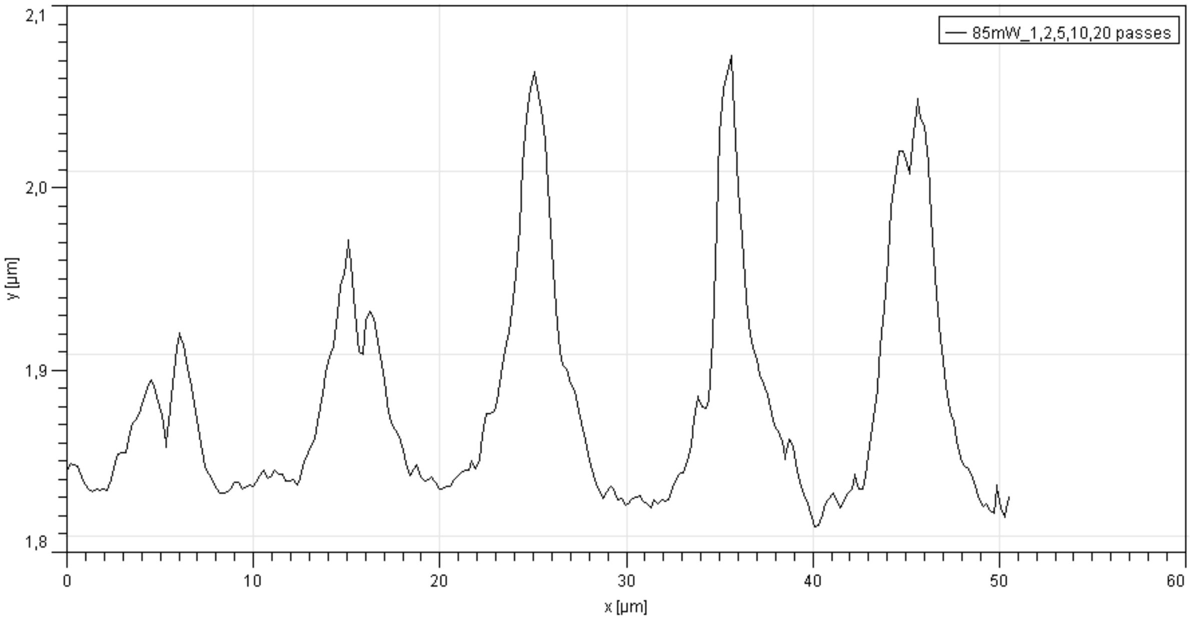

**Figure 82** ***Results on copper at 10µm/s for several fluences 0.36, 0.32, 0.24, 0.15 and 0.075 J/cm², and different number of passes, respectively from the left to right 1, 2, 5, 10, 20 passes.***

## 50 µm/s

410 mW (0.36 J/cm²)

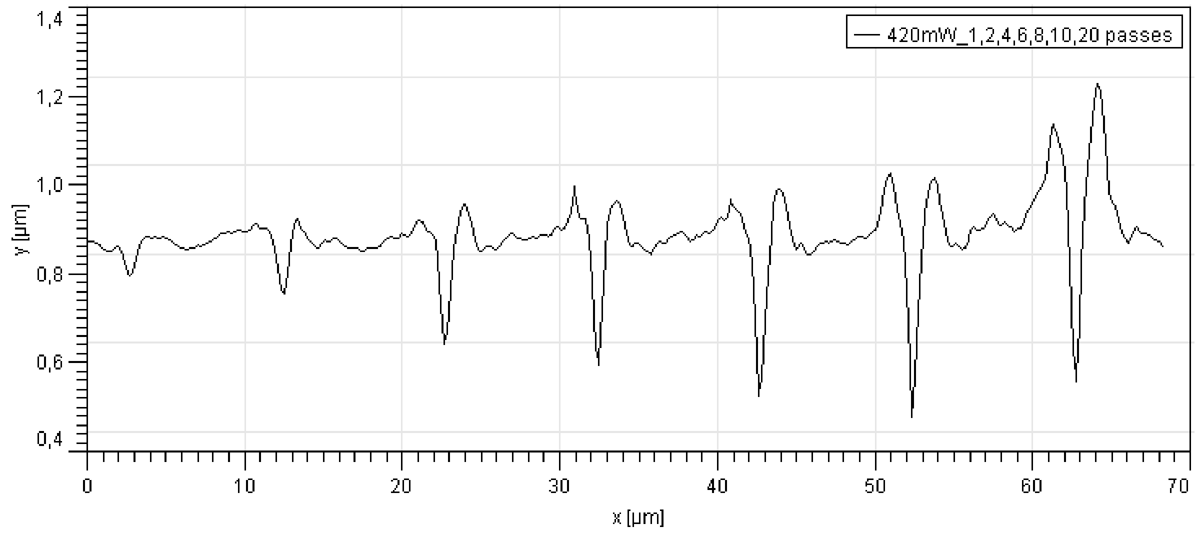

365 mW (0.32 J/cm²)

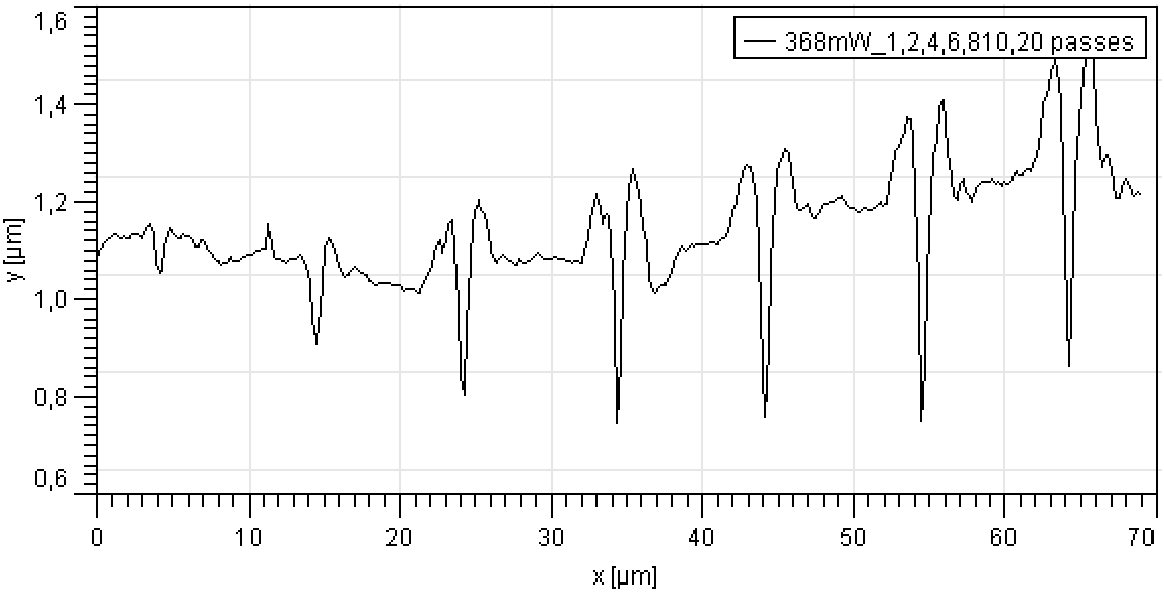

280 mW (0.24 J/cm²)

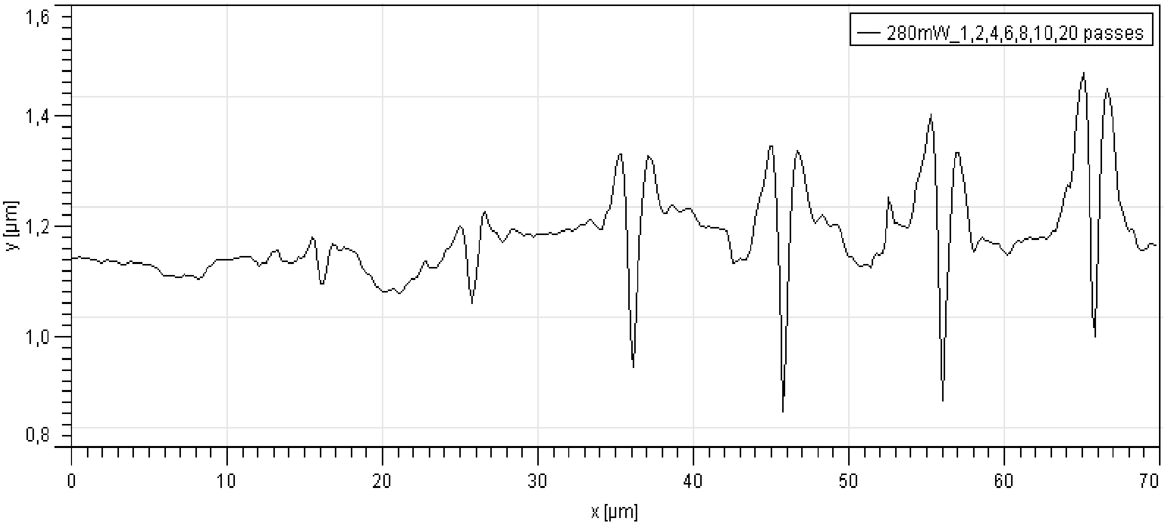

175 mW (0.15 J/cm²)

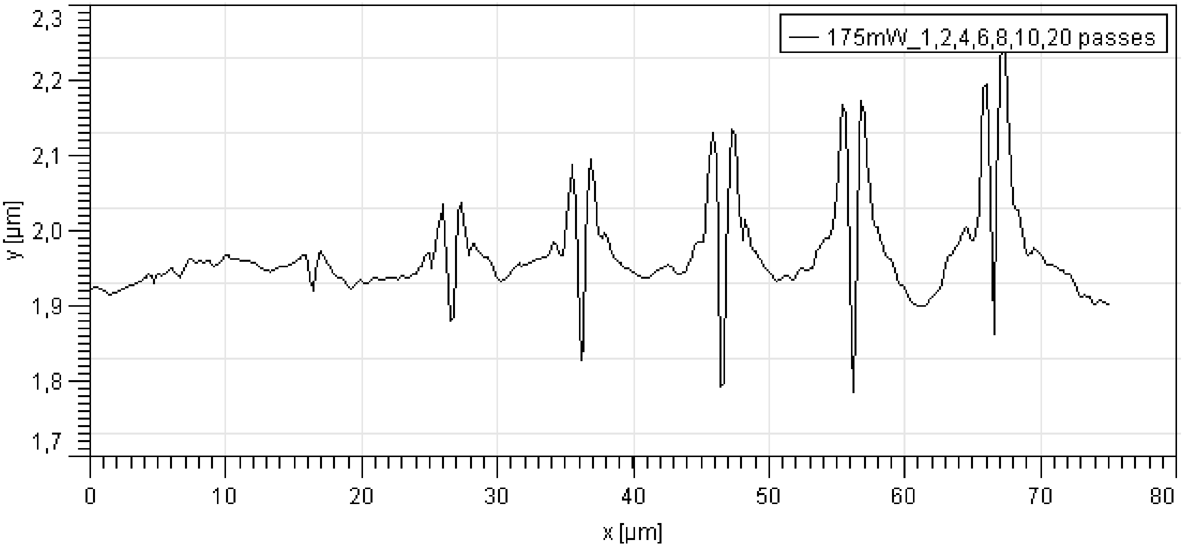

85 mW (0.075 J/cm²)

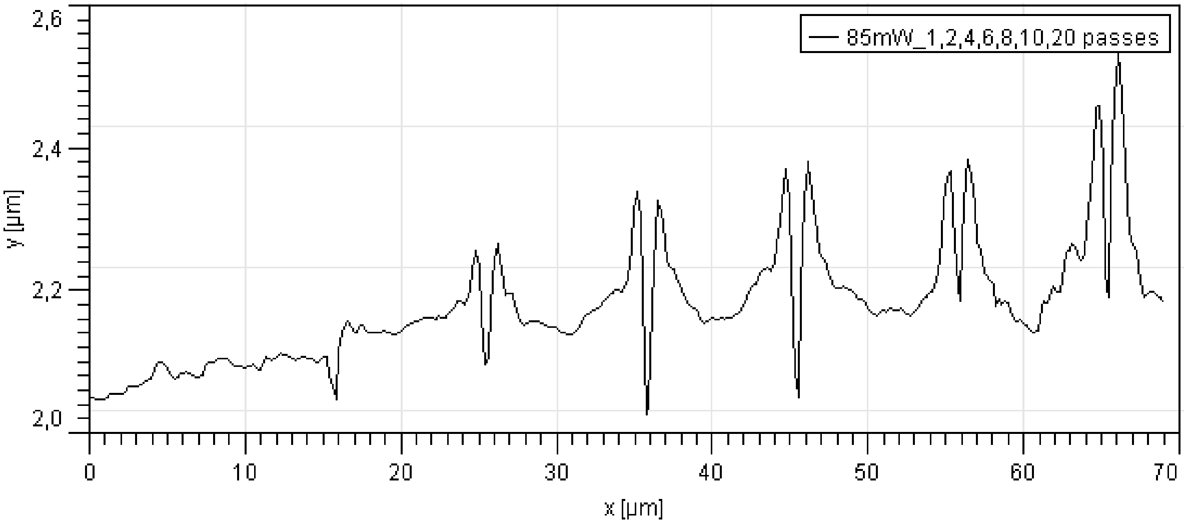

**Figure 83** ***Results on copper at 50µm/s for several fluences 0.36, 0.32, 0.24, 0.15 and 0.075 J/cm², and different number of passes, respectively from the left to right 1, 2, 4, 6, 8, 10, 20 passes.***

# 100 µm/s

410 mW (0.36 J/cm²)

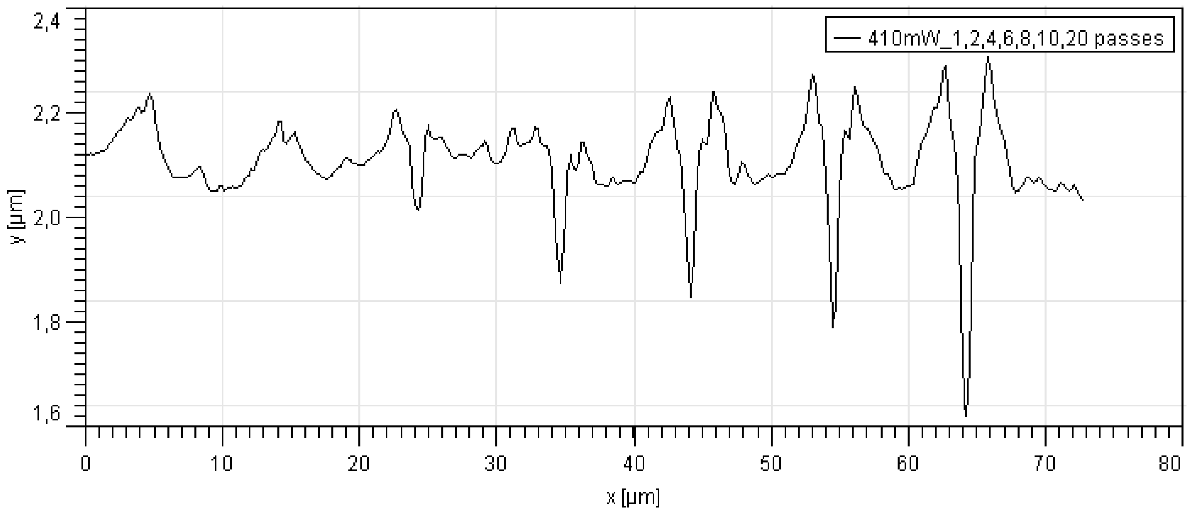

360mW (0.31 J/cm²)

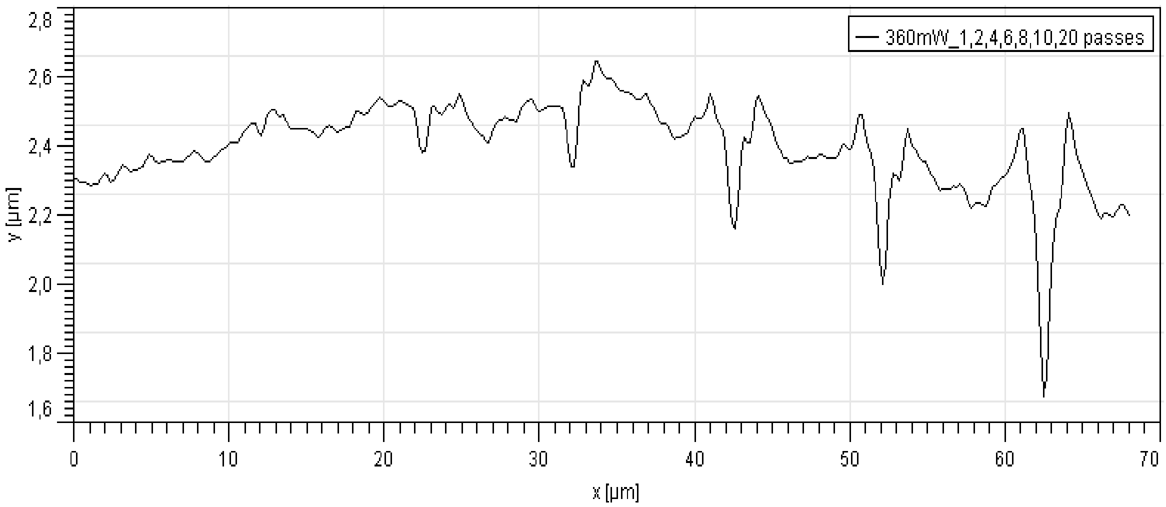

280 mW (0.24 J/cm²)

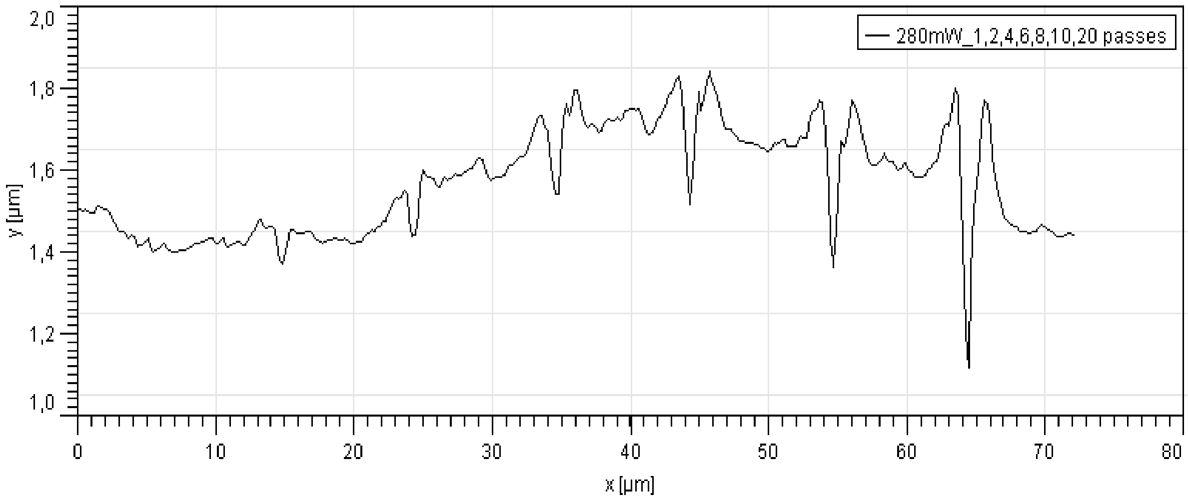

**Figure 84** ***Results on copper at 100µm/s for several fluences 0.36, 0.32 and 0.24 J/cm², and different number of passes, respectively from the left to right 1, 2, 4, 6, 8, 10, 20 passes.***

# Own Publication list

## Reviewed papers

R. Le Harzic, M. Stark, H. Schuck,, P. Becker, E. Lai, **D. Bruneel**, F. Bauerfeld, D. Sauer, T. Velten and K. König

"Nanostructuring with Nanojoule Femtosecond Laser Pulses", *Journal of Laser Micro/Nanoengineering (JLMN)* **3**, 106-113 (2008).

**D. Bruneel**, G. Matras, R. Le Harzic, N. Huot, K. König, and E. Audouard

"Micromachining of metals with ultra-short Ti-Sapphire lasers: Prediction and optimization of the processing time", *Optics and Lasers in Engineering* **48**, 268-271 (2010).

**D. Bruneel**, E. Audouard, K. König and R. Le Harzic

"Flexible tool for two photon laser nanoprocessing and large area mapping with high resolution", *Optics and Lasers in Engineering* **48**, 1278-1284 (2010).

## Proceedings

R. Le Harzic, C. Wüllner, **D. Bruneel**, C. Donitzky, and K. König

"Femtosecond refractive eye surgery: study of laser parameters for even more efficiency and safety", Proc. SPIE 6632, 663217 (2007), (Ophthalmic Technologies XIX , BIOS2007, Photonics West, 21-22 January 2007, San Jose, California, USA)

R. Le Harzic, C. Wüllner, **D. Bruneel**, C. Donitzky, and K. König

“New developments in femtosecond laser corneal refractive surgery”, Proceedings of the Fourth International WLT-Conference on Lasers in Manufacturing (2007)

(Laser world of photonics 2007, June 2007, Munich, Germany)

R. Le Harzic, M. Stark, H. Schuck, P. Becker, E. Lai, **D. Bruneel**, F. Bauerfeld, D. Sauer, T. Velten , K. König

“Nanostructuring with Nanojoule Femtosecond Laser Pulses”, Proceeding of the Laser Precision Fabrication conference (LPM), (2007)

(LPM (Laser Precision Fabrication), 24-28 April 2007, Vienna, Austria)

**D. Bruneel**, M. Schwarz, E. Audouard, K. König, R. Le Harzic

“Development of a powerful tool for nanostructuring and multiphoton imaging with nanojoule femtosecond laser pulses”, Proc. SPIE 7201, 720117 (2009)

(Laser Applications in Microelectronic and Optoelectronic Manufacturing VII, LASE2009, Photonics West, 24-29 January 2009, San Jose, California, USA)

**Poster**

**D.Bruneel**, E. Audouard, N.Huot, R. Le Harzic, K. König

“Nanomarquage femtoseconde “, Opto 2007, 3eme journée d’étude : Marquage, micro et nano gravure,25-27 septembre 2007, Paris, France

# Acknowledgments

My thanks go firstly to Pr. E. Audouard, R. Le Harzic, and Pr. K. Konig. Pr. E. Audouard proposed to me to work on this so interesting topic. I would like to thank him for having guided me all along this difficult work. I also thank for all discussions we could had, concerning sciences but not only. I have to confess that I was very impressed concerning his erudition, and his positivity. He is unmistakably a great driving force for the research to industry translation.

I would like to thank Pr. K. Konig, to have accepted to be my german supervisor, and to have enabled the possibility for me to integrate the team of laser Microsystems at the Fraunhofer IBMT.

I want to particularly thank Dr. R. Le Harzic for his help and good advices. He often unlocked pressing situations. He also followed all my work not only during the period I was at the Fraunhofer institut, but from the beginning to the end of this thesis. Thanks to him for all the help he gave me for my arrival and all along the period at the Fraunhofer IBMT. I have really appreciated to work with him, for discussing, and trying to solve problems with efficiency. Thanks again for translating and helping me in all the administrative German staff.

I would like to express a special thanks to Jean-Philippe Colombier, with who I liked to discuss about physics of the interaction of femtosecond pulses with the matter and the time he passed doing the very long hydrodynamic simulations in trying to understand high repetition rate interactions of femtosecond pulses with the matter.

I would like to thank all people with who I have worked during this time at the laboratory Hubert Curien. I think especially to the team of ultrafast laser processing, with Sébastien, Benjamin, Romain, Nicolas, Matthieu, Sébastien, … and from the company impulsion with Hervé Soder as the director, Julien, Gregory, Anthony and Alexandra. I also thank all the team of laser and Microsystems of the Fraunhofer institute with who I really enjoyed to work and shared good moments inside the team, I think about Ronan, Iris, Martin, Daniel D., Franck, Aisada, and, of course, Daniel S. for his efficiency and his great availability.

I want to thank my family who throughout this long trek has shown great support and without which the various severe tests met would have been as more difficult to overcome. I especially express a thought to my grandmother who left us during this time while maintaining her great presence and her good temper until the end.

I would like to thank all my friends, I think especially to Nico, Marie, Laurent, Claire, Tobias, Elodie, and all others for good moments passed together and which were very noticeable during this period. A special thought to Gonzague, Tobias and Christophe for great discussions and their support during all these four years. Thanks to Claire, Nico, and Tobias with who I spent very good time travelling and discovering new landscapes, new cities like Berlin, Munich, Pragues, and more … where we could discover another culture, other mores, as well as typical events, I particularly think about German Christmas markets, or the festival of wine in Stuttgart (and yes, German white wine is good too), without forgetting the legendary festival “Oktoberfest” in Munich, and so many anecdotes associated to each of these moments. Thanks to Tobias for giving us a very human welcome during this time. I keep in mind unforgettable remembers of time spent in Germany.

I would like to thank my neighbours of St Etienne, women across the landing, for their generosity, their kindness, and their humanity. They are to me, worthy people of the “cause stéphanoise”.

I would like to thank French-German University and the région Rhône-Alpes for grant support which helped me a lot when I was abroad. And thanks to the CNRS for funding me during all this time.

# Declaration

I hereby declare that this thesis is the result of my own independent investigation and that all contributions from other sources are duly acknowledged. No part of this thesis was previously submitted for a degree at universities of Saarland, and of Saint Etienne or another university.

Hiermit versichere ich an Eides statt, dass ich die vorliegende Arbeit selbständig und ohne Benutzung anderer als der angegebenen Hilfsmittel angefertigt habe. Die aus anderen Quellen oder indirekt übernommenen Daten und Konzepte sind unter Angabe der Quelle gekennzeichnet.

Die Arbeit wurde bisher weder im In- noch im Ausland in gleicher oder ähnlicher Form in einem Verfahren zur Erlangung eines akademischen Grades vorgelegt.

David Bruneel

Saint Etienne, 5 October 2010

# Curriculum Vitae

**David Bruneel**

Born September 21, 1982 in Montreuil-sur-mer (France)

**Education**

- 2003-2005 Master's degree in Engineering (Specialization in optics and electronics), TELECOM Saint-Etienne, the State School of Engineering of the University of Saint-Etienne, France.
- 2001-2003 Institut of technology specialized in physics and instrumental techniques, University of Lille, France.
- 2001 High school diploma, specialized in physics and industrial techniques, Lycée E. Woillez, Montreuil-sur-mer, France

**Professional experience**

- October 1rst, 2006 – September 30, 2009 PhD thesis of engineering "Femtosecond laser ablation for controlling micro and nanostructuration" realized at Laboratoire Hubert Curien in Saint Etienne (France) and at the Frauhofer Institut für Biomedizinische Technik (IBMT) in Sankt Ingbert (Germany).
- January 1rst, 2010 – until now Reasearch assistant at the Laboratoire Hubert Curien of the University of Saint Etienne (France).
- March 1, 2006 – August 31, 2006 Training period of six months as an engineer realized at the Fraunhofer Institut für Biomedizinische Technik (IBMT) in Sankt Ingbert (Germany).
- April 1, 2003 – June 30, 2003 Industrial training period in Valeo industry at Etaples (France)